In: New Topics in Crystal Growth Research ISBN 1-59454-837-4
Editor: George V. Karas, pp. 1-83

Chapter 1

OPTICAL IMAGING AND CONTROL OF CONVECTION AROUND A CRYSTAL GROWING FROM ITS AQUEOUS SOLUTION

K. Muralidhar, Atul Srivastava and P. K. Panigrahi
Department of Mechanical Engineering
Indian Institute of Technology Kanpur
Kanpur 208 016 UP (India)

ABSTRACT

The importance of convection in determining crystal growth rates and crystal quality has been emphasized in the literature. However, measurement of convection patterns has posed certain difficulties. In this context, laser measurement techniques have become popular, though primarily as a flow visualization tool. The nature of convection and its relationship to solute distribution, crystal growth rates and quality remains to be fully established. For this reason, the dependence of the convection patterns on the process parameters has been explored in the present study. The process parameters varied are cooling rate of the solution and the rotation rate of the growing crystal. Crystal rotation is seen in this work as a means of diminishing the impact of buoyancy. It can also be an alternative to growth under microgravity conditions. The crystal size plays an influential role in determining the relative importance of buoyancy and rotation. An independent study of crystal size has also been presented.

Mapping of convection patterns as well as the concentration field in the growth chamber is required to understand the mechanism of crystal growth and to establish appropriate conditions for growing large defect-free crystals. Unlike growth from melt and vapor, growth of a crystal from an aqueous solution is particularly amenable to optical visualization since the solution is transparent. It is possible to generate images of the convective field by exploiting changes in the refractive index that accompany changes in the density of the medium. The visualization technique is thus useful for on-line monitoring of the growth process.

Optical techniques are ideal for mapping the properties of the solution during a crystal growth experiment because they are non-intrusive and inertia-free. In addition, the images recorded can be interpreted as path integrals in the direction of line-of-sight.

Local properties can be subsequently reconstructed by using principles of tomography. In the present study, images from three refractive index-based methods namely, interferometry, schlieren and shadowgraph are presented. The suitability of these measurement techniques to image, analyze and interpret the convective field around a growing crystal is explored. The crystal material chosen for experiments is potassium-di-hydrogen-phosphate (KDP). The choice of KDP was based on the availability of refractive index and supersaturation data in the literature for image analysis.

The three optical measurement techniques have been validated in the context of buoyancy-driven convection in a rectangular differentially heated cavity. This study is concerned with the imaging of buoyancy-driven convection in a fluid medium that is confined in a horizontal differentially heated rectangular cavity. The horizontal surfaces of the cavity provide a temperature difference, for initiating convection in the fluid. The vertical side walls are thermally insulated. Experiments have been conducted in a cavity of length 447 mm and 32 mm vertical height. The cavity is square in cross-section, and the imaging direction is parallel to its longer side. Convection in air and water have been investigated. Quantities of interest are the temperature profiles in the fluid medium and wall heat transfer rates.

A direct comparison of the refractive-index based techniques shows that interferometry is best suited when density gradients in the fluid medium are small. For high density gradients, shadowgraph images contain the greatest amount of information. While interferograms are easy to analyze, it is difficult to retrieve concentration data from a shadowgraph. As a balance between ease of analysis and sensitivity to density gradients, schlieren emerges as the best option for crystal growth applications.

On the basis of schlieren imaging, results obtained in the present work show that the growth rates are well-correlated with regions of large concentration gradients. Rotation serves to diminish concentration gradients near the crystal by homogenizing the solution. Accordingly, the growth rate is seen to be the highest in the buoyancy-driven convection regime, while the quality of the grown crystal is superior in the presence of rotation. The three dimensional distribution of concentration shows a strong correlation with the topography of the growing crystal.

Key words: Convection, Supersaturated solution, Ramp rate, Rotation, Imaging, Interferometry, Schlieren, Shadowgraph, Tomography, Crystal quality.

1. INTRODUCTION

Large crystals with a high degree of perfection are required in a variety of applications. Optical crystals of good quality find utility in critical technology areas such as high power lasers, higher harmonic generation and in nuclear fusion. A class of such crystals can be grown from their supersaturated solution in water, during a slow cooling process. Growth of such crystals from an aqueous solution is one of the commonly used techniques in the industry. The technique can be used for growing optical crystals such as KDP and proteins such as lysozyme. A crystal growing from its aqueous solution creates a three-dimensional solute distribution in its vicinity. The solutal concentration gradients and hence the gradients in the density of the solution are responsible for the evolution of buoyancy-driven convection currents in the growth chamber. The buoyant convection currents influence the magnitude of the concentration gradients prevailing along the growth surfaces. In turn these control the stability of the growth process and the overall crystal quality. The concentration gradients in

the growth chamber are significantly altered when the crystal is given rotation. Rotation can hence be viewed as a method of controlling convection during the growth process.

Low temperature solution growth methods are applicable to materials that have moderate to high solubility in temperatures up to100^oC at atmospheric pressure. A number of organic and inorganic materials fall in this category and can be crystallized using this technique. The advantages here include relatively low temperature handling of the equipment and a good degree of temperature control to within $\pm 0.01^oC$. The grown crystals show full natural morphology. In addition, online studies of surface growth features and growth rate studies of different faces are possible. Since temperature gradients involved in a given process are low, thermally generated strains in the grown crystal are small. The disadvantage of low temperature solution growth is the slow growth rates (0.1 to 10 mm per day). In many cases the ease of solvent inclusion into the growing crystal is a limiting factor. Since many crystals are grown from water as the solvent, the grown crystal is hygroscopic in nature; this limits its use to applications in which water molecules are excluded in the lattice. A large fraction of the crystals produced from low temperature solutions are grown by using water as a solvent owing to its high solvent action, chemical stability, low viscosity, low toxicity and low cost. Other solvents include ethanol, methanol, acetone, carbon tetrachloride, hexane, and xylene. Examples of technologically important crystals grown from a low temperature aqueous solution include potassium di-hydrogen phosphate (KDP), potassium di-deuterium phosphate (DKDP), tri-glycine sulphate (TGS), potassium acid phthalate (KAP), lithium arginine phosphate (LAP), and urea. Recently, low temperature solution growth method has found its applications towards the growth of protein crystals such as lysozymes.

A crystal growing from its aqueous solution creates a three-dimensional solute distribution in its vicinity. The mechanism involved is the withdrawal of the solute from the solution, causing the solute concentration to decline in the neighboring solution. The solutal concentration gradients, and hence the gradients in the density of the solution are responsible for the evolution of buoyancy-driven convection currents in the growth chamber [1]. The convection currents are the main drivers for the solute from the solution rich in salt as it is transported to the surface of the growing crystal. In the absence of convection, solute transport is mainly by molecular diffusion. Since diffusion coefficients in liquids are small, small fluid velocities greatly increase mass transfer (over the diffusion values) and hence the growth rate of the crystal. It is understandable that changes in the symmetry pattern of the flow field and unsteadiness can lead to a lowering of the crystal quality and the growth rate. Hence an optimum strength of convection currents is desirable to maintain a balance between the quality of the growing crystal and its growth rate. The strength and orientation of buoyancy driven convection currents are intricately linked with the size and morphology of the growing crystal. These in turn depend upon the process parameters namely the supersaturation level of the solution and the rate at which it is cooled. More recently, convection has been found to be quality-limiting mechanism in the growth of protein crystals from their solution. Here, convection has the capability of distorting the effects of mechanisms such as surface tension and magnetic fields and thus influences the crystal growth process.

Buoyancy-driven convection currents influence the magnitude of the concentration gradients prevailing along the growth interfaces. In turn, the gradients control the stability of the growth process and the overall crystal quality. It has been experimentally noted that growth in free convection regime is often limited by density stratification in the vicinity of the

growing crystal leading subsequently to unwanted nucleation of solute in the growth chamber. The concentration gradients in the growth chamber are significantly altered when the crystal is given a rotation. An optimum rotation rate tends to stabilize the perturbations along the rotational axis eventually leading to an axisymmetric concentration distribution over the crystal. The stirring of the solution also reduces the natural convection-induced temperature oscillations by homogenizing the bulk solution. Rotation can hence be viewed as a method for controlling convection during the growth process by diminishing the impact of buoyancy.

To ensure the growth of high-quality large crystals, it is important to understand from a fundamental point-of-view, the transport phenomena involved during solute deposition from the solution to the crystal surfaces. Simultaneously, visualization techniques are required to monitor the crystal growth process itself during its progress. Unlike growth from melt and vapor, growth from an aqueous solution is particularly amenable to flow visualization, since it is transparent. It is possible to generate images of the convective field by exploiting changes in the refractive index that accompany changes in the density of the medium. Optical visualization techniques are thus useful for online monitoring of the growth process.

Optical techniques are ideal for mapping the properties of the solution during a crystal growth experiment. Since a probe need not be introduced in the field of study, they are non-intrusive and practically inertia free. Over the past decade, laser measurement techniques have become popular, though primarily as a flow visualization tool. Recent work however has emphasized the possibility of quantitative measurements as well. A majority of optical techniques are field techniques in the sense that an entire cross-section of the physical region can be mapped. They require the medium to be transparent, and are thus suitable for the measurements in liquids. Optical methods that utilize the dependence of refractive index of light on density (and indirectly on concentration and temperature) can be configured in many different ways. Three available routes are:

1. Interferometry, where the image formation is related to changes in the refractive index with respect to a reference environment,
2. Schlieren, where light deflection in a variable refractive-index field is captured, and
3. Shadowgraph, where the reduction in light intensity on beam divergence is employed.

In the context of crystal growth from an aqueous solution, a unique relationship can be established between the refractive index and the local density of the medium under study. Under normal process conditions, the solution is practically incompressible and the density does not depend on pressure. At any time instant, the solution is also at a spatially uniform temperature. Hence, density changes correlate with those in concentration alone, and the three methods become applicable for concentration field measurement in the fluid medium. The three techniques referred above yield the path integral of the density field in the direction of line-of-sight. The distribution of density in three dimensions can then be extracted from the recorded images using principles of tomography.

The present article reports measurement of the solute concentration distribution around a KDP crystal growing from its aqueous solution under slow cooling conditions. The choice of KDP (molecular mass 136.09) was based on the availability of refractive index and supersaturation data in the literature for image analysis. The solution adjacent to the crystal is

depleted of the salt and is close to the saturated state, while it is supersaturated in the far-field. The difference in solute concentrations drives a diffusive mass flux in the initial stages of growth, while the flux is controlled by fluid convection at later times (Figure 1). In the context of crystal growth, the present article contains discussions on refractive-index methods, their validation in a buoyancy-driven flow experiment, comparison of interferograms, schlieren and shadowgraph for crystals growing under nominally identical experimental conditions, schlieren imaging and analysis of convection patterns, possibility of control by rotation, and tomographic reconstruction of the concentration field around the growing crystal. The physical problem taken up for validation and comparison of the three optical methods is buoyancy-driven convection in a fluid medium confined in a rectangular cavity (Gebhart *et al.* [2]). The fluid is heated from below, cooled from the top and the cavity has insulating side walls. The flow pattern associated with this configuration shows a sequence of transitions from steady laminar to unsteady turbulent flow.

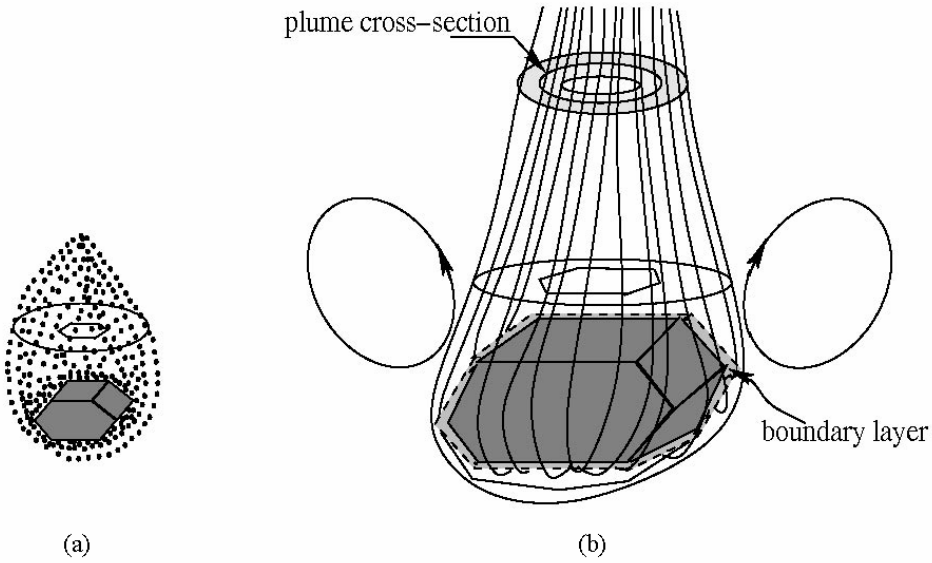

Figure 1. Schematic drawing of the concentration distribution around a growing crystal. (a) Diffusion dominated growth shown by dots, (b) Growth in stable convection regime in the presence of a buoyant plume. Arrows indicate fluid motion in the bulk of the solution.

2. LITERATURE REVIEW

The following sections present a survey of the published literature on imaging fluid convection using optical techniques. The review covers imaging and characterization of the convective fields induced due to thermal gradients, solute concentration gradients and measurements of three-dimensional temperature and concentration fields using tomography algorithms. The emphasis is on the survey of published literature related to the imaging of buoyancy-driven convection during crystal growth processes from an aqueous solution.

2.1. Imaging of Heated and Thermally Buoyant Flows

Buoyancy-driven flow and heat transfer are performance-limiting steps in several engineering processes. Examples can be seen in applications ranging from cooling of electronic components, growth of semiconductor crystals to material processing. Lewis *et al.* [3] conducted a quantitative study of temperature distribution using shadowgraph. The focus was on the determination of the temperature field in a laser ignition experiment wherein an ethylene-air mixture was heated by a high power laser, and the hot gas was illuminated with a collimated laser beam. To cross-check the results obtained from the shadowgraph experiments, the authors determined the temperature field under similar test conditions using Rayleigh light scattering and demonstrated a good agreement between the results obtained from these two approaches. Kosugi *et al.* [4] applied the schlieren technique to experimentally record gas temperature profiles in the shock region of excimer lasers and correlated them to the xenon concentration in helium gas. Muralidhar *et al.* [5] studied transient natural convection in a square cavity in the intermediate Rayleigh number range with air as the working fluid using a Mach-Zehnder interferometer. Chandrasekhara *et al.* [6] discussed a high-speed phase locked interferometry system designed and developed for real-time measurements of dynamic stall for flow over a pitching aerofoil. Zhong and Squires [7] used interferometry to evaluate organized structures in high-speed flow past a circular cylinder. The authors reported the similarities between compressible and incompressible wakes as well as similarities in the turbulent structures. Dupont *et al.* [8] discussed the use of electronic speckle interferometry for visualizing isotherms as well as streamlines in a Rayleigh-Benard configuration. Schopf *et al.* [9] adopted a shadowgraph approach for the study of convective flow in a water-filled square cavity which was differentially heated and cooled from the opposing vertical sidewalls. Tanda and Devia [10] performed a quantitative schlieren study of free convective heat transfer from heated plates and heat transfer from vertical parallel channels to the surrounding fluid. Howle *et al.* [11] carried out flow visualization of convective flow in a porous medium using the shadowgraph method. Agrawal *et al.* [12] described a color schlieren approach to temperature field measurements in gas jets using white light. Dezhong and Tiange [13] applied real time laser interferometric tomography for the measurement of three-dimensional temperature fields generated by two heated rods.

A review of the literature shows that laser measurement techniques that depend on refractive index changes in the fluid medium are regularly used in engineering research. Extension of these techniques to map three dimensional properties of the flow field and flow unsteadiness is to be seen in specialized applications.

2.2. Three-Dimensional Reconstruction of Density Fields

Recent literature on the application of refractive index based methods to the study of three-dimensional flow and thermal fields is presented here. Snyder and Hesselink [14] carried out instantaneous optical tomographic reconstruction of non-stationary fluid flow using holographic interferometry. The authors determined the spatial distribution of helium concentration in a co-flowing jet of helium in air. Watt and Vest [15] studied structures of turbulent helium jets in air by recording path integral images based on the refractive index

variation with a phase-shifted interferometer. Subsequently, the authors reconstructed the helium concentration field over the jet cross-section. Michael and Yang [16] discussed measurement of the three-dimensional temperature field in Rayleigh-Benard convection. The authors used a Mach-Zehnder interferometer, while reconstruction was performed using an iterative algebraic reconstruction technique. McMackin and Hugo [17] employed high-speed optical tomography system for imaging dynamic transparent media. The system was used to obtain spatially resolved high-speed cross-sectional temperature images of a round heated jet. Agrawal *et al.* [12] employed quantitative rainbow schlieren deflectometry with tomography for measurements of temperature in three-dimensional gas flows. The beam deflection data acquired from the schlieren images at multiple viewing angles were used to reconstruct refractive index data and temperature distributions with a modified convolution back projection (CBP) tomographic algorithm. Ko and Kihm [18] applied laser speckle photographic tomography to reconstruct the concentration field generated by asymmetric single and double helium jets in air. Mishra *et al.* [19] conducted an interferometric study of Rayleigh-Benard convection in air at intermediate Rayleigh numbers using tomography with limited projection data. More recently, Mishra *et al.* [20] carried out a detailed evaluation of iterative tomography algorithms for convection in a cylindrical cavity. The authors addressed the problem of handling incomplete and limited projection data that is frequently encountered in the engineering context.

In the above discussion, holography as a technique for determining the fluid density in three dimensions has not been included. In the opinion of the authors, laser imaging followed by tomography is a more convenient route for studying three dimensionality in flow and thermal fields.

2.3. Laser Imaging of Convection Around a Growing Crystal

Optical techniques have been employed to image the convective field around a growing crystal from its aqueous solution and quite a few studies have been reported. These experiments are described below in some detail.

In an early paper, Chen *et al.* [21] studied convection phenomena during the growth of sodium chlorate crystals from their aqueous solution using time-lapse schlieren cinematography. The authors addressed three major issues in their study: 1) Determination of conditions for transition from stable to unstable convection as a function of supersaturation of the solution and crystal size; 2) Characterization of plume width, its unsteadiness, and eddy frequency; 3) Effect of convection on the growth rate of the crystal. In addition, the authors studied the effect of mechanical shock on stable convection in the vicinity of the transition point to instability in an attempt to measure the strength of the convection currents. Grashof number based on solutal concentration was used to define the index of stability of the convective phenomena and an empirical relation was established between its critical value (at which transition from stable to unstable convective motion takes place) and the crystal height. The study also showed a good correlation between the strength of convection currents with plume characteristics such as its width and unsteady movement. Average growth rate of the crystal was measured by weighing as well as sizing the crystals before and after each experiment. The mass transfer rate was reported in terms of Sherwood number, a non-dimensional parameter. The authors also fitted an empirical relationship between Grashof

number and the average dimensionless concentration gradient at the growth interface of the crystal. In a separate study with sodium chlorate growing from its aqueous solution, Chen *et al.* [22] showed that with increasing supersaturation and horizontal crystal dimensions, the behavior of the convective plume changed from steady laminar flow to oscillatory flow with periodic shedding of eddies in the upward direction. The authors reported an improved correlation between Sherwood number and Rayleigh number. The latter is a parameter (like Grashof number) that governs the strength of buoyancy-induced convection currents in the growth chamber. The study showed that the growth rate was slightly higher when the convective plume was laminar than when it was irregular. The horizontal growth rate of the crystal was shown to be greater than the vertical growth rate, with the ratio tending to decrease with increasing plume instability.

In one of the earliest studies on protein crystals, Shlichta [23] reviewed the feasibility of using optical techniques for mapping convection, temperature and solute concentration in the solution around a growing protein crystal. Techniques considered were schlieren, interferometry and holography. In terms of sensitivity, the study showed that schlieren (based on the knife-edge principle) and interferometric techniques are marginally sensitive whereas phase-contrast schlieren, ultraviolet solute absorption, and laser Doppler anemometry are capable of mapping the velocity field in the crystal vicinity. In addition, author proposed an optical technique based on absorption-interferometry for simultaneous mapping of concentration and temperature in the solution around a growing crystal. Double-exposure holography and birefringence (measured as changes of the interference color of the crystal mounted between crossed polarizers) were shown to be suited for online measurement of growth rates of the protein crystal from its aqueous solution.

Bedarida [24] employed holographic interferometry (one beam and multi-directional) for the study of crystal growth from an aqueous solution. The mean value of the concentration field averaged over the width of the solution was obtained and the growth rates of the crystal faces were estimated. Three-dimensional information was derived from the multi-directional holographic technique by reconstructing solute concentration on planes parallel to the crystal face.

Bredikhin *et al.* [25] experimentally studied growth kinetics of KDP crystals growing from an aqueous solution in the free convection regime. Movement of the crystal faces with time was measured by a laser interference-polarization technique. The growth rates of the crystal faces in free convection regime were compared to those in forced convection (achieved by pumping solution in the growth chamber). It was shown that a significantly higher growth rate can be achieved in the forced convection regime. In addition, the authors also studied the effect of impurities such as Al^{3+} and Fe^{3+} on the crystal growth rate.

The role of buoyancy-driven convection was emphasized by Onuma *et al.* [26] in a case study of barium nitrate crystal growing from its aqueous solution. The authors employed schlieren technique and Mach-Zehnder interferometry for visualizing the convective field around the growing crystal. The effects of diffusion boundary layer and buoyancy driven convection upon the growth kinetics of crystals were investigated in relation to the bulk supersaturation of the solution. Schlieren technique using white light was used for qualitative observation of the growth process. An interferometer was used to measure quantitatively the gradient of the refractive index within the diffusion boundary layer. The authors classified convection patterns into three regimes: diffusion dominated, unstable movement of weak convective plume, and stable convection plume, depending upon the level of supersaturation

of the solution. The study demonstrated the effect of strength and orientation of buoyancy-driven convection currents on the growth rates of the individual faces of the crystal. The top face was seen to grow faster when the convection plume moved laterally and a higher growth rate of the side faces was observed in the presence of a stable convective plume. In a later work [27], the authors studied the effect of buoyancy-driven convection upon the surface morphologies (micro-topography) of different faces of $Ba(NO_3)_2$ and CdI_2 crystals. Schlieren technique was employed to visualize the buoyancy-driven convection currents. Onuma *et al.* [28] employed Mach-Zehnder interferometer for simultaneous measurements of the growth rate and surface super-saturation of K-alum crystals growing in an aqueous solution with varying flow velocities. The authors demonstrated that the two-dimensional profile of supersaturation levels varies significantly with flow velocity.

Bedarida *et al.* [29] illustrated the use of diffraction techniques based on the principle of phase measurements to study concentration and temperature gradients in aqueous solutions. As a case study, sodium chlorate crystals were used. The authors demonstrated that the technique is particularly useful for making local measurements in the solution over a small volume (whose dimensions are of the order of the wavelength of light) of the solution. In view of its simplicity and low electric power requirements the technique is useful for microgravity applications in outer space.

A Mach-Zehnder interferometer was also employed by Mantani *et al.* [30] for electronic measurement of concentration gradient around a KDP crystal growing from its aqueous solution. The authors established a linear relationship between the refractive index gradient and the growth rate of the crystal. Onuma *et al.* [31] constructed a microscopic Mach-Zehnder type real time phase shift interferometer for the measurement of concentration distribution around a growing or dissolving crystal in free convection regime. Sodium chlorate ($NaClO_3$) crystal was used to measure the surface concentration under different conditions of convection. It included relatively steady as well as fluctuating concentration fields. The study showed that the phase-shift interferometer has around 25 times higher sensitivity compared to the conventional two-beam interferometer. It also has higher time resolution to capture the fluctuations in the concentration field. Using Abel transformation, the authors obtained the actual surface concentration distribution of the growing crystal from the quasi-three-dimensional concentration profile. Sunagawa *et al.* [32] investigated transport phenomena during the growth and dissolution of barium nitrate ($Ba(NO_3)_2$), and K-alum crystals, their effects on the growth kinetics and degree of perfection of the grown crystals. The authors employed monochrome schlieren technique for visualizing convection as well as the diffusion boundary layer around growing and dissolving crystals. For quantitative measurements of concentration variation Mach-Zehnder interferometry was adopted. For *in-situ* observations of surface micro-topographic features and growth rate measurements of the growing crystal the authors used an optical microscope as well as a Michelson interferometer. The authors recommended the use of polarization microscope for *in-situ* identification of dislocation characteristics of individual growth hillocks (growth centers). The study emphasized the importance of solution flow in the growth chamber for achieving uniform supersaturation level over a wider surface area of the growing crystal by minimizing the effect of the buoyant plume.

Yu *et al.* [33] proposed holographic phase-contrast interferometric micro-topography (HPCIM), phase conjugation interferometry (PCI) and laser diffractometry as measurement techniques for studying real-time crystal growth and electrode processes. KDP was taken as

the sample material for conducting experiments. The authors demonstrated the use of the HPCIM technique for 1) quantitative measurements within the boundary-layer and interface patterns during the crystal growth process, 2) precise measurement of saturation for controlling supersaturation level of a given solution, and 3) studying phenomena taking place at the electrode-electrolyte interface. Phase conjugation interferometry (PCI) was recommended over the conventional Michelson interferometry for the characterization of surface morphology such as slope of the growth hillock and step heights of the growing crystal. For precise measurement of crystal growth rates, the authors proposed a laser diffraction metering technique (LDMT) for low-temperature solutions, high-temperature solutions and vapor-phase crystal growth processes.

Kleine *et al.* [34] carried out an experimental study of diffusion around a growing crystal from its aqueous solution using dark field-type schlieren microscope. The viability of the method was demonstrated by the *in situ* measurement of concentration distribution in the diffusion field around silver dendrites. The dendrites were growing from an aqueous $AgNO_3$ solution by electrolysis. The microscope enabled the calculation of solute iso-concentration lines around the growing crystals. The technique was shown to be rugged and relatively insensitive to vibrations compared to interference techniques. The drawback related to the fact that the gradients in concentration along x and y directions could not be simultaneously recorded. Hence it was not suitable for applications in rapidly changing and complex diffusion fields. Kransinski [35] conducted experiments to study the evolution of the diffusion field around a KDP crystal growing in gel. The optical technique employed for visualization of concentration distribution in gel was speckle interferometry. The linear kinetic coefficient for the KDP crystal growing in gel was calculated from the shape of concentration profiles and its value was shown to be significantly lower than that obtained in the case of solution growth. The author compared the results with the simulation based on the one-dimensional diffusion model. Bredikhin *et al.* [36] proposed a technique based on the optical schlieren method for *in situ* investigation of the morphology of a large growing KDP crystal (8×8 cm^2 cross-section) under rapid growth conditions and for monitoring the crystal growth process to provide quality control. The surface morphology of the crystal was characterized in terms of inclination angles of growth hillocks (measured with a sensitivity of 2' using the proposed technique) on the crystal surface. The authors showed that when the growth rate of the crystal exceeds an optimal value, a wavy structure appears on the crystal surface. The waviness can lead to the origin of micro-inclusions and formation of inter-layers in the crystal. The proposed optical technique was shown to be useful towards controlling the morphology of the growing face by optimizing experimental conditions.

Inoue *et al.* [37] studied the effect of supersaturation and super cooling of the aqueous solution on the growth faces of $Na_2S_2O_3.5H_2O$ crystals. The authors employed the schlieren method and the Mach-Zehnder interferometer for *in situ* observation of the formation process of spherulites. It was shown that the growth shapes changed from prismatic (normal growth) to spherulite (abnormal growth) with an increase of supersaturation level of the solution. Piano *et al.* [38] demonstrated the use of electronic speckle interferometry (ESPI) for investigating convective phenomena around a growing KDP crystal. It was used for the measurement of concentration gradients as well as growth velocities of the crystal faces. The authors showed the potential of the technique for studying diffusion phenomena by capturing the refractive index gradients at the sugar-water interface in a solution of sugar in water. In a separate study [39], the authors performed dissolution and growth experiments for KDP

crystals and observed convection using electronic speckle interferometry. The authors showed the presence of three regions of different densities around the dissolving/growing crystal that were independent of the geometry of the cell. The potential of ESPI was also demonstrated for calculating the temporal and spatial distribution of the solute concentration around the growing crystal.

Duan and Shu [40] applied phase shift interferometry for the study of the kinetics of sodium chlorate ($NaClO_3$) crystals. Both crystallization and dissolution phase of the crystal in its aqueous solution were considered. The optical technique was employed to visualize the convective plume in the crystal vicinity and for *in situ* measurement of the distribution of refractive index gradient. The sensitivity of the optical diagnostic system was shown to be higher than that of the conventional two-beam interferometry. In addition to the visualization of convective phenomena, the potential of phase-shifting interferometry for *in situ* imaging and characterization of interfacial morphology of a growing KDP crystal was demonstrated by Booth *et al*. [41]. The method was applied to monitor the (101) face of the crystal growing from its aqueous solution. The formation and evolution of solution-flow induced step bunches were imaged using the optical technique. In a separate application of real-time phase-shifting interferometry, Maruyama *et al.* [42] observed transient double diffusion fields around a rapidly growing sodium chlorate crystal from its aqueous solution. A two-dimensional transient numerical code was also developed to simulate the diffusion field around the crystal and an accurate measurement of solutal gradients in the crystal vicinity was carried out using the computer code. The authors estimated the growth rate of the crystal by combining experimental data with results of numerical simulation. Bredikhin *et al.* [43] employed the schlieren method with some improvements (over the set up as used in [36]) to achieve a higher optical resolution. Competing growth centers and step bunching in KDP crystal growth from its aqueous solution were investigated. The study focused on the morphology of (100) and (101) crystal faces when fed by impingement controlled solution flow. Schlieren observations showed that the brightness difference between the neighboring slopes of the hillocks is proportional to the angle between them and hence can be used as the basis for characterizing the surface morphology of the growing crystal face. The authors concluded that the mechanisms of step bunching and competition between growth centers are essential for good crystal quality. They are quite affected by the solution flow. When the flow is weak, multi-center growth occurs and an increase in flow intensity results in single-center growth of the crystal face.

In a recent study, Srivastava *et al.* [44] compared interferometry, schlieren and shadowgraph for studying buoyancy-driven convection patterns around a growing KDP crystal from its aqueous solution. While the spatial distribution of concentration differences in the vicinity of the crystal was revealed by all the techniques, it was concluded that the laser schlieren technique is best suited for process control. The basis of this observation was ease of instrumentation, image clarity and simplicity of data analysis. The study also brought out the limitation of free convection crystal growth experiments in the form of density stratification around the growing crystal. In a subsequent work [45], the authors studied the effect of ramp rate and crystal rotation on the convective field around a growing KDP crystal. Laser schlieren technique was employed as a diagnostic optical tool to map the concentration field around the crystal. It was shown that buoyancy-driven convection intensifies with increasing ramp rate as well as with increasing size of the crystal. Rotation tends to diminish the concentration gradients and improves the symmetry and uniformity of concentration

distribution over the crystal faces. The findings of [44] and [45] are discussed at length in Section 9 of this article.

2.3.1. Protein Crystals

Optical techniques are presently being applied for visualization and control of buoyancy-driven convection in the growth of protein crystals. Convection currents have an adverse impact on the quality of the growing protein crystals. Steps have to be taken to suppress the buoyancy-induced flow during the growth process. Miyashita *et al.* [46] made use of a two-beam Michelson interferometer for *in situ* observation of solute concentration distribution around a growing lysozyme crystal from its aqueous solution. From the experimentally recorded interferograms, concentration profiles around the crystal, growth rates and diffusion coefficient of the lysozyme molecules were estimated. Vekilov and Rosenberger [47] experimentally studied the effect of solution flow on the growth kinetics and interface morphology of protein lysozyme crystals growing from their aqueous solution using laser interferometry. The authors showed that continuous circulation of the solution at an optimum rate provides an alternative to microgravity. Higher kinetic stability for the solute transport is achieved that in turn results in higher crystal quality. Hou *et al.* [48] employed the two-beam Michelson interferometer to visualize concentration gradient layers around tetragonal lysozyme crystals growing from gel. Gel was used as a solvent in order to suppress convection and mimic the microgravity environment. The surface concentration properties (its width and gradients) around the crystal as measured in gel were found to be noticeably different from that measured in an aqueous solution. In particular, concentration gradients were wider and transport rates were slower for gel-grown protein crystals. Yin *et al.* [49] reported an interferometric study of concentration measurement in a protein solution under the influence of a strong magnetic field. The growth process of tetragonal crystal of lysozyme was investigated using a Mach-Zehnder interferometer. The study showed that the crystal growth process under the influence of a magnetic field was slower when compared to that without a magnetic field. However, there was no significant effect of varying the magnitude of the magnetic field on the buoyancy-driven convection currents in the lysozyme solution. Sazaki *et al.* [50] employed two-beam Michelson interferometry for determining the solubility curve of protein lysozyme crystals. The equilibrium temperature of the crystals in solution was estimated on the basis of the bending of interference fringes at a given protein concentration. The study showed that the technique is insensitive to the impurities in the solution. It is comparatively less time consuming while compared to other conventional methods used for solubility measurements. Kawaji *et al.* [51] employed two different techniques, namely, photo chromic dye activation and particle tracking velocimetry, for investigating the occurrence of Marangoni and natural convection during the growth of lysozyme protein crystals. Marangoni convection is related to gradients in the interfacial tension, while natural convection arises from density gradients in the bulk of the solution. The visualization technique of the authors made use of a photo chromic dye material with a UV light absorption spectrum that changes its molecular structure upon UV light irradiation. The photo chromic reaction changes the liquid from clear to visible colors, resulting in the formation of visible dye traces. The velocity of the liquid containing the photo chromic dye can be obtained from the displacement of the dye traces over a given interval of time. In particle tracking velocimetry, small tracer particles are dispersed in the fluid and are illuminated with a visible laser light sheet. Flow velocities can be estimated by determining

the displacement of the tracer particles with time. The fluid velocity estimates made by the two techniques indicated that the protein crystal growing from an aqueous solution is highly resistant to Marangoni convection. Ramachandran and Leslie [52] have recently shown that magnetic fields may be useful in mimicking the microgravity environment of space and can be employed for controlling the strength of convection currents during the growth of protein crystals. The authors analyzed the physical phenomena using a mathematical model and validated the results against the experimental observations.

The survey of articles above clearly shows that the importance of fluid convection in crystal growth from an aqueous solution is well-recognized. The use of laser measurement techniques is also found to most suitable for monitoring convection when the growth process is in progress.

2.4. Reconstruction of Three Dimensional Concentration Field Around a Growing Crystal

The use of tomography for the measurement of three-dimensional concentration field around the growing crystal has found limited application in the area of crystal growth. Gatti *et al.* [53] carried out three-dimensional measurements of concentration field using multidirectional holographic interferometry. The authors proposed a mathematical technique for interferometric data processing. The concentration field was reconstructed from the projection data using a numerical algorithm that was based on the "sinc" method developed earlier by Sweeny and Vest [54]. The projections were collected over a limited range of view angles. Notcovich *et al.* [55] investigated the three-dimensional temperature field around heavy ice (D_2O) growing from super cooled heavy water using interference tomography. Heavy water was used for the experiments since dn/dT, the variation of refractive index of normal water with temperature is small (with a maximum in refractive index at 4^oC). Heavy water has a maximum value of refractive index at 7^oC. In addition the authors also measured the two-dimensional concentration field around sodium chloride (NH_4Cl) crystals growing from a supersaturated solution in water. The authors explained the morphological transition of the crystal faces at high growth velocities. In a recent study [56], the authors of the present article have investigated the three-dimensional concentration field around a KDP crystal growing from its aqueous solution using a laser schlieren technique. Growth experiments were conducted in the diffusion as well as convection-dominated regime. Convolution back projection (CBP) tomography algorithm was employed for the reconstruction of the concentration field in the planes above the growing crystal. The study revealed symmetry of the flow field away from the crystal in the convective regime of the growth process. However, the concentration distribution was seen to be unsymmetrical during transition from the diffusion regime towards the establishment of a stable convective plume. This study is described in detail in Section 9.3.

Despite the availability of considerably large amount of literature on the application of optical techniques to investigate the crystal growth processes, the nature of convection and its relationship to solute distribution, crystal growth rates and quality has not been fully understood. The effects of process parameters such as level of supersaturation of the solution, cooling rate, and rotation of the growing crystal on quality and growth rates has not been studied. Optical techniques have predominantly served as the visualization tools to study the

growth kinetics and surface morphologies of the crystals growing from their aqueous solutions. The application of tomography based on optical imaging of a variable refractive index field to investigate the three-dimensional nature of convection currents and its effects on the solute distribution around the growing crystal is yet to be fully explored.

3. OBJECTIVES OF THE PRESENT WORK

The importance of convection in determining crystal growth rates and crystal quality has been recognized by a variety of authors. Over the past decade, laser measurement techniques have become popular, though primarily as a flow visualization tool. Recent papers, however, have emphasized the possibility of quantitative measurements using optical methods. Against this background, results are discussed in the present article in the following sequence:

1. **Convection in a rectangular cavity.** The literature on refractive index based methods shows that of the three methods, interferometry has been predominantly applied for qualitative as well as quantitative analysis of the thermal fields in buoyancy-driven convection. Schlieren finds potential applications towards qualitative visualization of the flow field and to a limited extent, it has been applied for quantitative studies. Shadowgraph has been extensively used for qualitative imaging. The three techniques, however, have not been jointly compared against a benchmark experimental configuration. The present work compares interferometry, schlieren and shadowgraph techniques for the measurement of temperature distribution in buoyancy-driven convection in a rectangular cavity. The top and bottom walls of the cavity are maintained at uniform temperatures at all times in an unstably stratified configuration. Fluid media considered are air and water. Temperature differences of 5-50 K for air and 3-10 K for water have been employed in the experiments. Over the range of temperature differences considered, flow was seen to become progressively unsteady, finally becoming turbulent.
2. **Comparison of optical techniques for a crystal growing from its aqueous solution.** Interferometry, schlieren and shadowgraph are employed to visualize the convection field around a growing KDP crystal from its aqueous solution. Experiments have been conducted under practically identical conditions. The goal of the study is to explore the suitability of these measurement techniques to image, analyze and interpret the convective field around a growing crystal.
3. **Schlieren study of convection around a crystal driven by buoyancy and rotation.** The specific goals here are to understand (a) changes in convection pattern at various stages of the crystal growth process, (b) role of convection in creating regions of high/low concentration gradients, (c) possibility of controlling the size of these regions by providing crystal rotation, and (d) to demonstrate the suitability of the schlieren technique for quantitative mapping of solutal concentration around the growing crystal. The process parameters studied are cooling rate of the solution and rotation rate of the growing crystal. Crystal rotation is viewed in this study as a means of diminishing the impact of buoyancy. The crystal size plays an influential role in determining the relative importance of buoyancy and rotation. An independent

study of crystal size has also been presented. Schlieren images have been analyzed to correlate the strength of convection currents with the concentration field and its gradients. The crystal quality has been gauged by examining the transparency of the crystal at the end of the experiment.

4. **Three dimensional concentration contours around a growing crystal.** Laser schlieren technique is employed to investigate the three-dimensional concentration field around a KDP crystal growing from its aqueous solution. The convective field is set-up in the growth chamber by inserting a KDP seed into its supersaturated solution followed by slow cooling of the solution. The projection data in the form of two-dimensional schlieren images have been recorded from four different view angles (0, 45, 90, and 135^{o}) by turning the crystal growth chamber. Since a circular growth chamber is employed in the present experiments, the entire width of the growth chamber for a given view angle could not be covered. Hence a single view provides only partial data, corresponding to the area localized in the vicinity of the growing crystal. The integrated values of concentration are obtained by analyzing the light intensity data of the schlieren images. Subsequently, the concentration fields at various horizontal planes above the crystal are reconstructed using the convolution back projection (CBP) algorithm. Owing to limitations in the optical system, the projection data required for tomographic inversion is often incomplete. Specifically, the number of view angles is small, and in addition, the entire field of view may not be scanned. The applicability of the inversion algorithms can then be ensured only when additional tests are conducted to validate the result obtained. Validation with numerically simulated data is reported in this work. The focus of the present study is to examine the symmetry of the concentration field in the vicinity of the growing crystal in the initial stages (diffusion-dominated growth) and in the stable growth regime (recognized by the presence of a steady convective plume rising from the crystal surface). Of interest is the relationship between the morphology of the crystal with the solutal concentration field around it, during the growth process.

The text is organized as follows. Sections 4.1-4.3 describe the apparatus employed in experiments, while Section 4.4 explains the experimental procedure. Sections 5.1-5.4 discuss interferometry, schlieren and shadowgraph individually in terms of the optical layout, principle of operation and data analysis. Section 6 presents a discussion on measurement errors and uncertainty. Sections 7.1-7.3 present principles of tomography, the CBP algorithm, extrapolation techniques for partial data and a validation study against a numerically simulated convection pattern. Section 8 provides detailed results of convection in a rectangular cavity using the three refractive-index techniques. Section 9 shows in greater detail the convection patterns, interaction of buoyancy and rotation, relationship between growth rates and concentration gradients, and preliminary results obtained from tomographic inversion of the schlieren data.

4. EXPERIMENTAL DETAILS

The apparatus used for experiments of the present study are described in the following sections. In experimental procedure followed for growth of KDP crystals is also discussed.

4.1. Convection in a Rectangular Cavity

Experiments are reported for studying fluid convection in a rectangular cavity. The temperature difference maintained across the horizontal surfaces of the cavity leads to unstable density gradients in the fluid medium. In turn, fluid motion in the form of closed loops is initiated in the cavity. The configuration studied, called Rayleigh-Benard convection is a problem of fundamental as well as practical importance. The flow patterns associated with Rayleigh-Benard convection show a sequence of transitions, leading from steady laminar to unsteady turbulent flow. The strength of convection is quantified by the Rayleigh number, a dimensionless parameter. [For a definition, see Nomenclature.] The Rayleigh number is a measure of the ratio of energy released in the buoyancy field to that lost by viscous dissipation. The values realized in the present experiments are quite large in comparison to the critical Rayleigh number of 1707 reported for a horizontal differentially heated infinite fluid layer at the onset of convection (Gebhart *et al.* [2]).

The apparatus used to study the buoyancy-driven convection in a horizontal fluid layer is shown schematically in Figure 2. The cavity is 447 mm long with a square cross-section of edge 32 mm. The test cell consists of three sections namely the top plate, the fluid layer enclosed in a cavity and the bottom plate. The top and bottom walls of the cavity were made of 3 mm thick aluminum plates. The flatness of these plates was manufacturer-specified to be within ±0.1 mm and was further improved during the fabrication of the apparatus. The central portion of the experimental apparatus is the test section containing the fluid medium. The side walls of the cavity were made of a 10 mm Plexiglas sheet. In turn the Plexiglas sheet was tightly wrapped with thick bakelite padding in order to insulate the test section with respect to the atmosphere. The height of the test section was 32 mm and was measured to be uniform to within ±0.1 mm. A window was provided in the direction of propagation of the laser beam. It was held parallel to the longest dimension of the cavity for recording the projected convective field in the form of two-dimensional images. The apparatus was enclosed in a larger chamber made of thermocole to minimize the influence of external temperature variations. The room temperature during the experiments was a constant to better than $\pm 0.5^{o}$C over a 10-12 hour period. Experiments were initiated by flowing water over the hot and cold surfaces respectively. After the start of the experiments, the surfaces reached a steady state within a few minutes. The thermal fields in air evolved over a longer period of time and stabilized over 5-6 hours. In water, dynamically steady patterns were realized in 1-2 hours. The thermally active surfaces were maintained at uniform temperatures by circulating a large volume of water over them from constant temperature baths. Temperature control of the baths was rated as $\pm 0.01^{o}$C; at the cavity location, direct measurements with a multi-channel temperature recorder showed a spatial variation of less than $\pm 0.1^{o}$C. For the upper plate, a tank-like construction enabled extended contact between the flowing water and the aluminum surface. Special arrangements were required to maintain good contact between water and the

lower surface of the plate. Aluminum baffles introduced a tortuous path to flow, thus increasing the effective interfacial contact area.

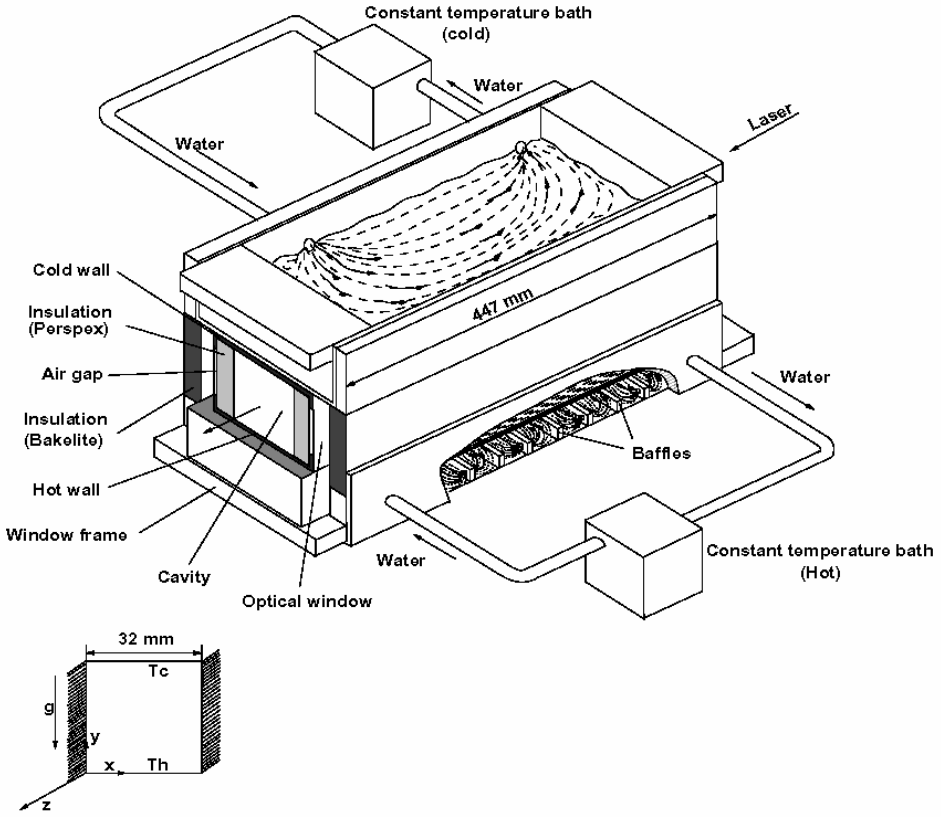

Figure 2. Schematic drawing of the rectangular cavity experimental set up

For air, the temperature differences applied across the cavity walls were in the range of 5-50 K. These correspond to Rayleigh numbers of 14×10^3 to 14×10^4. In experiments with water, the temperature differences applied were in the range of 3-13 K. These correspond to Rayleigh numbers of 25×10^5 to 13.5×10^6 respectively. The Rayleigh numbers realized in the experiments can be seen to be quite large in comparison to the critical value of 1707, indicating the presence of strong fluid motion in the cavity.

4.2. Convection Around a Growing Crystal

The apparatus in which experiments have been conducted on convection around a crystal in a top-hanging arrangement is discussed. The apparatus in which the crystal is held over a platform is described in Section 4.3.

Experiments that compare images of convection around the crystal recorded by interferometry, schlieren, and shadowgraph have been conducted in a growth chamber made of glass (17 cm diameter and 22 cm height) as shown in Figure 3. Glass used for the

experimental chamber has the advantage of being a smooth surface on which unwanted nucleation cannot take place. In addition, glass is chemically non-reactive towards the KDP solution. The crystal growth chamber is in turn, placed in a Plexiglas tank. Temperature of the solution inside the growth chamber is maintained at prescribed levels by thermostatically controlled water circulating in the outer tank. The temperature of water is stabilized in the outer tank to within $\pm$ 0.1^{o}C with the help of a programmable temperature controller (*Eurotherm*). A K-type thermocouple wire fixed to the outer surface of the growth chamber provides the feedback to the controller. With this arrangement, ramp rates could be applied to cool the solution over long periods of time. For example, a linear change in temperature of the solution from 25 to 36^{o}C over a period of 60 hours was closely realized in the present set of experiments. Sufficient insulation is provided on the outer surface of the entire assembly to reduce thermal interaction between the growth cell and the ambient.

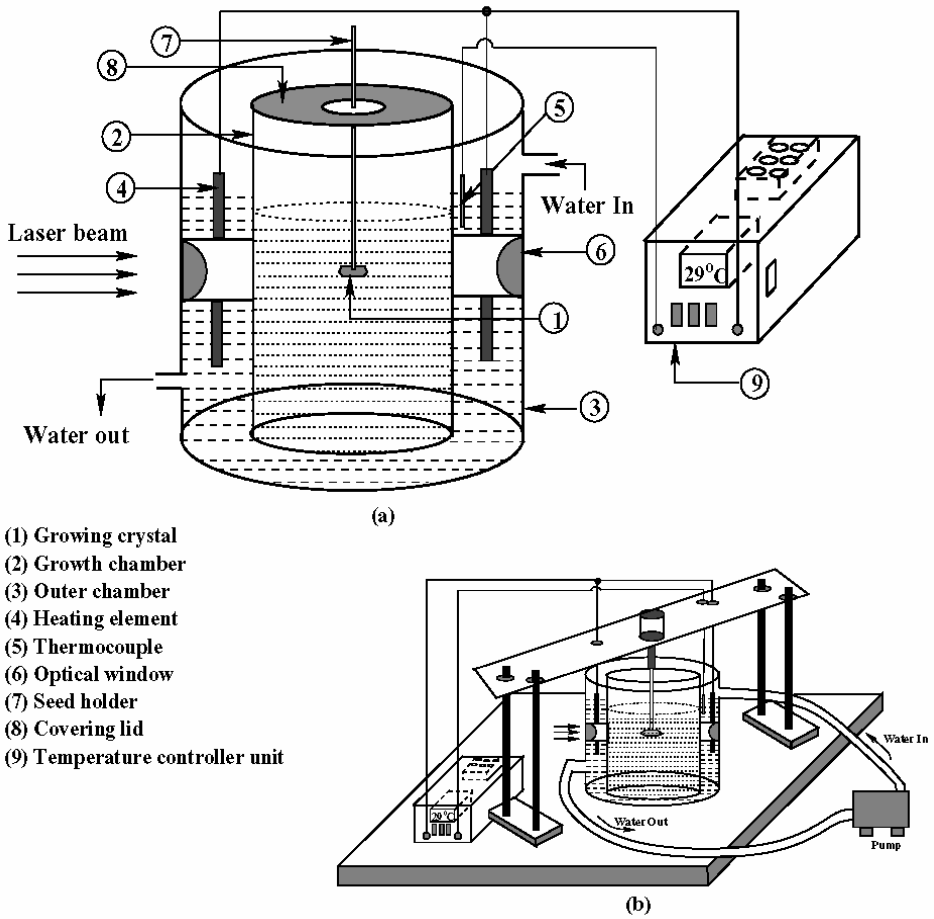

Figure 3. (a) Schematic diagram of the crystal growth chamber, and (b) complete assembly

For visualization of the concentration field by the schlieren technique, circular optical windows (*Stranda*, BK-7, 60 mm diameter, 5 mm thickness, λ/4 flatness) have been fixed on the walls of the growth chamber at opposite ends. The growth process is initiated by

introducing into the growth cell a spontaneously crystallized seed crystal fixed at one end of a thin glass rod. The glass rod (diameter 3 mm) is small enough not to disturb the convection plume rising above the crystal. Rotation to the growing crystal is imparted with the help of a stepper motor (12V, 0.6A, *RS components)*.

For experiments employing interferometry, a double-walled compensation chamber is placed in the path of the reference beam. In order to ensure identical conditions in terms of the undisturbed optical path length, the volumetric capacities of the compensation chamber and growth chamber are kept equal. The inner cell of the compensation chamber contains the KDP solution that has a salt concentration corresponding to saturation conditions at the ambient temperature of 25^oC. In the growth process, the temperature range utilized is 25^oC-36^oC, and no deposition was seen in the experiments anywhere in the cell. The solution in the test section and the compensation chamber are at practically identical temperatures through out the duration of the experiment. This is accomplished by splitting the outlet of the water-circulating pump into two parts, one leading to the growth chamber and the other to the compensation chamber. In the absence of a crystal, the optical path lengths in the test and the compensation chamber could be balanced during the cooling of the solution. Consequently, there was no fringe formation (in the infinite fringe setting mode) and fringe deformation (in the wedge fringe setting mode) from either thermal disturbances or those related to small differences in concentration. Fringe formation in the presence of the crystal occurred due to salt concentration differences in the solution with respect to the average value in the compensation chamber.

In the present set of experiments, the growth of the seed crystal is initiated by slow cooling of the supersaturated solution. Two values of ramp rates have been employed: 0.05^oC/hour and 0.1^oC/hour. The rate at which the solution is cooled plays an important role in controlling the strength of convection currents, and hence the growth rates and crystal quality. Low rates keep the degree of supersaturation to a small value. The growth process is then diffusion-dominated and is inefficient in terms of the size of the crystal grown. On the other hand, very high values of the ramp rate give rise to vigorous convection currents resulting into deterioration of the crystal quality. At intermediate cooling rates, high crystal quality is to be expected.

Stirring the solution reduces the natural convection-induced temperature oscillations by homogenizing the bulk solution. Hence the importance of optimum rates of rotation in crystal growth processes has gained recognition. The two most widely used stirring mechanisms are the rotation of the seed and/or the rotation of the crucible. In the present work, experiments have been conducted by continuously rotating the growing crystal at 15 rpm.

4.3. Crystal Growth Chamber for Tomographic Projections

Tomographic projection data are recorded by viewing the convection pattern at various angles over the range of 0 to 180^o. If the pattern is strictly steady, projections can be recorded by turning the crystal through small incremental angles. This approach has the drawback of creating unsteadiness in the flow field. Results obtained by turning the crystal have been discussed in the context of validating the tomographic algorithm with measured data. An appropriate technique is to keep the growth chamber fixed and turn the axis of the source-detector system. This route could not be followed in the present study owing to the physical

size of the laser, CCD camera and the accompanying optical components. Instead, the growth chamber along with the crystal was turned through definite angles to image the concentration field. The curvature of the beaker led to ray-bending problems and prevented scanning of its entire width. The portion of the solution visible through optical windows alone has been used for measurement. Unlike the top-hanging arrangement of Section 4.2 (where the supporting rod disturbed the convective plumes), experiments have been conducted here using a crystal mounted above a platform.

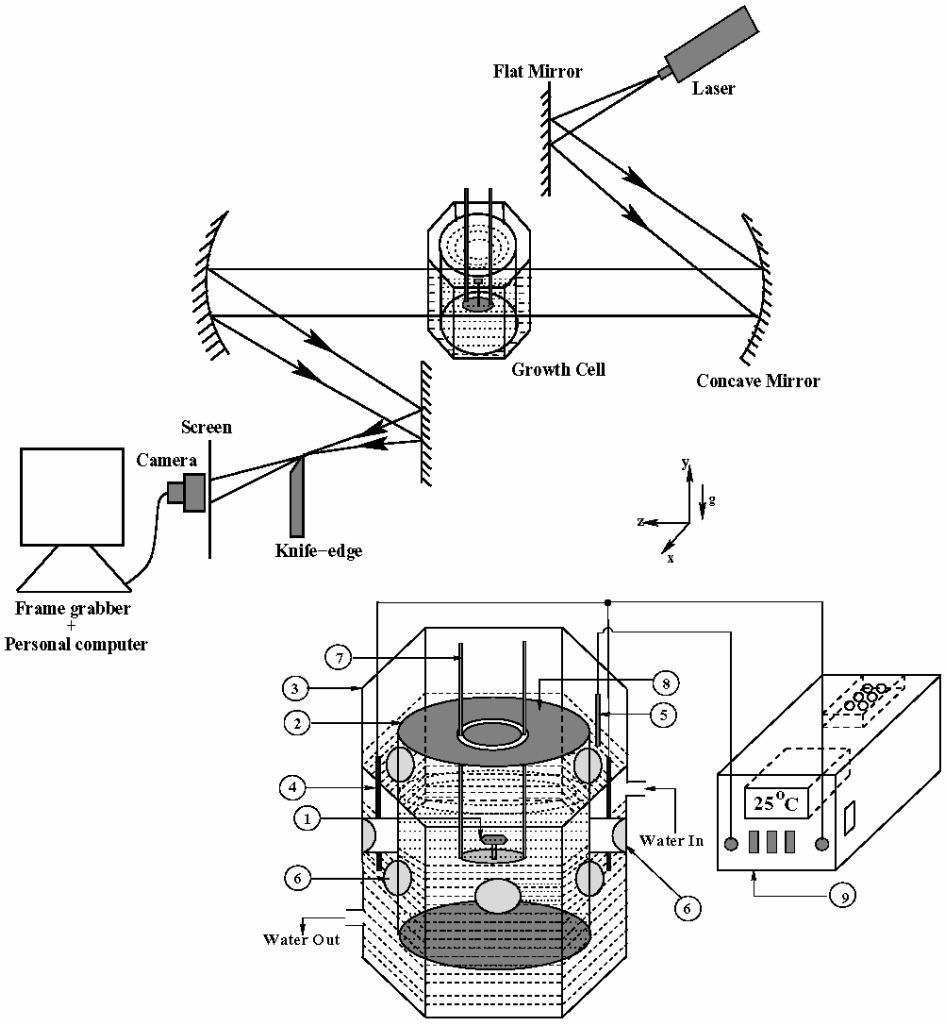

Figure 4. Schematic diagram of the four-view crystal growth chamber placed in the path of the laser beam in a *Z*-type schlieren set up. (1) Growing crystal on a platform, (2) Growth chamber, (3) Outer chamber, (4) Heating element, (5) Thermocouple, (6) Optical window, (7) Seed holder (platform configuration), (8) Covering lid, (9) Temperature controller unit.

The crystal growth chamber used in the present experiment is shown schematically in Figure 4. It comprises of a glass chamber that holds the KDP solution, has a diameter of 16.5 cm with a height of 23 cm. For visualization of the concentration field by the schlieren technique, circular optical windows (BK-7, 40 mm diameter, 5 mm thickness, $\lambda/4$) are fixed

on the glass beaker at opposite ends. A total of eight such windows permit passage of the laser beam for four view angles. Parallelism and straightness of the optical windows are crucial for generating meaningful images, and considerable precautions have been taken in this regard. The Plexiglas tank surrounding the growth chamber is octagonal in plan. It ensures large enough volume for the circulating water to keep the KDP solution at the required temperature level over a considerable period of time. Four heating elements placed diametrically opposite in the outer chamber maintain the temperature of circulating water, and hence the KDP solution. Electrical input to the heating elements is regulated by a programmable temperature controller (*Eurotherm*). As in the apparatus discussed in Section 4.2, a K-type thermocouple wire fixed to the outer surface of the growth chamber provides the feedback to the controller. Uniformity of temperature within the solution is ascertained by recording temperatures at various locations using 26 gage K-type thermocouples. With this arrangement, it was possible to reduce the temperature of the solution from 36 to 25^{o}C linearly with time over a time frame of 60 hours.

The salt-solution has an initial temperature that is high enough to keep it from becoming fully saturated. A KDP seed crystal spontaneously crystallized in a second vessel is placed on a glass platform and introduced in the growth cell. When the bulk temperature is lowered, the solution becomes super-saturated with salt that in turn deposits on the crystal. The solution adjacent to the crystal is now close to being saturated with the dissolved salt. A crystal growing from its aqueous solution thus creates a three-dimensional solute distribution in its vicinity. The solutal concentration gradients and the accompanying gradients in density of the solution are responsible for the appearance and evolution of buoyancy-driven convection currents in the growth chamber.

4.4. Experimental Procedure

The crystal growth experiments were performed in the following manner. A supersaturated solution of KDP powder is prepared in distilled, de-ionized water. The amount of KDP salt to be dissolved is determined from its solubility curve [57] at an average temperature of 35^{o}C. The solution is stirred long enough to ensure complete dissolution of the solute. It is filtered using Whatman-100 filter paper to remove residual microscopic particles. The solution is maintained at relatively high temperature for about 4-5 hours using water circulation from the temperature control unit. Subsequently, the solution is cooled by applying a suitable ramp rate, 0.1^{o}C/hour in the present study. When the solution reaches a value right enough for it to become saturated, a KDP seed is introduced into the solution using a thin glass rod. The orientation of the seed crystal is adjusted in such a way that the prismatic faces ({100}) are placed normal to the direction of the laser beam. Experiments are allowed to run for a considerably longer duration of time (≈60 hours) in order to allow the growth of large crystals. Precautions are taken to avoid external disturbances and vibrations that may introduce unsteadiness in the flow field. For the experiments discussed below, the crystal size increased from 0.3 cm^3 to 3 cm^3 in 60 hours, while preserving high crystal transparency.

5. LASER MEASUREMENT TECHNIQUES AND DATA ANALYSIS

The optical configurations for interferometry, schlieren and shadowgraph as well as data retrieval from optical images are discussed in the following sections (see Goldstein [58] and Settles [59] for a longer discussion.).

5.1. Optical Arrangement

For measurements, a continuous wave helium-neon laser (Spectra Physics, 35 mW) has been used as the coherent light source. A monochrome CCD camera (*Sony*, Model: XC-ST50) of spatial resolution of 768×574 pixels was used to record the convective field. The camera was interfaced with a personal computer (HCL, 256 MB RAM, 866 MHz) through an 8-bit A/D card. Interferograms, schlieren and shadowgraph images presented in this work have been subjected to image processing operations to improve contrast; the data analysis for recovering the field concentration is, however, based on the intensity changes in the original images.

The layout for each of the three imaging techniques used in the present work is shown in Figure 5. The Mach-Zehnder interferometer used in the present study is shown in Figure 5(a), and has been described earlier by Mishra *et al.* [19,60]. It has two mirrors and two 50% beam splitters of 150 mm diameter. The mirrors are coated with 99.9% silver and employ a silicon dioxide layer as a protective layer. The interferometer floats on pneumatic legs to isolate the optics from external vibrations. Experiments have been carried out in the infinite as well as the wedge fringe setting [58]. In the infinite fringe setting, the optical path difference between the test and the reference beams is initially zero. When a density disturbance is introduced in the path of the test beam, it is seen as a set of fringes over which the depth-averaged concentration field is a constant. In the wedge fringe setting, the optics is slightly misaligned to produce a set of straight fringes. When exposed to a thermal or concentration field, the fringes are displaced to an extent depending on the change in temperature or concentration. The fringes in the wedge fringe setting of the interferometer are thus representative of the temperature variation in the rectangular cavity and concentration profile in the crystal growth chamber. In the present study, the infinite fringe setting initially produced an image of uniform brightness indicating true constructive interference between the test and the reference beams. In the wedge fringe setting, the fringes were seen to be straight and horizontal.

The schlieren system used in the present work is of the ***Z***-type, as shown in Figure 5(b). The optics includes concave mirrors of 1.30 m focal length and 200 mm diameter. Relatively large focal lengths make the schlieren technique sensitive to the concentration gradients [58-59]. The knife-edge is placed at the focal length of the second concave mirror. It is positioned to cut off a part of the light focused on it, so that in the absence of any optical disturbance, the illumination on the screen is uniformly reduced. The initial intensity values in the experiment were chosen to be less than 20, on a gray scale of 0-255. The knife-edge is set perpendicular to the direction in which the density gradients are to be recorded. In the present study, the gradients are expected to be predominantly in the vertical direction of gravity, and the knife-edge has been kept horizontal.

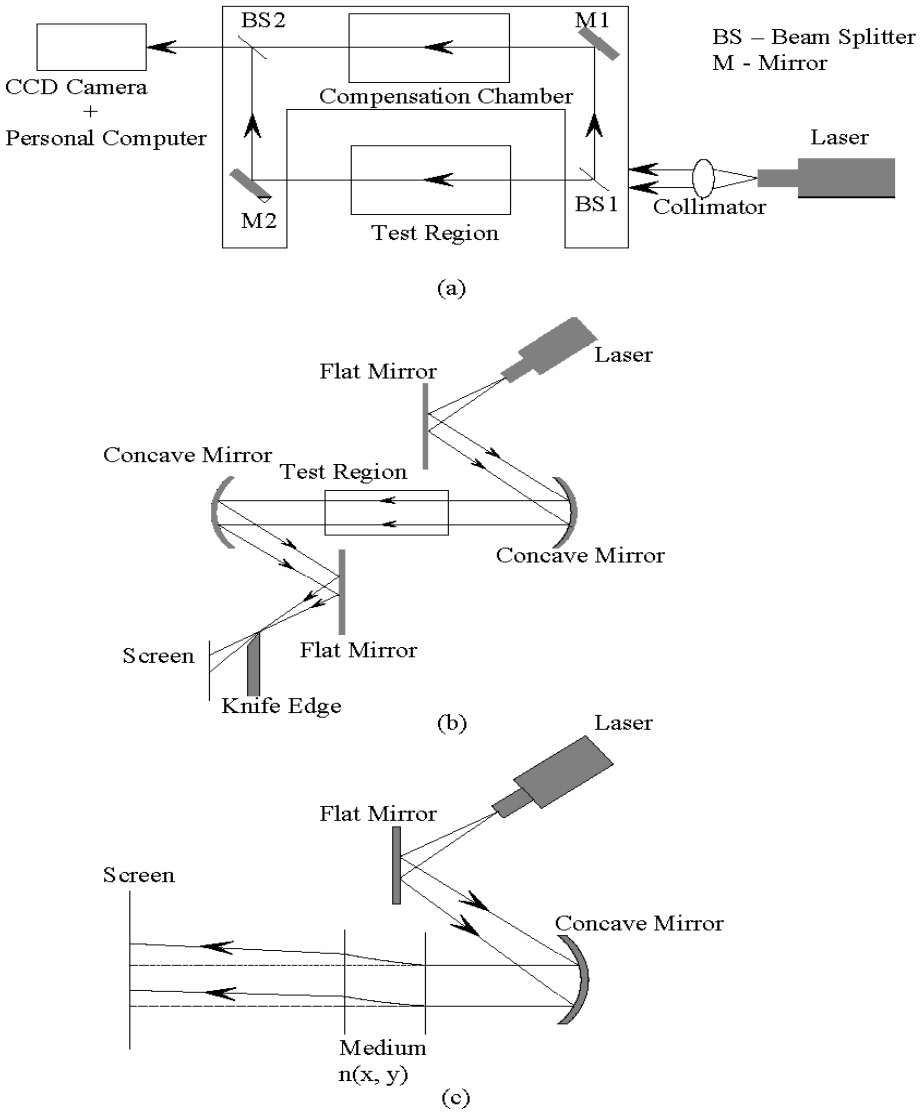

Figure 5. Optical layout of a (a) Mach-Zehnder interferometer, (b) Schlieren and (c) Shadowgraph.

Shadowgraph images have been recorded using the same optical components as employed in the interferometry setup by first blocking the reference beam and allowing the test beam alone to fall on the screen (Figure 5(c)). Shadowgraph images have also been recorded from the schlieren apparatus by collecting the refracted light beam emerging from the test cell. The position of the screen on which the shadowgraph images are displayed plays an important role in data analysis [9, 58]. The screen position is chosen so as to improve the image contrast, while extracting the dominant features of the flow field. Beam refraction from regions of high concentration gradients can interfere with those passing through one of nearly constant concentration. This factor is taken into account while fixing the camera position. The initial intensity distribution in shadowgraph experiments before inserting the seed corresponds to the Gaussian intensity variation of the laser source itself.

5.2. Image Processing

The three optical methods generate images that are path integrals of the refractive index fields and in turn, the concentration (or temperature) distribution in the fluid medium. The integrals can be simplified if the fields being studied are strictly two-dimensional. In general, the local information can be extracted using principles of tomography [61-62]. In the present work, the images have been interpreted as carrying information of the solutal concentration (or thermal) field that is an average along the direction of propagation of light.

The determination of the concentration/temperature field from interferograms requires several intermediate steps, including (a) noise removal, (b) edge detection, (c) location of intensity minima within fringe bands, and (d) fringe thinning. Step (d) involves fitting a smooth function through points of intensity minima within a single fringe, as obtained in step (c). In addition, assigning temperatures to fringes, followed by transferring the data to a Cartesian grid are important. The fact that fringe thickness is small in regions of high concentration or temperature gradients has not been used in the present work. The analysis and interpretation of fringe patterns in interferometry has been discussed in detail by various authors [63, 64]. The approach described in [64] has been implemented in the present study.

In contrast to interferometry where information is localized at the fringes, a schlieren image carries information related to the local temperature/concentration in the form of an intensity distribution. The advantage here is that data is available at the pixel-level of the camera. Drawbacks include the errors due to superimposed noise associated with scattering and the possibility of device saturation. In the present work, the first factor is taken to be less significant because the field variable is obtained by integrating the intensity distribution (see Section 5.3), an operation that tends to smooth noisy profiles. The second factor was circumvented by reducing the laser intensity using neutral density filters. The local temperatures (and concentrations) were then determined by numerically integrating the appropriate governing equation in the direction normal to the knife edge.

5.3. Data Reduction

The present section examines the suitability of the three optical techniques of the present study for quantitative analysis of the convective field within a rectangular cavity and during crystal growth. An aspect shared by the three techniques is that they generate projection data, namely information that is integrated in the direction of propagation of the light beam. The result of analysis is thus a concentration (or temperature) that is ray-averaged over the length L of the growth chamber. The steps involved in the analysis of the experimental images are briefly discussed below.

Refractive index techniques depend on the fact that for a transparent material, refractive index and density share a unique relationship, called the Lorentz-Lorentz formula [58]. In addition, if pressure changes within the fluid region are small, density will be uniquely related to solute concentration and temperature. The functionality is often linear since changes in concentration and temperature are often small in many applications. In rectangular cavity experiments, temperature is the only dependent variable and density (and hence refractive index) relates to temperature. Though the crystal growth process is driven by the cooling process of the solution, the ramp rate is often small enough for thermal equilibrium to prevail

for short periods of time through out the experiment. In the present analysis, it is assumed that the aqueous solution has negligible temperature gradients. Hence, refractive index becomes a measure of concentration itself. The material property that determines the sensitivity of the optical measurement is *dn/dC*, where *n* is the refractive index and *C* is solute concentration.

The following discussion is presented in terms of solutal concentration. It is equally applicable to imaging thermal convection.

Interferometry: For a light source of wavelength λ, the change in concentration required per fringe shift in the infinite fringe setting is given by the equation [58]

$$\Delta C_{\varepsilon} = \frac{\lambda / L}{dn / dC} \tag{1}$$

The fringe positions are to be determined from interferogram analysis. In the wedge fringe setting, it can be shown that the fringe displacement from the initial position is proportional to the change in concentration with respect to the portion of the solution where the fringes are undisturbed. These results hold under the approximation that refraction effects are small.

Schlieren: Image formation in a schlieren system is due to the deflection of light beam in a variable refractive index field towards regions that have a higher refractive index. In order to recover quantitative information from a schlieren image, one has to determine the cumulative angle of refraction of the light beam emerging from the growth chamber as a function of position in the *x*-*y* plane. This plane is defined to be normal to the light beam, whose direction of propagation is along the *z*-coordinate. Using principles of ray-optics, the total angular deflection δ can be expressed as [58-59]

$$\delta = \frac{1}{n_a}\int_0^L n \frac{\partial(\ln n)}{\partial y} dz$$

where *n* is the refractive index at any point in the solution. The change in the intensity field (ΔI) relative to the background intensity distribution (I_k) can now be related to the refractive index field directly as

$$\frac{\Delta I}{I_k} = \frac{f}{a_k n_a}\int_0^L \frac{\partial n}{\partial y} dz \tag{2}$$

where n_a (~1) is the refractive index of the ambient, a_k is the size of the focal spot at the knife edge, and *f* is the focal length of the de-collimating mirror. This equation shows that the schlieren technique records the average gradient of refractive index over the path of the light beam. In terms of the ray-averaged refractive index, the governing equation for the schlieren process can be derived as:

$$\frac{\Delta I}{I_k} = \frac{f}{a_k}\frac{\partial n}{\partial y}L \tag{3}$$

where L is the length of the path traversed by the light beam through the growth chamber, namely its diameter. Equation 2 requires the approximation that changes in the light intensity occur due to beam deflection, rather than its physical displacement. The concentration gradient is related with the refractive-index gradient of the KDP solution using the following relation [30]:

$$\frac{\partial N}{\partial y} = \frac{9n}{2\alpha(n^2+2)^2}\frac{\partial n}{\partial y} \tag{4}$$

Here N is the molar concentration of the solution and α is the polarizability of the KDP crystal (=4.0 cm^3/mole). Combining Equations 3 and 4 and integrating from a location in the bulk of the solution (where the gradients are negligible), the concentration distribution around the growing crystal can be uniquely determined.

The contribution of refraction of light at the confining optical windows has been accounted for by applying a correction factor in Equation 3 for the angle of deflection with which the beam emerges from the growth chamber. It can be shown using Snell's law that the correction factor is equal to the refractive index of the KDP solution (=1.355) at the ambient temperature.

Shadowgraph: The shadowgraph arrangement depends on the change in the light intensity arising from beam displacement from its original path. Shadowgraph analysis requires tracing the path of individual rays through the aqueous solution. When subjected to linear approximations that include small displacement of the light ray, a second order partial differential equation can be derived for the refractive index field with respect to the intensity contrast in the shadowgraph image [57]. With D as the distance of the screen from the optical window on the beaker and Δ as the Laplace operator in the x-y plane, this equation is

$$\frac{\Delta \boldsymbol{I}}{\boldsymbol{I_k}} = \boldsymbol{LD}\left[\Delta\{\ln\, \boldsymbol{n}(\boldsymbol{x},\boldsymbol{y})\}\right] \tag{5}$$

Equations 3 and 5 have to be suitably integrated to determine the refractive index, and hence the concentration field. Integration of the Poisson equation (5) can be performed by a numerical technique, say the method of finite differences. When the approximations involved in Equations 3 and 5 do not apply, optical techniques can be used for flow visualization alone.

In interferometry, one can measure concentration values only at those points where fringes appear. The quantity of information is also limited by the number of fringes (infinite fringe setting) or their deformation (wedge fringe setting). Schlieren and shadowgraph generate information about the refractive index field at every pixel of the image in the form of intensities.

6. UNCERTAINTY AND MEASUREMENT ERRORS

Errors in the experimental data are associated with misalignment of the apparatus with respect to the light beam, noise generated at different stages of the experiment, including the imperfections of the optical components, and the intrinsic unsteadiness of the convection process itself. All experiments were conducted several times to establish the repeatability of the convective patterns, for the parameter range of interest. A quantitative assessment of errors and uncertainty was possible in experiments on convection in a rectangular cavity because of knowledge of the lower and upper surface temperatures.

A series of cross-checks have been enforced to validate the quantitative results obtained from experiments in the rectangular cavity. These include predicting the temperature of the cold top wall by starting from the lower hot wall, as well as comparing steady heat transfer rates across the cavity against published correlations. For example, an interferometry experiment with hot and cold temperatures of 305.5 K and 300.5 K yielded the cold wall temperature as 300.2 K. For temperatures of 300 and 320 K, the hot wall temperature was predicted to be 319.65 K. In schlieren, temperatures of 300 and 320 K were predicted as 301 and 319 K. The errors were considerably smaller at lower temperature differences across the cavity where the flow field was clearly steady. The comparison with correlations of average heat fluxes across the cavity for various temperature differences is discussed in Section 8.

In experiments with air, the time-dependent movement of the fringes during interferometry and the time-wise change in intensity for schlieren were not severe enough at the lower end of temperature differences, specifically the lower end of the Rayleigh number range. For Ra>51,000 unsteadiness was a source of uncertainty in the local temperature profiles as well as the wall heat transfer rates. Quite often, unsteadiness was a source of measurement uncertainty in air. It was less serious in water as well as the aqueous solution of KDP. Analysis of convection patterns in the KDP solution could be carried out under conditions of mild unsteadiness by averaging a time-sequence of images. The results obtained in the present work can be taken to be quantitatively meaningful for the lower range of Rayleigh numbers. For very high Rayleigh numbers, the images are purely representative of the instantaneous thermal/solutal fields in the fluid region.

An additional check carried out in the crystal growth experiments was one of solutal mass balance. Since the convective field was imaged from various angles, it was possible to independently determine the average concentration of KDP on a given plane. These averages were within 0.1% of each other as long as the convection plume was steady. Larger discrepancies were seen in those experiments where the convection process was strongly unsteady. Only those images that satisfied the mass balance check were used for tomographic reconstruction.

7. THREE DIMENSIONAL RECONSTRUCTION FROM SCHLIEREN DATA

The schlieren image yields gradients of refractive index and hence concentration. As discussed in Section 5.3, the gradient information can be integrated to yield data in terms of concentration itself. Subsequently, the concentration field on selected horizontal planes above the growing crystal can be reconstructed using principles of tomography [61-62]. For this

purpose, the left side of Equation 2 is interpreted as projection data of the refractive index gradient.

The schlieren images have been utilized to reconstruct the concentration field on horizontal planes above the crystal. For this purpose, images have been recorded at four different view angles. Since these images are time-separated, the present study is restricted to a steady convection conditions. Minor changes in the concentration field with time have been accounted for by averaging a sequence of four successive images. The schlieren images recorded during the initial transients as well as late stages of growth when convection is unsteady have not been utilized for three dimensional reconstructions.

Application of interferometric tomography for buoyancy-driven convection has been discussed earlier by Mishra *et al*. [19]; also see the related review article [64].

7.1. Computed Tomography

Tomography has been used in the present work to reconstruct two-dimensional concentration fields over individual horizontal planes from their one-dimensional projections. The third dimension is filled by moving from one plane to the next in the third (vertical) direction. The recording configuration shown in Figure 6 is the parallel beam geometry. The convolution back projection (CBP) algorithm has been used in the present study for tomographic reconstruction. Significant advantages of this method include its non-iterative character, availability of analytical results on convergence of the solution with respect to the projection data, and established error estimates [61-62,65]. The treatment of reconstruction for partial data adopted in the present work differs from that of Mishra *et al.* [20] where an iterative approach has been followed.

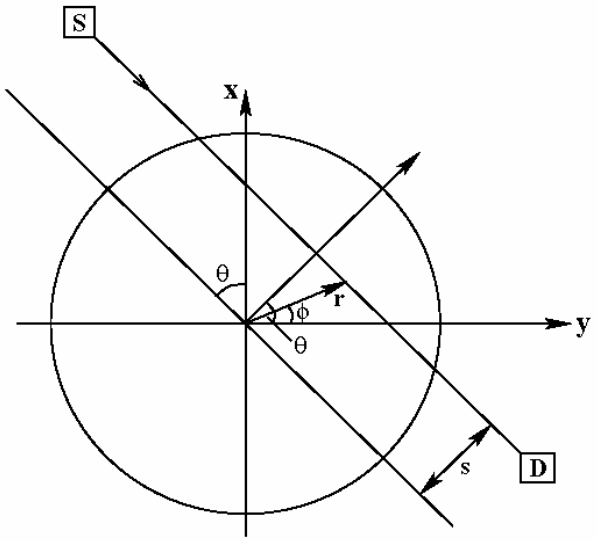

Figure 6. Schematic drawing of data collection using parallel beam geometry. S-source, D-Detector, s-perpendicular distance from the center of the object to the ray, θ-view angle, and (r,φ)-polar coordinates.

In an experiment, projection data can be recorded either by turning the crystal growth chamber or the source-detector combination. The latter is particularly difficult due to stringent requirement of alignment. With the first option, it is not possible to record a large number of projections, owing to the inconvenience of installing plane optical windows in a circular beaker. Further, for a cylindrical growth chamber, the entire field of interest cannot be imaged due to the curvature of the test cell. Instead, the central core region (corresponding to the size of the optical windows), that includes the growing crystal, has been recorded. In this respect, the projection data set is incomplete. In order to generate a complete projection data set for each view angle, an extrapolation procedure has been adopted and is discussed in Section 7.2.

Projection data has been recorded for four view angles of 0, 45, 90, and 135^o in the present experiments. The data for 180^o is taken to be identical to that for zero angle. Information for intermediate view angles has been generated by employing linear interpolation on the experimentally recorded data.

7.2. Extrapolation Scheme

The experimental set up employed in the present work enables only a part of the aqueous solution in the beaker to be scanned by the laser beam, being limited by the size of the optical windows. The projection data is thus incomplete, as shown schematically in Figure 7. Specifically, the experimental data in the form of the schlieren images covers about 25% of the beaker diameter. In order to successfully apply the CBP algorithm for tomographic inversion, one needs projection data over the entire width of the physical domain for each view angle. In the present work, the experimentally recorded partial data has been extrapolated to derive information about the portion of the solution beyond the optical windows. In all experiments, the region inclusive of the crystal has been imaged; extrapolation is applied to the portion of the field from the edges of the laser beam to the walls of the beaker.

The applicability of extrapolation to the present study can be justified on the basis of two factors: First, the concentration level away from the growing crystal, corresponding to the supersaturated solution is practically constant. This is confirmed in the recorded schlieren images where the changes in the intensity are found to be localized in the vicinity of the growing crystal alone. These images are discussed in the subsequent sections. Secondly, the information content of schlieren images decrease with the geometric path length of the light beam within the beaker, as indicated by the integration limits in Equation 2. The diminishing chord length of the beaker towards the edges shows that the measurement procedure de-emphasizes concentration variation occurring towards the sides of the beaker. Specifically, the chord length is zero at the extremities of the beaker. The approximation involved in extrapolating concentration outside the measurement volume is thus expected to be less serious in predicting the concentration field closer to the center of the beaker and hence the crystal location. Further justification can be based on the fact that concentration is continuously distributed in the fluid volume.

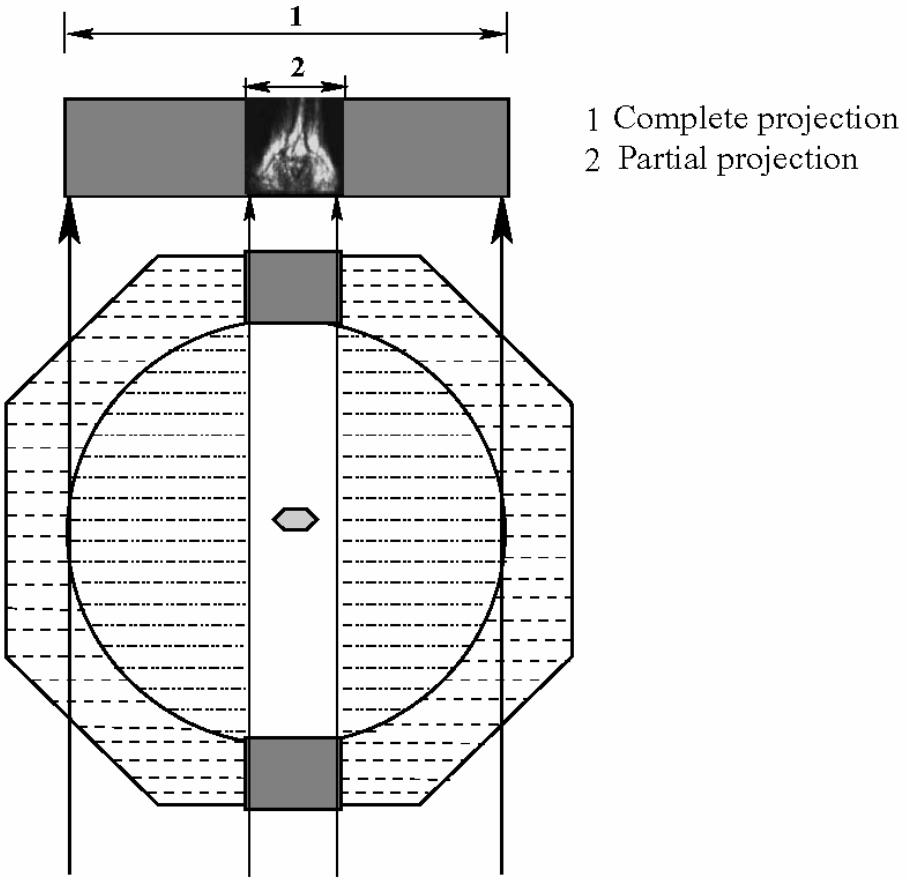

Figure 7. Definition of partial projection data

In the present work, a tenth order polynomial has been used to extrapolate the concentration distribution, starting with the portion covered by the optical windows. Polynomials of order 5 to 10 produced practically identical results. The limiting values of concentration in the far field, and the necessity of maintaining slope-continuity in the concentration distribution at every point have been enforced. An independent check on the accuracy of the experiment, data analysis and extrapolation is the conservation of solutal mass in each of the projections. Mass balance was found to be better than 0.01% in all the experiments analyzed using tomography. Minor imbalances are subsequently rectified by normalizing the data-set. To account for changes in the integration length along the direction of the laser beam, the extrapolated data is multiplied by the local chord length as one proceeds from the center towards the periphery of the growth chamber. This projection data is used for tomographic reconstruction of the concentration field over a horizontal plane of the solution. The above approach has been successfully tested in the context of numerically simulated buoyancy-driven convection and is discussed in Section 7.4.

7.3. Convolution Back-Projection

In the convolution back-projection algorithm (CBP), the reconstructed function, $f(r,\phi)$, is evaluated by the integral formula [61,62,65]:

$$f(r,\phi) = \int_{0}^{\pi} \int_{-D/2}^{D/2} p((s' - s);\theta) q(s) ds d\theta \tag{6}$$

where

$$q(s) = \int_{-Rc}^{Rc} |R| W(R) \exp(i 2\pi R s) dR$$

Here $p(s;\theta)$ is the projection data and s is the perpendicular distance of the data ray from the center of the object. In addition, θ denotes the source-detector line with respect to a fixed axis (and hence the view angle), D is the diameter of the growth chamber, and s' is the s-value of the data ray passing through the point (r,ϕ). The symbol R is the Fourier frequency, $q(s)$ is the convolving function of Equation 6, and $W(R)$ is the filter function. Also see Figure 6 for an explanation on the notation used. The filter function vanishes outside the interval $[-R_c,+R_c]$ and is an even function of R. Here R_c is the Fourier cut-off frequency and is taken to be $1/2\Delta s$, Δs being the ray spacing. The reconstruction obtained is specific to the choice of the filter function [61-62]. A Hamming filter h54 has been used in the present study. For $|R| < R_c$, it is given by the formula

$$W(R) = 0.54 + (1 - 0.54)\cos\left(\frac{\pi R}{R_c}\right)$$

As discussed by Natterer [62] and Munshi [65], this filter emphasizes the smooth features of the concentration variation, while suppressing small-scale (fine structure) fluctuations. This is quite appropriate to the present study for the following reason. Density variations in the solution arise primarily because of the deposition of the solute on the growing faces of the crystal as the solution is cooled at a given rate. Since the crystal growth rate is slow, one encounters density variations that are distributed in the entire solution, while rapid fluctuations in concentration do not appear [44-45]. Hence, it is of interest to reconstruct the dominant pattern in the concentration field rather than its secondary features.

7.3. Validation of Reconstruction Procedure with Simulated Data

The goal of the present work is to obtain concentration distribution on selected planes above the crystal growing from its aqueous solution from the schlieren images. These images require to be extrapolated to fill the width of the beaker. The extrapolation step combined

with the convolution back-projection algorithm is first validated against simulated data. The physical problem considered is buoyancy-driven convection in a differentially heated circular fluid layer with upper and lower walls maintained at specified temperatures. The side wall that is circular is thermally insulated. The fluid considered is air and the Rayleigh number based on the height of the fluid layer is set at Ra=12,000. The temperature distribution in the fluid layer has been obtained by numerically solving the governing equations of flow and energy transport on a fine grid. For definiteness, the thermal field is taken to be axisymmetric; accordingly the isotherms on individual planes of the fluid layer are circular. The physical realizability of axisymmetric convection in a circular cavity around a Rayleigh number of 12000 has been discussed at length by Velarde *et al.* [66] and Leong [67].

With the solution for temperature determined numerically, the projection of the thermal field is obtained by path integration. The accuracy of reconstruction with partial data has been examined in the present study against the available numerical solution.

Errors have been reported in the present section on three grids, namely 64×64, 128×128 and 256×256. Here the first number represents the number of view angles along which projections have been recorded, and the second indicates the number of rays for each view. The definitions of errors considered are:

$$E_1 = \max[(T_{\text{orig}} - T_{\text{recon}})] \quad \text{absolute maximum temperature difference}$$

$$E_2 = \sqrt{\frac{1}{N}\sum\left[T_{\text{orig}} - T_{\text{recon}}\right]^2} \qquad \text{RMS error}$$

Here T_{orig} and T_{recon} are the original and reconstructed temperature fields respectively and N is the total number of grid points on the reconstructed plane. All temperatures generated by simulation are dimensionless and fall in the range of 0 to unity. The difference between error norms E_1 and E_2 arises from the fact that the former highlights large isolated errors, while the latter reveals trends that are applicable for the entire cross-section.

The validation of the reconstruction procedure with simulated data is summarized in Figure 8. Figure 8(a) shows isotherms of the thermal field in the fluid layer for a given view angle. This data is presented in the form of contours of the path integrated temperature field. Since the thermal field is axisymmetric, the projection data for all other view angles are identical to Figure 8(a). The reconstruction over a horizontal plane of the fluid layer is shown in Figure 8(b). Results obtained with complete projection data (marked 100% in 8b(i)) and partial data (60% in 8b(ii) and 30% in 8b(iii), symmetrically placed about the center) are also shown. The axisymmetric nature of temperature distribution is brought out in all the reconstructions. This can be taken as a validation of the extrapolation procedure used to convert partial to an approximate but complete data set. A quantitative comparison of the reconstructed temperature profiles along the diameter of the cavity for different combinations of rays and views are shown in Figure 8(c). Profiles obtained with full as well as partial data are reported. For the complete data set, a perfect match between the original and reconstructed profiles can be seen for grid sizes of 128×128 and 256×256, while small errors are to be seen for the 64×64 grid. The extent of deviation from the original increases as the fraction of incomplete data increases. Noticeable errors are to be seen when only 30% of the

original data is used, the rest of it being derived by extrapolation. Errors in reconstruction were found to be significantly higher when the partial data set was used without extrapolation.

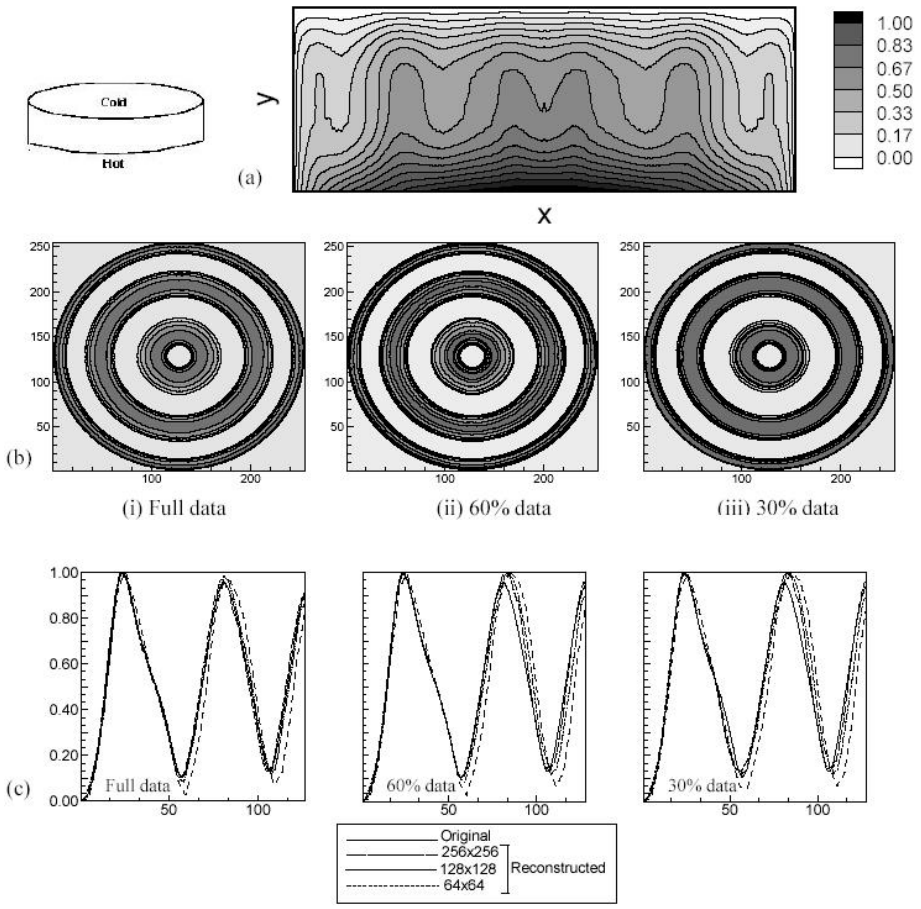

Figure 8. Buoyancy-driven convection in a differentially heated circular cavity. (a) Complete projection data in the form of isotherms for the differentially heated circular fluid layer; (b) Reconstructed temperature contours at y/H=0.65 for full (i) 100% and partial (60% (ii), 30% (iii)) projection data; and (c) Comparison of original and reconstructed non-dimensional temperature distribution along the radial direction for the three different combinations of rays and views.

The magnitudes of errors as a function of discretization of the fluid layer and size of the partial data set are summarized in Table 1. Since the difference between the minimum and maximum temperatures is unity, the percentage error is obtained as $100 \times E_1$ and $100 \times E_2$. In Table 1, error E_1 is consistently seen to be higher than E_2, the latter being an average over the entire field. Both errors decrease as the grid size (number of rays and views) increases. For a given grid size, errors increase as the fraction of original data used in reconstruction decreases. When only 30% of the original is used (the rest being obtained by extrapolation), the maximum errors on a 64 × 64 grid are 17.3% (absolute maximum) and 7.6% (RMS).

Figure 8 shows that the corresponding reconstructions are qualitatively meaningful, and hence these error magnitudes may be taken to be within limits.

Table 1. Comparison of the original and reconstructed temperature fields in terms of errors E_1 and E_2 for buoyancy-driven convection in a circular cavity

Date Type		Rays×Views	E_1	E_2
Full Data		256×256	0.052	0.028
		128×128	0.109	0.056
		64×64	0.124	0.058
Partial Data	60%	256×256	0.095	0.039
		128×128	0.148	0.061
		64×64	0.152	0.067
	30%	256×256	0.122	0.051
		128×128	0.148	0.072
		64×64	0.173	0.076

8. BENCHMARK EXPERIMENT: A COMPARISON OF INTERFEROMETRY, SCHLIEREN AND SHADOWGRAPH

A direct comparison of images of convection seen in interferometry, schlieren and shadowgraph is presented here. The physical experiment considered is a differentially heated fluid layer enclosed in a rectangular cavity (Section 4.1). In the initial discussion, the temperature difference across the cavity is 10 K in the experiments, while the fluid medium in the cavity is air. The corresponding Rayleigh number has been calculated to be 6×10^4. The interferograms, schlieren and shadowgraph images are compared on the right column of Figure 9. The fringes of an interferogram are lines of constant temperature. With reference to the discussion in Section 5.3, temperature here is to be interpreted as an integrated value over the length of the cavity. It should be noted that fringe shapes in a circular geometry are harder to interpret owing to a change in the geometric path length in a direction the path of the light beam [68-69]. The spatial coordinates of the fringes can be used to obtain the temperature profile. For schlieren and shadowgraph, the information regarding the thermal field is contained in the light intensity variation. The respective thermal properties recovered are the local values of the first derivative and the Laplace operator applied to the temperature. These quantities have been plotted for the mid-plane of the cavity on the left side of Figure 9. The individual data points are specific to the mid-plane of the cavity, while the solid line indicates the overall trend. The shaded circles of the left column indicate the gradients calculated from interferometric data (for schlieren) and from schlieren data (for shadowgraph). A good overall match is a confirmation of the result that schlieren is a derivative of the interferometric field, and the shadowgraph in turn is the derivative of the schlieren. The appearance of dense fringes near the horizontal walls is indicative of high temperature gradients at these locations. This is brought in the schlieren image in the form of an increase in intensity as well as the data points. The central region is a zone of nearly constant temperature, where the gradients

(and the light intensity values) are close to zero. Thus, the schlieren images and interferograms correlate quite well with each other. They also correlate with the shadowgraph, once it is realized that in this approach, light is redistributed over the image. In a shadowgraph image, light from the region close to the cold top wall deflects towards the lower hot wall, where the light intensity shows a maximum. Thus, high gradients are represented in a shadowgraph by regions of very low as well as very high light intensity. In the central core, the change in light intensity with respect to the initial setting is small. Thus the Laplacian operation of temperature in this region yields a practically zero value. The thermal lensing effect that distorts the shape of the cavity cross-section is most visible in the shadowgraph.

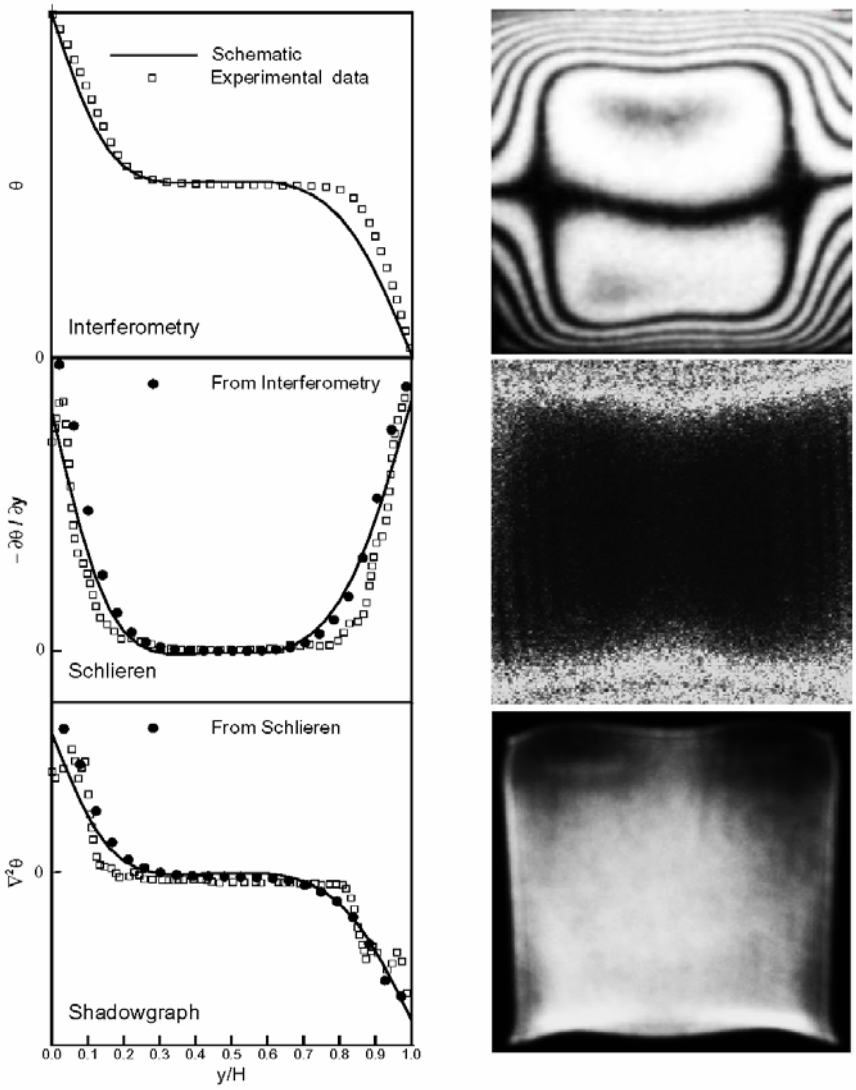

Figure 9. Comparison of the data recovered from the three optical techniques (left column). The corresponding experimental images are shown in the right column. $Ra=6\times10^4$. The solid line in the left column is representative of the trend seen at any vertical section of the image.

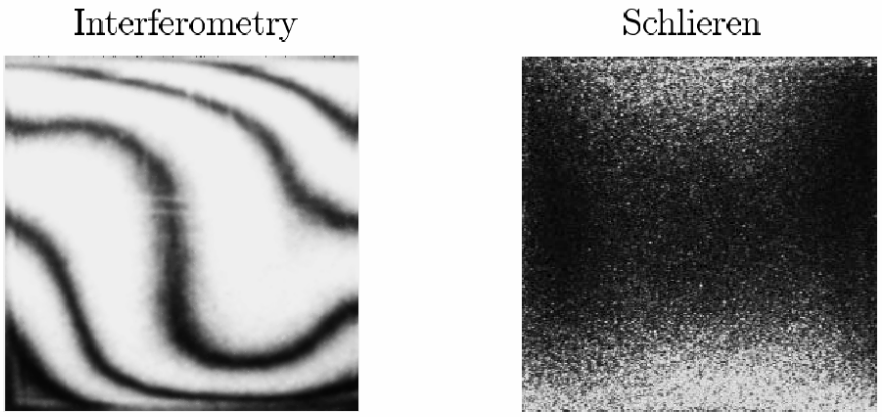

(a) Ra=1.30×10^4

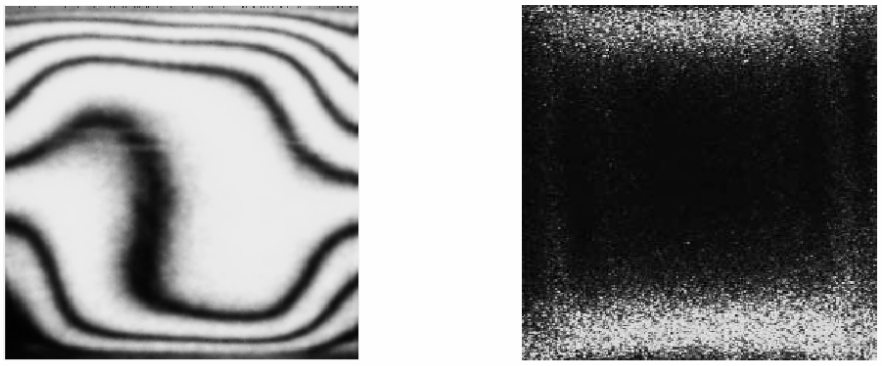

(b) Ra=2.60×10^4

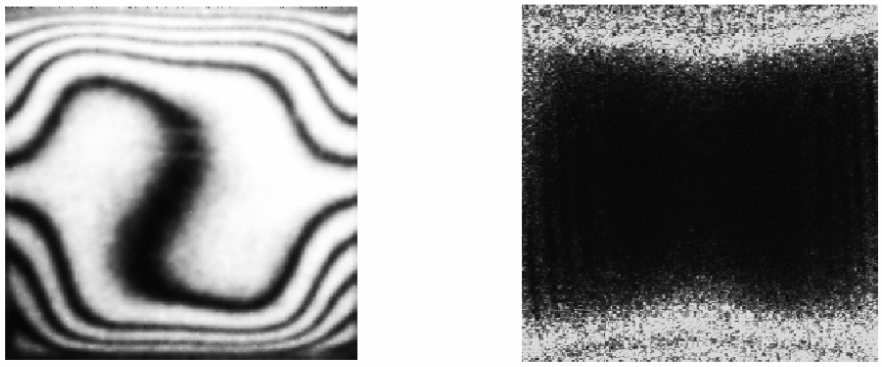

(c) Ra=5.00×10^4

Figure 10. Interferometric and schlieren images for the lower range of Rayleigh numbers in air.

Quantitative analysis of the temperature field and wall heat transfer rates is reported for the lower range of cavity temperature differences (and hence Rayleigh number). Clear shadowgraph images could not be recorded for small temperature differences and have not been shown. At higher temperature differences, the field was seen to become unsteady. The discussion for larger cavity temperature differences is based on qualitative comparison of the three imaging techniques.

Low Rayleigh numbers: Figure 10 shows the steady state interferometric and schlieren images for the lower range of Rayleigh numbers namely $1.3\times10^4<Ra<5\times10^4$. At $Ra= 1.3\times10^4$, the interferogram has only a few fringes. The number of fringes in the experiments was uniformly found to be consistent with the estimate $(T_h\text{-}T_c)/\Delta T_\varepsilon$, the denominator being given by Equation 1. The number of fringes increases with Rayleigh number, along with the fringe density near the horizontal walls. With respect to the schlieren images, it can be seen that the increase in light intensity is distributed over the cavity cross-section at the lowest Rayleigh number. As Rayleigh number increases, the brightness is limited to the wall region, and its size progressively diminishes. The schlieren image clearly brings out a boundary-layer type of flow structure in the cavity. The above experiments have been validated against a numerical model and the comparison has been found to be good [70].

A comparison of the steady dimensionless temperature profiles in the cavity as obtained from interferometry, schlieren, and numerical simulation is presented in Figure 11. Temperature profiles at two column locations (x/h = 1/4 and 3/4) have been considered. The comparison has been presented for the three Rayleigh numbers referred in Figure 10. The shape of the temperature profile, characteristic of buoyancy-driven convection in a Rayleigh-Benard configuration is reflected in all the three approaches. The slopes of the individual curves near the walls give a measure of the wall heat flux. The comparison between the experiments and simulation is seen to be good. Schlieren measurements compare marginally better with numerical simulation, as against interferometry. This is because in interferograms, information about the thermal field is available only at the fringes. Constructing a complete temperature profile requires interpolation between fringes, and is a source of error. In addition, the number of fringes at low Rayleigh numbers is small.

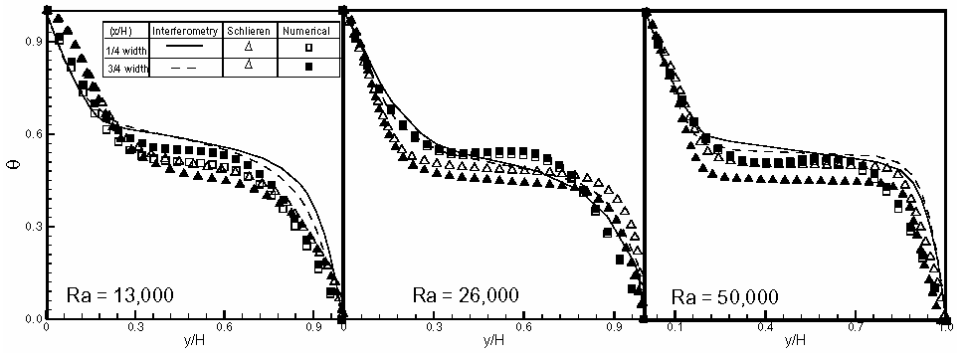

Figure 11. Convection in an air-filled cavity. Non-dimensional temperature profiles as a function of the vertical coordinate.

Under steady conditions, the average wall heat flux is also equal to the energy transferred across any horizontal plane of the cavity. Average heat transfer rates at the hot and the cold

walls of the cavity have been calculated in terms of Nusselt number and presented in Table 2. Further, they have been compared against the experimental correlation of [2]. The correlation summarizes the observations of a number of authors and cavity dimensions. Consequently, it has a large uncertainty level of ±20%. The average Nusselt numbers predicted by the two optical techniques match well with each other, with a maximum difference of ±5%, that occurs at the lowest Rayleigh number (Ra= 1.4×10^4) of the present work. The hot and cold wall Nusselt numbers are also reasonably close, indicating a good energy balance in the data reduction procedure. The discrepancies are higher in interferometry at this Rayleigh number owing to the formation of just a few fringes in the cavity.

Table 2. Wall-averaged Nusselt numbers at the lower (hot) and the upper (cold) walls for convection in a rectangular cavity with air as the working fluid. Comparison of experiments with correlation of [2]. Symbol I in brackets indicates values calculated from interferograms; symbol S indicates values from a schlieren image

Rayleigh number	Nu (cold)	Nu (hot)	Nu ([2])
1.4×10^4	2.38 (I) 2.28(S)	1.965(I) 2.07(S)	2.615
2.7×10^4	3.32(I) 3.50(S)	3.13(I) 3.10(S)	3.03
5.1×10^4	3.56(I) 3.37(S)	3.51(I) 3.38(S)	3.45

High Rayleigh numbers: Convection in a cavity subjected to a large temperature difference and hence a high Rayleigh number is discussed in the present section. The shadowgraph images were quite clear in these experiments and have been included for comparison. In each of the experiments, a true steady state was not attained even after the passage of a long period of time. Secondly, interferograms were subjected to large refraction errors. The cavity viewed through the schlieren and shadowgraph layouts looked deformed once again due to refraction. Hence, the present discussion is purely descriptive and quantitative data has not been reported. Rayleigh numbers considered are Ra=8.5×10^4, 1.13×10^5 and 1.4×10^5.

Figure 12 shows representative images of the convective field recorded after the passage of 8-9 hours of real time. At Ra=8.5×10^4, the interferogram shows nearly straight dense fringes parallel to the horizontal walls. These are indicative of near-parallel flow near the hot and the cold walls. The flow turns at the corners, leading further to fringe curvature and separation. The flow field is symmetric about the centerline of the cavity. These trends are well-reproduced by schlieren and shadowgraph images.

The movement of the fluid medium in the cavity cross-section has the shape of a roll. The roll size can be determined directly from the optical images since the fringes as well as the intensity fields should turn along at corners with the local velocity vector. The roll sizes of Figure 12 have been compared in Table 3, and are found to be quite close. The three experimental techniques reveal a reduction in the roll size with increasing Rayleigh number. The nature of unsteadiness in the convective field as recorded by the three optical techniques has been discussed by the authors elsewhere [70].

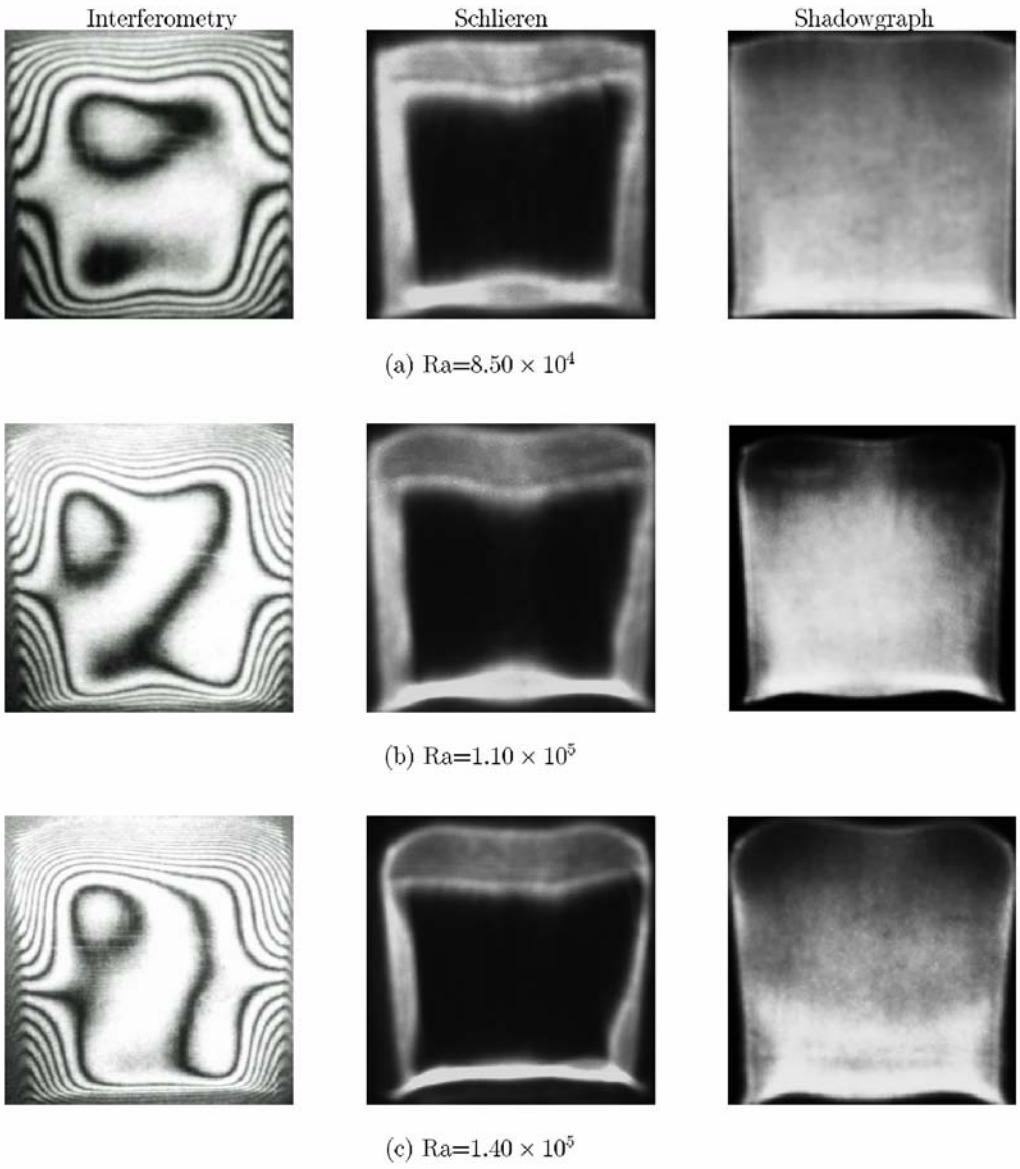

Figure 12. Interferometric, schlieren and shadowgraph experimental images for the higher range of Rayleigh numbers in air.

Table 3. A comparison of roll sizes of convection seen relative to the cavity height in the three optical techniques; effect of increasing Rayleigh number

Rayleigh number	Interferometry	Schlieren	Shadowgraph
8.50×10^4	0.270	0.278	0.310
1.10×10^5	0.258	0.252	0.252
1.40×10^5	0.210	0.242	0.220

Thermal imaging of the test cell filled with water is reported in the following discussion. The vast difference in the properties of air and water leads to certain difficulties in temperature measurement in a water-filled cavity. Specifically, the following issues are to be noted:

1. Even for modest temperature differences, the equivalent Rayleigh numbers are very high. Consequently, the convective field reaches the unsteady, turbulent regime quite early.
2. The temperature drop per fringe shift is small in water. Thus the fringe density in interferograms is high, making data analysis difficult.
3. The sensitivity of the refractive index to temperature is high. Thus the deformation of the cavity size as seen on the screen is large and leads to ambiguity in data analysis.

In view of these complications, it is natural that shadowgraph should be best suited for temperature measurement in water. A comparison of interferometry, schlieren and shadowgraph for a temperature difference of 4 K ($Ra=2.5\times10^6$) is presented in Figure 13. The optical images contain information that is path-integrated in the direction of propagation of light, but are functions of time. Figure 13 shows that the shadowgraph has the most well-defined intensity variation and is the easiest to analyze for the present experiment.

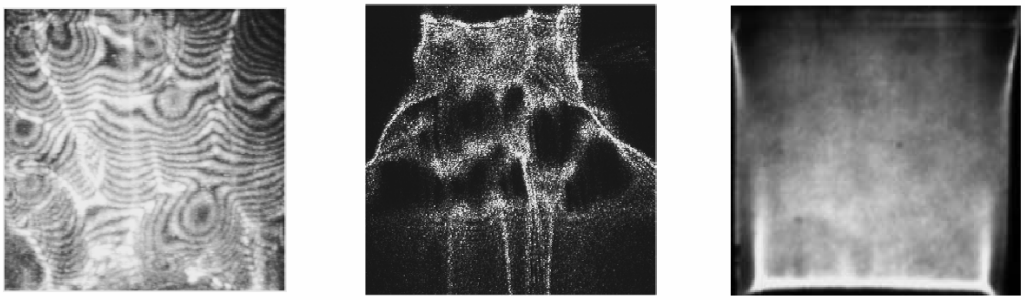

Figure 13. Comparison of (a) interferometry, (b) schlieren and (c) shadowgraph for buoyant convection in a water-filled cavity at $Ra=2.5\times10^6$.

A comparison of shadowgraph images over a range of high Rayleigh numbers in water is shown in Figure 14. The light intensity variation shows the flow evolving from a boundary-layer type behavior at the lowest Rayleigh number towards large scale structures (namely, plumes) at the highest Rayleigh number. Beyond $Ra=5\times10^6$ the flow is unsteady as well. The images shown in Figure 14 have been time-averaged over a few seconds so that the dominant spatial features are captured.

Convection in water at high Rayleigh numbers in the presence of an air-water interface has been studied by Punjabi *et al.* [68]. A sequence of shadowgraph images recorded in the experiments is shown in Figure 15.

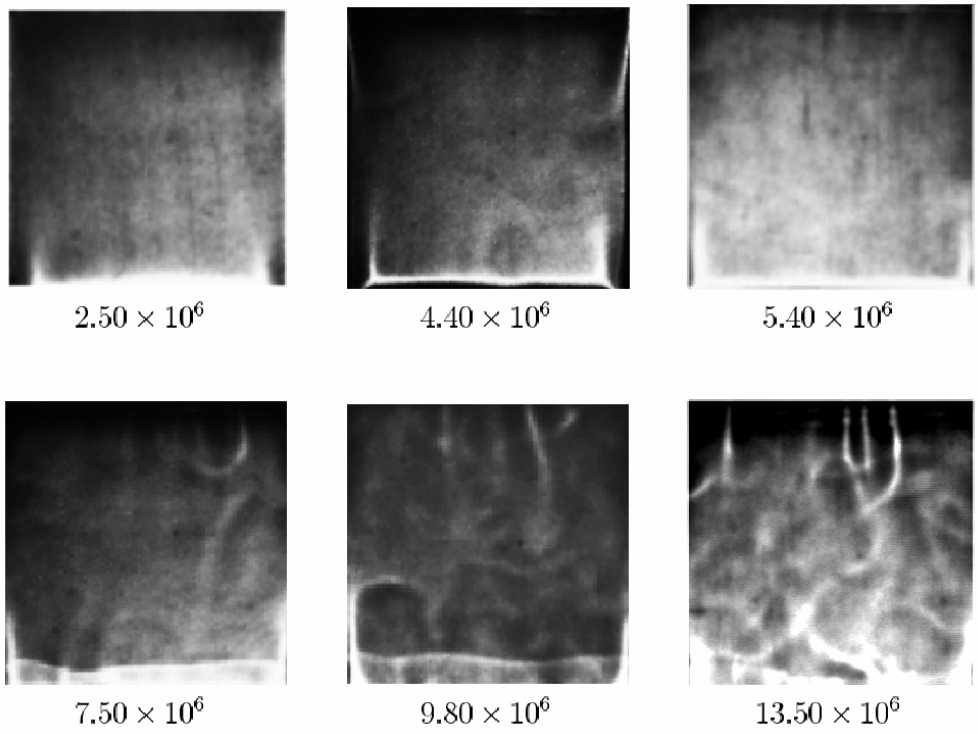

Figure 14. Shadowgraph images of the convective field with increasing Rayleigh number in water.

Based on the above discussion, the following conclusions can be drawn.

1. In low temperature gradient experiments, all the three techniques correlate well with one another. Interferograms are limited by few fringes in air, and too many fringes in water. The shadowgraph image does not show sufficient contrast for analysis. In this respect, the schlieren technique is most amenable to data reduction.
2. In high gradient experiments, both schlieren and shadowgraph yield clear images. The interferograms are however corrupted by refraction errors. Schlieren and shadowgraph track the temporal response of the fluid medium in the form of the light intensity variation.
3. In high Rayleigh number experiments with water, the flow field is turbulent. Shadowgraph images are seen to be meaningful, as against interferograms and schlieren. The shadowgraph images reveal a considerable amount of physical information, including boundary-layers, plumes and time scales. It can be independently used to improve existing models of engineering turbulence.

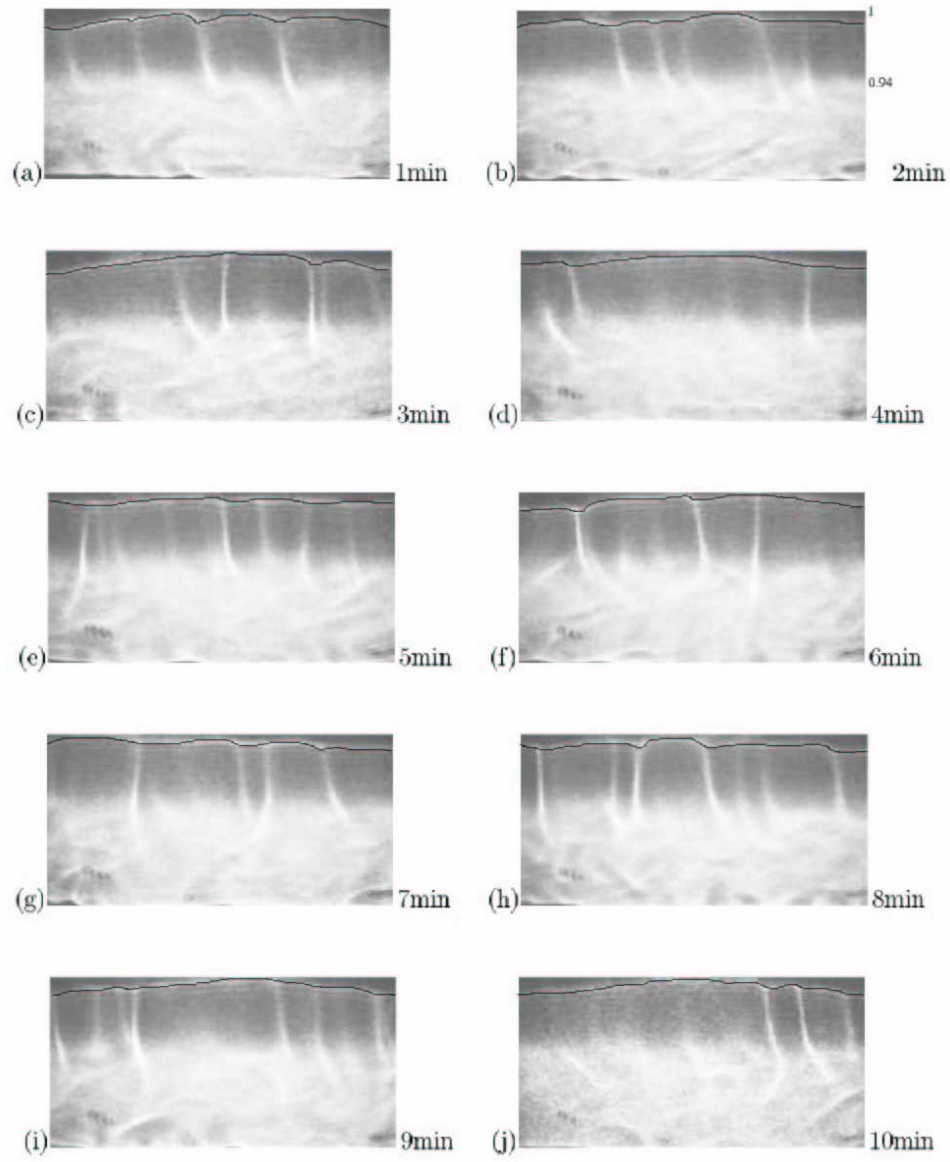

Figure 15. Shadowgraph images showing the deformed interfaces in a cavity half-filled with water, the rest being air; Interfaces are emphasized in black.

9. CONVECTION PHENOMENA DURING CRYSTAL GROWTH

For a purely buoyancy-driven growth process, the driving potential of flow is the maximum concentration difference occurring in the solution. In addition, the strength of convection is also governed by the length scale, typically the size of the growing crystal. With time, the solution is depleted of the salt, though there is an increase in the length scale related to the change in size of the crystal. Jointly, the strength of convection can increase with time, till the solution in the growth chamber is fully depleted of salt. This state is characterized by

stable stratification of the solution, the convection currents diminishing in strength to negligible levels. The growth of the crystal practically stops at this stage. Growth can be resumed when the grown crystal is immersed in a fresh supersaturated solution and the ramp rates are re-introduced. The resulting convection patterns would be different from the first stage because of a change in the crystal size. When the crystal is imparted rotation, velocities are created in the angular direction in the horizontal plane, in addition to the buoyancy-driven motion in the vertical plane. However, the two motions are interlinked through the radial component of velocity. The linkage is such that rotational motion leads to Coriolis forces that re-direct fluid motion. However, homogenization of the solution is the dominant factor that reduces concentration gradients, diminishes the driving potential and hence suppresses fluid motion arising from buoyancy. The critical speed at which buoyancy is practically suppressed will depend on the crystal size and overall concentration difference available in the solution. The resulting solutal concentration distribution at the surface of the crystal influences the growth rate and quality.

The process of solute deposition leading to crystal growth occurs on a hierarchy of length and time scales. At the small scale, solute particles arrange themselves as a part of the crystal structure. The pyramidal structure seen at later stages of growth is initiated at this point. The experiments conducted in the present work do not yield information on this aspect of the growth process. At the larger scale (the length scale of the crystal itself), concentration gradients are set up that feed solute to the crystal. These gradients naturally control the rate of crystal growth. The uniformity in distribution of the concentration gradients determines the crystal quality. The present research aims at investigating physical mechanisms at the scale of the crystal in terms of the solutal concentration distribution.

9.1. Comparison of Interferometry, Schlieren and Shadow-Graph in a Crystal Growth Experiment

The applications of interferometry, schlieren and shadowgraph as tools for visualization of buoyant convection and on-line monitoring of KDP crystal growth from its aqueous solution are discussed in the present section. The ramp rate here is around 0.2^{o}C/hour that is quite high in comparison to the rates employed in Section 9.2. The resulting convection patterns, as a result, form earlier in the experiments discussed. Images of the time-evolution of the convective field in the growth chamber have been recorded. The three measurement techniques are compared in terms of image quality and the potential for extracting quantitative information.

9.1.1. Convection Patterns

When a seed of the crystal is inserted in the solution, the initial temperature difference between the two leads to the dissolution of the seed itself. The local density of the solution increases, and consequently the solution descends vertically from the crystal. With the passage of time, thermal equilibrium is established, and density differences within the solution are solely due to concentration differences. Adjacent to the crystal, the solute deposits on the crystal faces, and the solution goes from the supersaturated to the saturated state. Thus the solution near the crystal is lighter than the solution away from it. The denser solution displaces the lighter fluid, and a circulation pattern is set up around the crystal. The

structured movement of the fluid, called a buoyant plume is essential for transporting the solute from the bulk of the solution to the crystal and determines the crystal growth rate. The plume is visible in the three visualization techniques: as fringe displacement in interferometry, and the spread of light intensity in schlieren and shadowgraph.

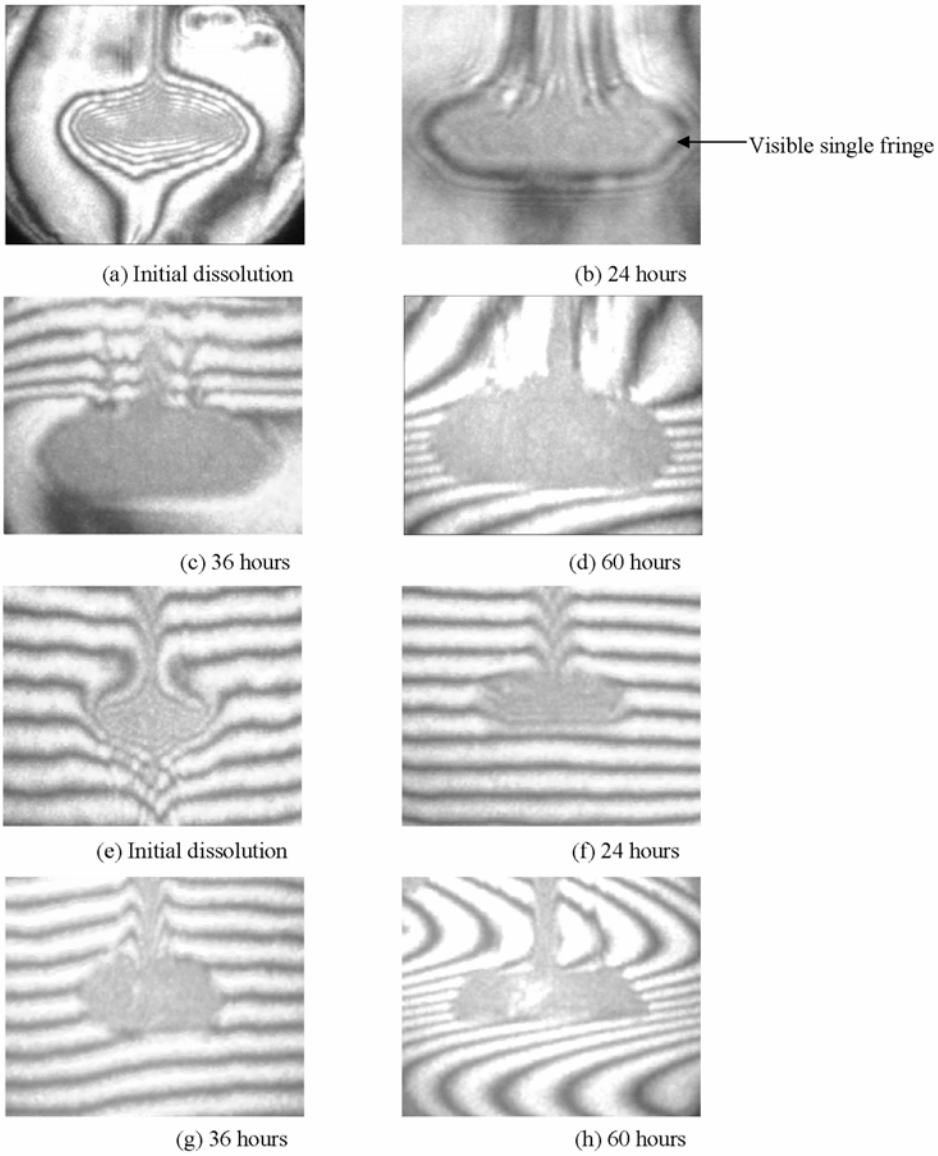

Figure 16. Time sequence of the evolution of interferograms around the growing crystal. (a-d) Infinite fringe setting; (e-h) Wedge fringe setting. The initial crystal size in the infinite fringe setting is greater than in the wedge fringe setting. Large fringe slopes in (e-h) very close to the glass rod are possibly distortions. The opposing fringe curvatures above and below the crystal in (h) show a lighter and a denser solution formed by stratification.

Figure 16 shows the formation and time-evolution of fringes in the infinite and wedge fringe settings of the interferometer around the growing crystal. The first image of the

transient shows the appearance of fringes due to crystal dissolution. This process increases the local density, causing the solution to descend vertically downwards. Hence, the fringe displacement is also in the downward direction (Figure 16(a)). Large concentration gradients in the vicinity of the dissolving crystal give rise to time-dependent fluid motion as well. A second factor contributing to unsteadiness is the change in the crystal geometry from rectangular to prismatic. As the crystal attains thermal equilibrium on one hand and its natural shape on the other, the concentration gradients gradually diminish. During a time period of 15-35 hours, the gradients were small enough to produce only a single visible fringe adjacent to the growing crystal (Figure 16(b)). The fringe was found to be stable with respect to time indicating uniform deposition of the solute around the growing crystal. Experiments in the wedge fringe setting of the interferometer reflect identical trends. The horizontal fringes deform vertically downwards (Figure 16(e-f)), and is followed by a phase when they are practically straight. Near the crystal, the solution is practically saturated, while it is supersaturated in the far field. The wedge fringes get displaced in regions of a large change in concentration with respect to the bulk of the supersaturated solution. With further cooling, the solution in the near-field becomes supersaturated with reference to the new temperature, additional salt deposits on the crystal, and the growth process is once again initiated. This leads to concentration gradients adjacent to the crystal, and a continuation of buoyancy-driven flow. In the time frame of 20-30 hours after the insertion of the KDP seed, the infinite and the wedge fringes showed considerable symmetry as well as stability in time, ensuring uniform growth on all the faces of the crystal. This time duration may be called the stable growth regime of the crystal.

With an increase in the crystal size, the influence of even mild concentration gradients is strengthened, increasing the fringe deformation. Over a longer duration of the experimental run time (> 50 hours), the solution is found to be layered (stratified) with respect to density (Figures 16(c-d) in the infinite fringe setting and Figures 16(g-h) in the wedge fringe setting). This is understandable because crystal growth takes place from a fixed volume of the solution in the growth chamber, and with time, the solution is increasingly depleted of salt. The density inversion suppresses convection to a point where the increase in the crystal size is negligible. The downward movement of these layers of constant concentration is driven by molecular diffusion, and contributes to a very slow increase in the crystal size. The appearance of straight horizontal fringes above the crystal in the infinite fringe setting, and opposed curvature of wedge fringes in the far-field can thus be taken as the limiting point where the growth process is to be terminated.

The initial size of the crystal used in the infinite fringe setting had to be larger than that of wedge fringes. This is because the convection patterns with a small crystal did not produce sufficient contrast in the interferograms, and could be recorded by the camera.

The growth sequence using schlieren and shadowgraph techniques is shown in detail in Figures 17 and 18. They confirm the evolution pattern of the convection field recorded by the interferometer. The first image in the schlieren and shadowgraph sequences shows initial dissolution of the seed just after its insertion into the solution. A sharp descending plume originating from the seed can be seen. The intensity contrast is related to an abrupt change in the solute concentration around the seed crystal, which creates a jump in the refractive index, and deflects the light beam into the region of relatively large concentration gradients. The schlieren arrangement is more sensitive to the change in concentration, producing a greater intensity contrast, when compared to the shadowgraph. After the initial dissolution, the

growth process of the crystal is initiated. The associated convection currents are larger, and a significant increase in the size of the bright region is seen. The schlieren image is more vivid (Figure 17), when compared to the shadowgraph (Figure 18). The images also reveal the extent of symmetry of the solutal distribution and the underlying flow field in the stable growth regime of the crystal. As in interferograms, schlieren and shadowgraph reveal the following sequence of events: (a) The plumes associated with crystal dissolution are unsteady; (b) the growth process enters a stable growth regime till the crystal size exceeds a critical value; and (c) the flow field approaches a stagnant condition when the solution becomes stratified.

The layering and stable stratification of the solution are seen for times greater than 55 hours (Figures 17(g-h) and Figures 18(g-h)). In the schlieren image, it leads to the region of brightness shifting away from the crystal. Figure 17(h) is an original unprocessed schlieren image. It shows a larger view of convection around the crystal, where stratification leads to a significant refraction and the appearance of a bright patch of light above the crystal. In shadowgraph images, the movement of the stratification front is visible as a bright band that descends vertically downwards. For times greater than 50 hours, the patch of light is localized around the crystal, while alternating bands of bright and dark regions are formed.

The schlieren (Figures 17(c-d)) and shadowgraph images (Figure 18(e-f)) in the stable growth regime show an upward movement of the buoyant plumes around the crystal. These plumes end in the bulk of the solution in the beaker, and descend in such a way as to form a closed loop. The images discussed in the present section pertain to the flow field adjacent to the crystal alone. The buoyant plumes in the stable growth regime are responsible for the deposition of the solute on the crystal surface. These convection plumes are almost steady and uniform in nature resulting in uniform and symmetric growth of the crystal. The gradient of concentration is larger near the crystal surface when compared to the bulk of the solution. This distribution can be visualized as a diffusion boundary layer around the growing faces of the crystal. The thickness of the boundary-layer can be identified as the region over which the light intensity is high. The vertically upward movement of the convective plumes results in the variation of the thickness of concentration boundary layer along the crystal faces. During the growth phase of the crystal, the boundary-layer is the thinnest on the lower side of the crystal, and the highest on the upper side.

The shadowgraph images are not as explicit as the schlieren, but they help in deciding the symmetry pattern of growth, time dependence, and the onset of stratification. It is to be expected that the shadowgraph images would show greater contrast when the gradients are very high, for example crystal growth in forced convection conditions.

9.1.2. Comparison of the Three Techniques

The knowledge of transport phenomena in the growth of crystals from their aqueous solution in the free convection regime is important for understanding the fundamental mechanisms involved and for fixing process parameters. As opposed to forced convection, the free convection technique has its own importance, for example in protein crystal growth where it is the only choice because of their delicate structure and the ease of managing defects. The creation of a homogeneous concentration field in the boundary-layer adjacent to the solution-crystal interface and uniform distribution of solute in the bulk solution are two major requirements. Refractive index-based optical techniques can be used to examine the nature of convection patterns as a function of time and hence the quality of the grown crystal.

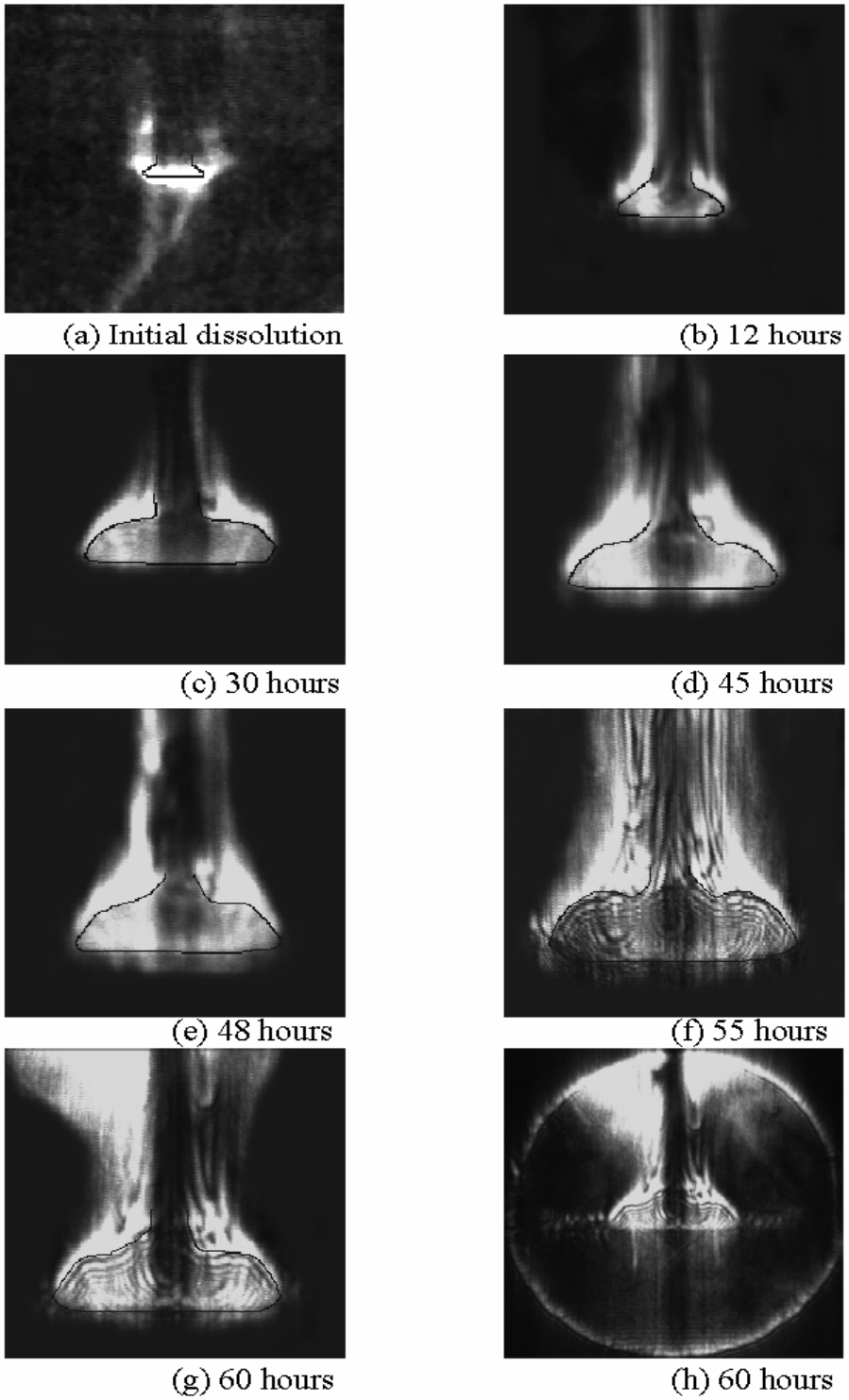

Figure 17. Evolution of schlieren images around the growing crystal from an aqueous solution. Images have been contrast-enhanced to reveal clearly the regions of high brightness. In (h) the original photograph as recorded by the camera is shown. The crystal position has been highlighted.

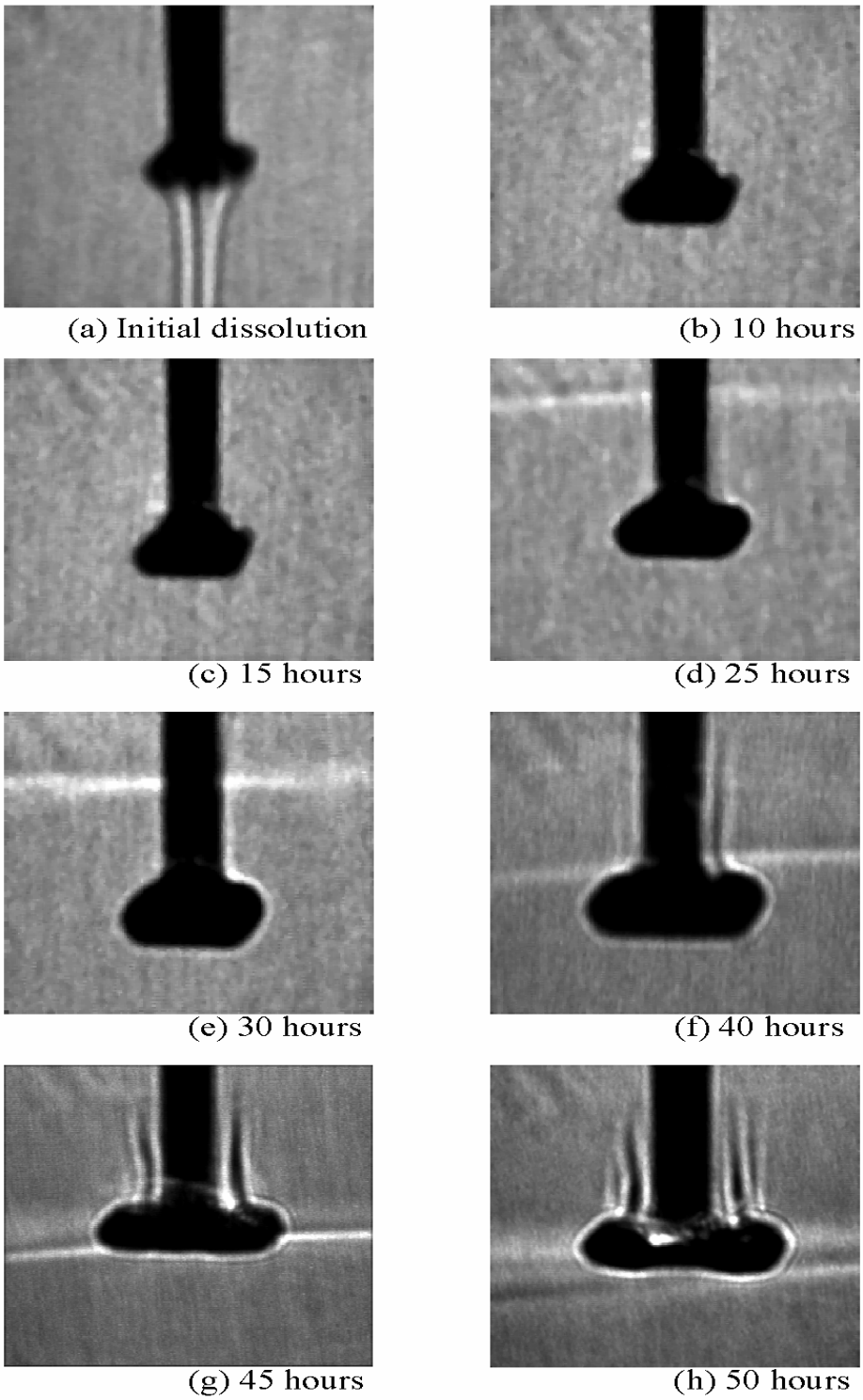

Figure 18. Evolution of shadowgraph images around the growing crystal from an aqueous solution. Images have been contrast-improved for clarity. A bright streak of light indicates the separation of the light solution from the heavy. The streak is seen to move downwards in (d-h), till it stabilizes just around the crystal.

A comparison of the images of the three techniques shows interferograms to be most vivid, since fringes deform and get displaced in relationship to the local velocity field. Thus, they offer the most direct information about concentration distribution as well as the underlying flow field in the solution. Schlieren and shadowgraph images reveal regions of high concentration gradients in the form of heightened brightness, though the former shows greater sensitivity. A review of Equations 1, 3 and 5 (Section 5.3) shows that interferograms are easy to analyze, schlieren requires integration of the intensity field, while shadowgraph requires the solution of a Poisson equation to recover the local concentration.

The three optical techniques under discussion yield images that are integrated values of the concentration field in the direction of propagation of the light beam. Thus, if the spatial extent of the disturbed zone in the solution is small, the information contained in the image is small. In the context of interferometry, the consequence could be the appearance of too few fringes in the infinite fringe setting and small fringe deformation in the wedge fringe setting. In schlieren and shadowgraph, weak disturbances show up as small changes in intensity and hence contrast. The difficulty can be alleviated in schlieren by using large focal length optics so that small deflections are amplified. In shadowgraph, image quality can be improved by moving the screen away from the test cell. Additional difficulties with interferometry are the need for maintaining identical experimental conditions in the crystal growth and the compensation chambers, careful balancing of the test and the reference beams, and limitations arising from fact that quantitative information is localized at the fringes. This discussion shows that configuring the interferometer as the instrument for on-line process control poses the greatest challenge, schlieren and shadowgraph being relatively simpler. Based on the above discussion, schlieren may be considered as an optimum while comparing the ease of analysis with the difficulty of instrumentation.

The quantitative description of the concentration field derived from the schlieren images is discussed in the following section.

9.2. Influence of Ramp Rate and Crystal Rotation on Convection Patterns

The present section discusses the application of the laser schlieren technique to monitoring convection in a crystal growth process from its aqueous solution, when the process parameters are varied. The cooling rate of the solution determines the amount of excess salt available in the solution for deposition on the crystal, and hence the potential difference for driving the convection currents. Ramp rates of 0.05 and 0.1^{o}C/hour have been studied in the present work. These values are smaller than the ramp rate of Section 9.1; consequently the stratification of the solution seen in those experiments was considerably delayed. The rpm of rotational motion fixes the degree of homogenization of the solution and hence, indicates a reduction in the strength of buoyant convection. Crystal rpm of 0 and 15 are studied through experiments. These values have been selected on the basis of their ability to permit growth of crystals of meaningful quality. The effects of ramp rate of the solution, crystal rotation and the size of the growing crystal have been correlated with the growth rate of the crystal. Results of the transient evolution of the convective field in the growth chamber in the form of two-dimensional schlieren images are reported. The images are quantitatively interpreted in terms of concentration contour maps and concentration gradient profiles. In order to bring out the influence of the process parameters, results have been presented in the

following sequence: 1. convection currents at a ramp rate of 0.05^{o}C/hour with rotations of 0 and 15 rpm; 2. convection currents at a ramp rate of 0.1^{o}C/hour with rotations of 0 and 15 rpm; and 3. effect of crystal size.

The nature of fluid motion around the crystal gives rise to *boundary-layers* in the flow and solutal concentration fields. These are relatively thin zones adjacent to the crystal faces where large changes in velocity and concentration take place. Large concentration gradients are revealed in a schlieren image as a brightened region against a darker background. The images discussed in the following sections show that the stable growth regime of crystal growth is accompanied by thin high intensity zones that originate at the crystal surface. Thus, it is clear that fluid motion and transport occur in the bulk of the solution, but are governed by the physical conditions imposed by the crystal. These are 1. a prescription of fluid velocity in terms of crystal rpm, and 2. concentration levels fixed by salt depletion from the aqueous solution.

9.2.1. Ramp Rate of 0.05^{o}C/Hour

Figure 19 and Figure 20 show the transient evolution of the convective field for experiments when the growing crystal is respectively held stationary in the solution and rotated at a constant speed of 15 rpm. The ramp rate to cool the solution in the two sets of experiments is 0.05^{o}C/hour. Insertion of the seed into its supersaturated solution can lead to an instantaneous temperature difference between them, followed by an initial dissolution of the crystal. This phase of the experiment is not included in the figures. With the passage of time, thermal equilibrium is established, and density differences within the solution are solely due to concentration differences. Adjacent to the crystal, the deposition of solute from the solution to the crystal surfaces results in a change of concentration and the solution goes from supersaturated to the saturated state. In the absence of rotation, the denser solution displaces lighter solution in the vicinity of the crystal and a circulation pattern is set up around the crystal. The fluid motion is largely in the vertical plane. With rotation, a radial pressure gradient creates an independent circulation loop that forms an alternative basis of solute movement. Here, the fluid particles around the crystal move in the radial direction, but conservation of mass ensures that vertical velocities be set-up once again. In the purely buoyancy-driven mode (0 rpm; also called *natural convection*), the strength and orientation of the convection currents is determined by the available concentration difference in the solution at any instant of time, and hence the cooling rate. On the other hand, an externally imparted rotation to the growing crystal (called *forced convection*) leads to homogenization of the solution, reduction in concentration gradients and hence a reduction in the strength of convection currents. Except for the initial stages of the growth process (where it is diffusion-dominated), these circulation patterns and their interaction form the basis of the transport of solute from the bulk of the solution to the growing crystal surfaces.

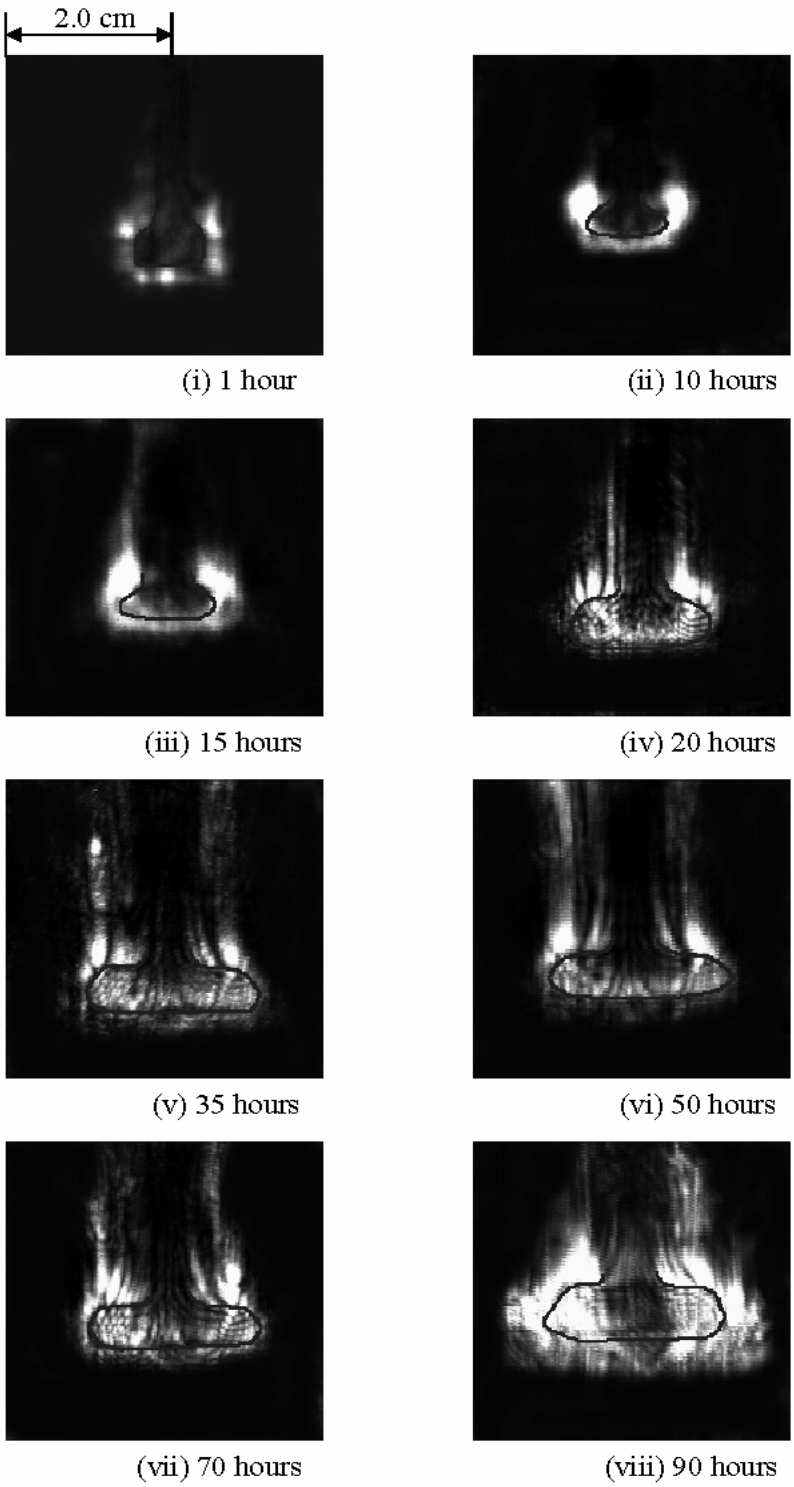

Figure 19. Schlieren images of the transient evolution of the convective field around crystal growing from its aqueous solution. (Ramp rate = 0.05°C/hour, rate of crystal rotation = 0 rpm).

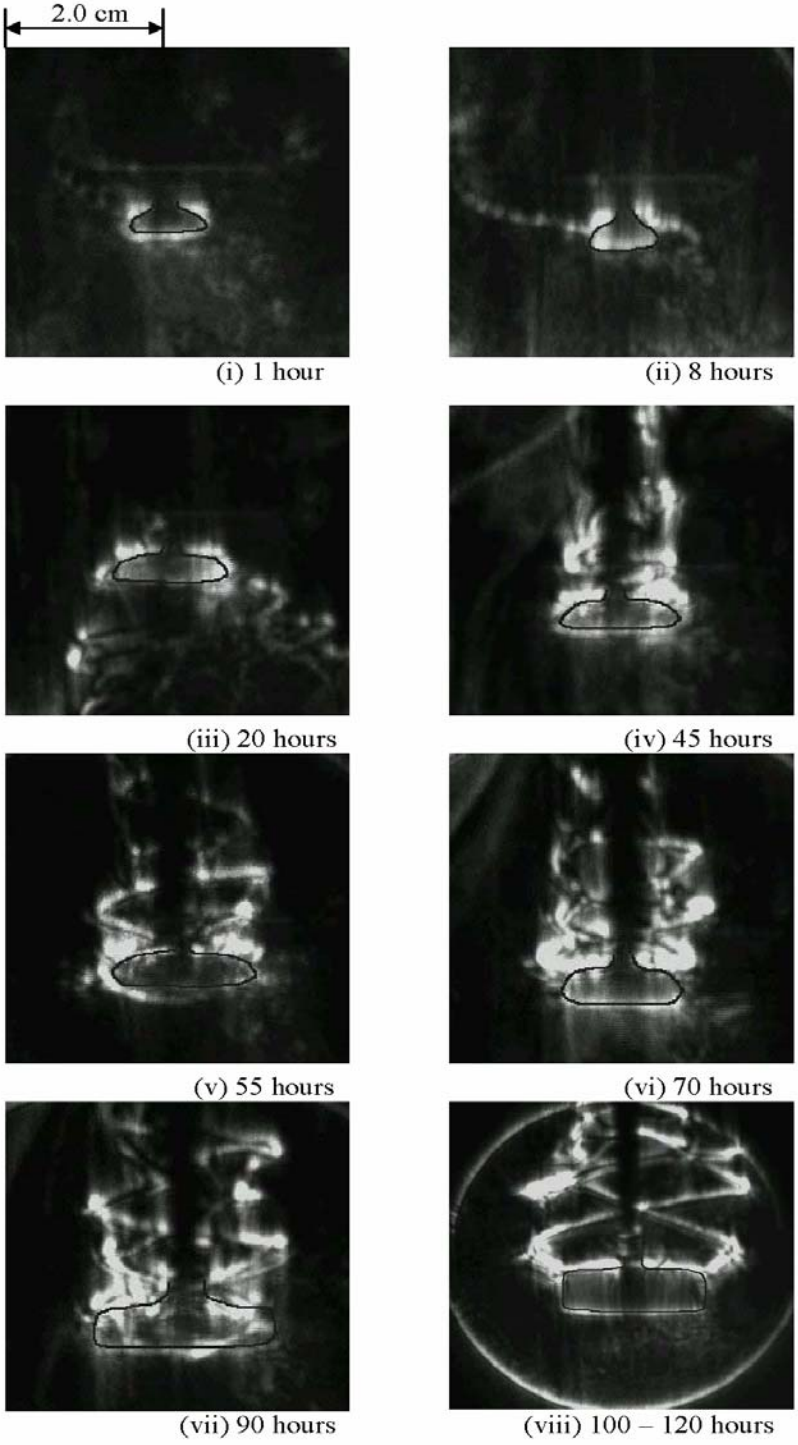

Figure 20. Schlieren images of the transient evolution of the convective field around a rotating crystal growing from its aqueous solution. (Ramp rate=0.05^{o}C/hour, rate of crystal rotation = 15 rpm).

Figure 19 shows the sequence of convection patterns in the purely buoyancy-driven mode. Growth in the initial stages of the experiments is accompanied by steady, weak convection, during which diffusion effects can be expected to be significant. Thus, for $t \leq 20$ hours, a slow growth of the crystal is to be expected. Concentration gradients are primarily localized in the vicinity of the growing crystal. With the passage of time, the size of the crystal increases, and the gradients grow in strength. This result is brought out in the schlieren images as an increase in the light intensity around the crystal. As defined by the bright region, the resulting flow creates a strong plume directly above the growing crystal. Over a longer period of time (20-90 hours), the plume structure remains unchanged. It indicates a stable growth regime for the crystal, where the buoyant plumes are steady and uniform in nature (Figure 19(v-vii)). A gradual evolution of the concentration gradients and the associated buoyant plumes ensure a relatively uniform concentration field in the vicinity of the growing crystal, thus leading to symmetric growth of the crystal at the greatest possible rate. As the crystal increases in size, the convection currents grow in strength. Beyond 90 hours, they are seen to become quite vigorous (Figure 19(viii)). Correspondingly, time-dependent movement of the plumes was seen in the experiments. This stage is characterized by local changes in the concentration gradients in the vicinity of the growing crystal, followed by a breakdown in the symmetry of the growth process. It is a limit on the time duration up to which a single growth experiment can be carried out in free convection regime, and the consequent limit on the size of the grown crystal.

The intensity contrast in the images of Figure 19, as well as their average intensity progressively increases with time, indicating a depletion of the salt in the aqueous solution. For long times, a stable stratification in density (and hence salt concentration) was obtained in the growth chamber [44]. The rate of increase of the crystal size was negligible at this stage.

Figure 20 shows the transient evolution of the convective field around a rotating crystal when the rpm is 15. The first image (Figure 20(i)) shows the existence of a diffusion boundary layer around the surfaces of the seed crystal, as seen by the almost uniform distribution of intensity all over the growing faces. After a growth period of about 10 hours, the gradients near the crystal increase in strength. There is a tendency for the plumes to rise vertically, demonstrating that buoyancy forces are larger than centrifugal, on an average. Unlike the schlieren images in Figure 19 where the buoyant plume moved almost symmetrically along the seed holder over a considerable part of the growth phase, the images shown in Figure 20(ii-iii) reflected temporary unsteadiness in the experiments and asymmetric behavior of the convection currents on either side of the crystal. The unsteadiness can be attributed to two factors: (a) temporary unsteadiness in convection due to the development of prismatic faces from the seed crystal, and (b) the dominance of centrifugal force over the buoyancy force due to crystal rotation, causing the convection currents to be pushed sideways (Figure 20(iii)). At all subsequent time periods, the combined effect of buoyancy and rotational forces govern the overall orientation and movement of the convection currents. As the crystal size increases, relatively stronger convection currents rising upwards due to buoyancy lead to stronger concentration gradients near its surfaces. The effective movement of the fluid particles is along a helical path, seen in Figures 20(iv-vii), but most clearly in Figure 20(vii). The width of the helical structure of the rising plumes scales well with the horizontal dimension of the growing crystal. The increasing strength of buoyant convection is evident from the vertical extent upto which the well-defined helical shape is preserved above the crystal. For example, the respective images for 45 hours (Figure 20(iv))

and 55 hours (Figure 20(v)) show a breakdown of helical structure in the central region between the upper face of the crystal and the free surface of the solution. Helical symmetry is preserved for the greatest vertical extent (i.e., the distance between the crystal and the free surface of the solution) during the time interval of 90-120 hours (Figures 20(vii-viii)). Hence, at a certain level of supersaturation and crystal size, a delicate balance exists between the rotational and buoyancy forces. The balance provides a geometric pattern to the plume, and hence favorable conditions required for the growth of good quality crystals from their aqueous solution is obtained. This particular phase of the growth process can be termed as the stable growth regime in which the crystals of highest transparency and symmetry can be grown. Unlike the growth process in purely buoyancy-driven mode, rotation enforces homogenization of concentration gradients around the crystal over the longer duration of experimental run time. Therefore, the possibility of solute stratification as observed in Figure 19(viii) (and at later times) is delayed.

Figure 20 shows that the convection regime is purely forced for short time, and is governed by crystal rotation (< 8 hours). The stirring effect is to be seen by the streaks of light in the image that spread out deep into the solution. Between 8 and 20 hours, the spread becomes narrower, as buoyancy forces re-direct the plume in the vertical direction. For times greater than 45 hours, the plumes show a swirl component, but are vertically directed. The relative importance of rotation and gravity is governed by the ratio of buoyancy and centrifugal forces. The force ratio can be shown to be proportional to the crystal size [2, 71]; hence buoyancy is the guiding force at later times, when the crystal has become large. However, rotation provides a kinematic condition for fluid motion (in the form of a boundary condition), causing the buoyant plumes to become helical, and hence structured.

Figure 21 shows the concentration contour maps (normalized between 0 and unity) around the growing crystal for 0 and 15 rpm. The value of C=0 represents the saturated state, with C=1 being the supersaturated condition at the temperature of the solution in the growth chamber. The maximum crystal size grown in each experiment has been used to non-dimensionalize the x and y coordinates. In the following sections, the normalized concentration gradient is based on the ratio of the maximum concentration difference and maximum crystal size. The contours in Figure 21(a), corresponding to zero rotation, indicate an almost uniform and symmetric distribution of solute in the growth chamber, both near the crystal and in the bulk of the solution for $t \leq 45$ hours. The contours shown in Figure 21(b) also reflect a similar trend over the comparable time period ($t \leq 55$ hours). Initially (t=1 hour) the contours are localized in the vicinity of the crystal surfaces, with the bulk of the solution being at the supersaturated state (C=1). This phase of the experiment corresponds to the growth process with transport across a diffusion layer, and correlates well with the schlieren images shown in Figure 19 where there is no well-defined upward movement of the buoyant plume. The effect of rotation of the growing crystal can be clearly seen in the contours shown for $1 \leq t \leq 55$ hours, for locations below the crystal (y=0). While those shown in Figure 21(a) (purely buoyancy-driven) depict a larger spread in the upward direction along the seed holder, contours corresponding to 15 rpm are relatively flat. Thus, a uniform distribution of solute is indicated in the solution in the presence of rotation, owing primarily to a mixing action. The vertically rising plume is narrower in the presence of rotation, but broadens with time. At t=45 and 90 hours, Figure 21(a) shows a slight breakdown in symmetry of the concentration contours below the crystal, with respect to the seed holder, though the plume maintains

symmetry. Rotation, on the other hand, enforces a better symmetry to the concentration distribution around the crystal. This is clearly visible at 55 hours in Figure 21(b). At 100 hours, the plume is strongly influenced by buoyancy and is as broad as in the case of no rotation. The swirl flow pattern superimposed on buoyant flow by crystal rotation imparts anti-symmetry to the iso-concentration contours. This pattern continues to represent a new form of symmetry for the growth of good quality crystals.

At t=20 hours, an asymmetric set of contours is seen in the region below the growing crystal. This temporary asymmetry in the concentration contours is in agreement with the corresponding schlieren image shown in Figure 20(iii). It is related to the joint influence of buoyancy and rotation. At other times, either rotation or buoyancy predominates, and symmetry in the concentration distribution is restored.

The growth rate of the crystal is related to concentration gradients, rather than concentration alone. This aspect is explored in Figure 22. The variations of the dimensionless concentration gradients averaged over each of the three different faces of the growing crystal (left <001>, right <001> and base <100>) with respect to experimental run time are shown in Figure 22(a) for 0 and 15 rpm. As expected, left-right symmetry of the crystal is realized in growth with and without rotation. The effect of rotation is to lower the overall concentration gradient when compared to that generated by buoyancy alone. The gradients on the lower face are small in comparison to the sides. On the lower face, density stratification is stable and buoyant motion is inhibited. The effect of rotation is then to increase the gradients here by inducing fluid movement. Evolutionary profiles on the top face of the crystal are not shown, since the image is adversely influenced by the presence of the seed holder.

In the purely buoyancy-driven experiment, the gradients on the side faces grow in strength with time, whereas the gradients along the lower face are small. The increase in the gradients on the side faces is consistent with the corresponding high intensity regions in the schlieren image sequence shown in Figure 19. The problem of high concentration gradients during the later stages of experiments (t≥60 hours) and also a significant difference in the relative distribution of these gradients over sides and lower faces of the growing crystal is seen to be overcome by rotation. The effect of rotation in equalizing the strength of the gradients over the three faces of the crystal is indicated by the proximity of the gradient profiles in Figure 22(a). Figure 22(b) shows the horizontal growth of the crystal with respect to the experimental run time. The growth rate with rotation is slightly lower when compared to that based on buoyancy alone; it is however practically linear. The growth rate with crystal rotation is comparatively lower because of two factors: (a) the lowering of concentration gradients in the vicinity of the growing crystal due to homogenization of the solution induced by crystal rotation, and (b) the rotation of the crystal introduces a radial (outward) velocity component that inhibits the transport of solute to its growing surfaces. Figure 22(c) shows photographs of the grown crystals for the two cases. The size of the finally grown crystal (after 90 hours) is larger in buoyancy-driven convection, but the crystal quality is superior in terms of transparency when growth is accompanied by rotation.

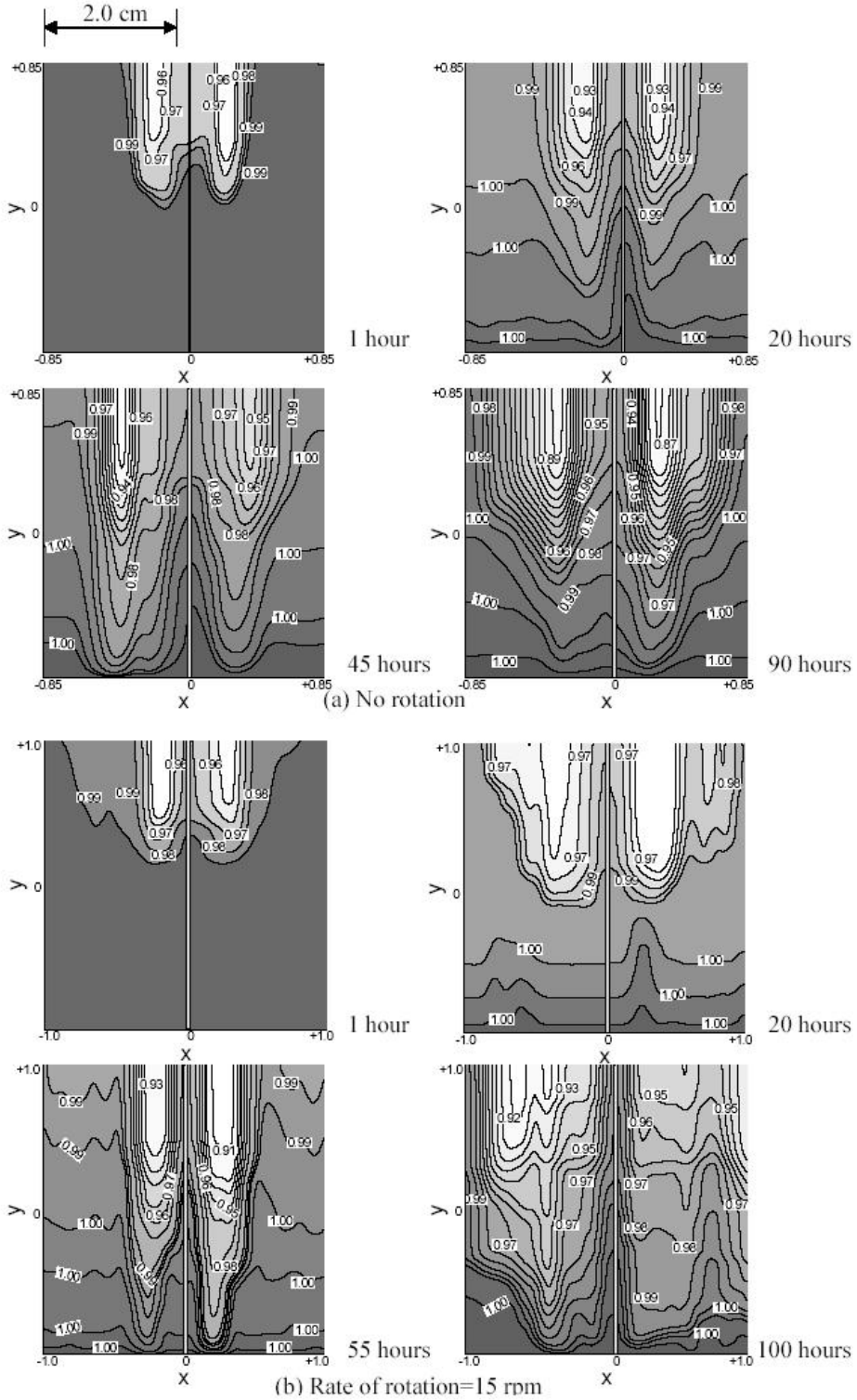

Figure 21. Concentration contours around a growing crystal with the passage of time with and without crystal rotation. The central vertical filled band in each plot represents the seed holder. (Ramp rate=0.05^{o}C/hour).

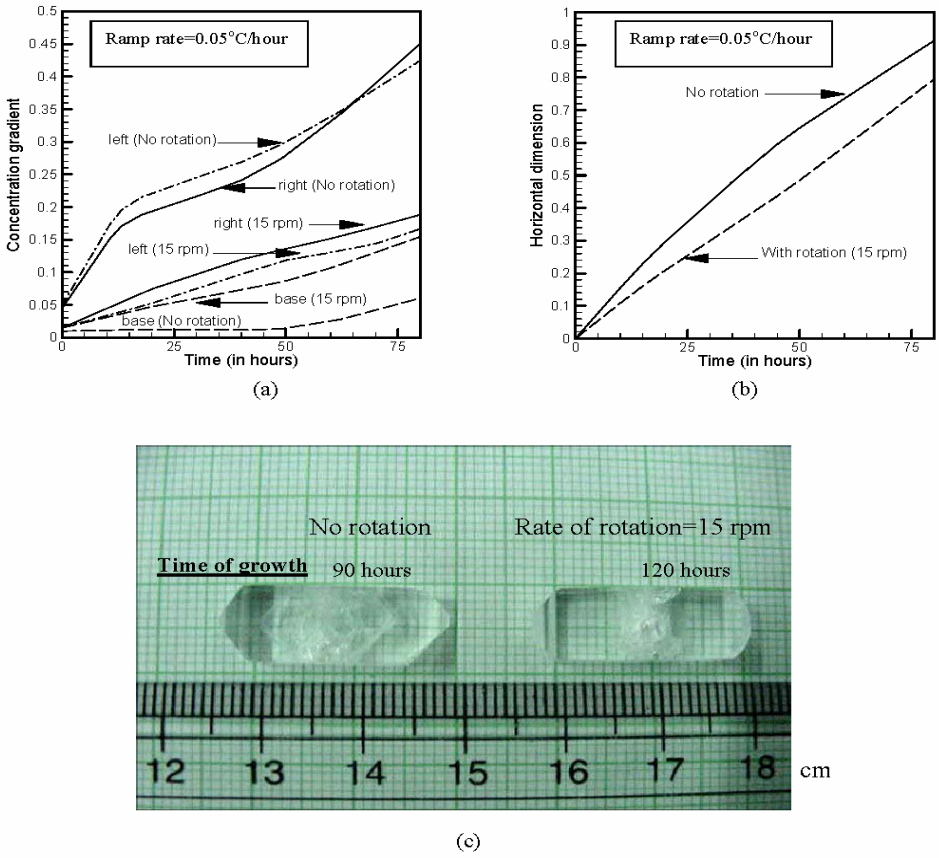

Figure 22. (a) Variation of normalized concentration gradients near the three faces of the growing crystal, (b) horizontal growth of the crystal relative to its maximum size as a function of time, and (c) photographs of grown crystals with and without crystal rotation. (Ramp rate=0.05°C/hour).

9.2.2. Ramp Rate of 0.1°c/Hour

When the ramp rate is increased, the amount of salt that is held in the supersaturated solution increases. The consequence is a greater driving potential for buoyant convection. There is an outer limit to the degree of super-saturation of the solution, though it was not reached in the present study. The growth process of a crystal when the solution is cooled at a higher ramp rate of 0.1°C/hour is discussed in the present section.

Figure 23 shows the transient evolution of the convective field in a purely buoyancy-dominated growth regime (0 rpm, 23(a)) and under the combined effects of buoyancy and rotation of the crystal (15 rpm, 23(b)). In comparison to the sequence shown in Figure 19 (ramp rate=0.05°C/hour, 0 rpm) the region in the vicinity of the growing crystal reveals a bright intensity distribution, indicating larger concentration gradients in the buoyancy-driven regime. The spread of the bright patch at t=1 hour shows that fluid motion has set in quite early. Thus, even the initial growth is not diffusion-controlled. The buoyancy-driven fluid motion is more vigorous at the higher ramp rate, leading to a greater vertical spread of the depleted solution, and a narrower plume. A clear movement of the buoyant plumes on either sides of the seed holder can be seen at t=35 hours in Figure 23(a), whereas at a comparable time instant, weak convection currents were observed at a lower ramp rate of Figure 19.

Schlieren images in Figure 23(a) show well-defined, strong buoyant plumes that transport solute from the bulk of the solution to the crystal surfaces at a faster rate. Consequently, the crystal size at 65 hours in Figure 23(a) is larger than that at 90 hours in Figure 19. Rotation of the growing crystal tends to diminish the high concentration gradients in the growth chamber. It is clearly seen from the schlieren images shown in Figure 23(b) for $t \leq 25$ hours. In contrast to pure buoyancy, the convection currents do not rise vertically upwards; instead they are dispersed in the solution as they are determined by the combined effects of buoyancy and rotational forces (Figure 23(b), t=25 hours). The sizes of the crystal and the convection pattern in the mixed regime (when rotation and buoyancy are of comparable magnitude) are similar in Figures 20 and 23(b). Furthermore, lower concentration gradients due to the homogenization of the solution are reflected by the weak intensity contrast in Figure 23(b) in comparison to that in Figure 23(a).

As the crystal size increases, vigorous convection currents in the solution due to buoyancy result in steep concentration gradients around the crystal (Figure 23(a), t=65 hours). In the presence of rotation (Figure 23(b), t=50 and 80 hours), the plumes orient themselves in the vertical direction, showing that buoyancy predominates over rotation. However, the flow field is clearly disorganized, leading to the appearance of light streaks that are smeared in the horizontal direction by the circulating flow. There is a considerable loss of symmetry in the concentration field at all time instants. At t=80 hours, the higher ramp rate removes a considerable amount of solute from the solution, leading to density stratification in the growth chamber (Figure 23(b)). Rotation has no impact on the concentration field at this stage.

In the presence of rotation, the influences of a lower and a higher ramp rate can be discussed as follows. In the former experiment, rotation imparts symmetry of the solute distribution, diminishes the gradients, the crystal growth rate and results in crystals of better transparency. In the latter, rotation has a less significant role. The solute distribution is homogenized, but there is no improvement in the symmetry of the concentration contours. The crystal growth rates remain high and the solution is density stratified in a shorter period of time. The growth of the crystal is halted at this point. The above discussion shows that for a given ramp rate, a judicious choice of crystal rotation can lead to an enhanced crystal quality, though a slower growth process.

Figure 24(a) shows the evolution of concentration gradients on the faces of the growing crystal for a ramp rate of 0.1^{o}C/hour. In the purely buoyancy-driven growth regime, the gradients on the side faces of the crystal progressively keep increasing. Thus, very high concentration gradients are obtained towards the late stages of growth. On comparing with the corresponding variation of concentration gradients with time in Figure 23(a), the effect of higher ramp rate of the solution can be clearly understood. The maximum non-dimensional value of concentration gradient for the ramp rate of 0.1^{o}C/hour is around 0.55 observed at t=60 hours. For the lower ramp rate (0.05^{o}C/hour), the corresponding value is 0.45 after 80 hours. To some extent, rotation lowers the monotonic increase in the concentration gradients in Figure 24(a), and improves the left-right symmetry. The difference is on the lower side, where rotation further diminishes concentration gradients, in comparison to growth without rotation. This result is the reverse of what is seen in Figure 22(a). The large gradients on the side faces, and low gradients on the horizontal faces leads to high growth rates of the horizontal dimension of the crystal (Figure 24(b)), that is relatively insensitive to rotation. The quality of the grown crystals (Figure 24(c)) is inferior in transparency to that obtained with a lower ramp rate (0.05^{o}C/hour) that is shown in Figure 23(c).

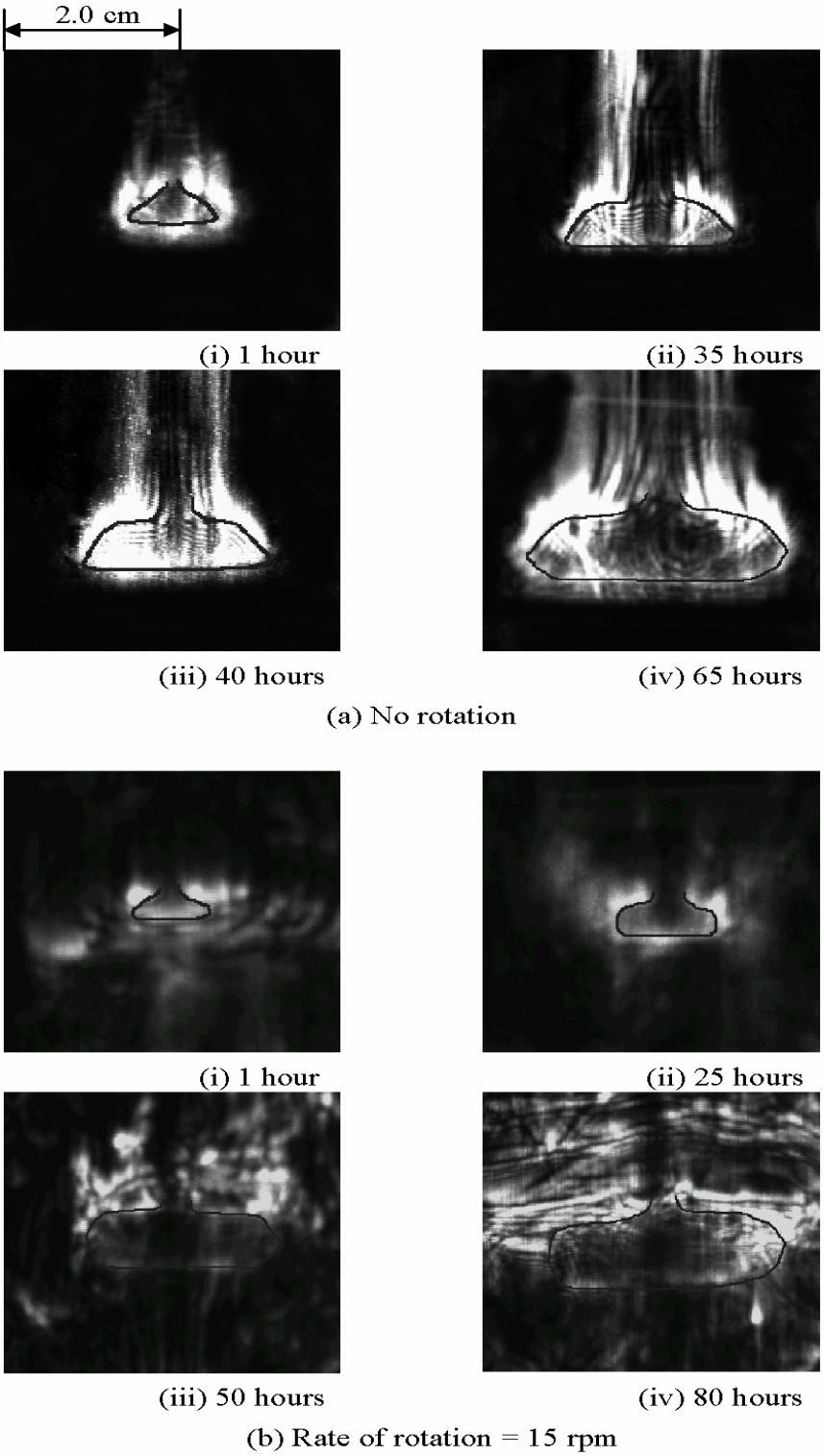

Figure 23. Schlieren images of the transient evolution of the convective field around a KDP crystal growing from its aqueous solution with and without crystal rotation. (Ramp rate = 0.1^{o}C/hour).

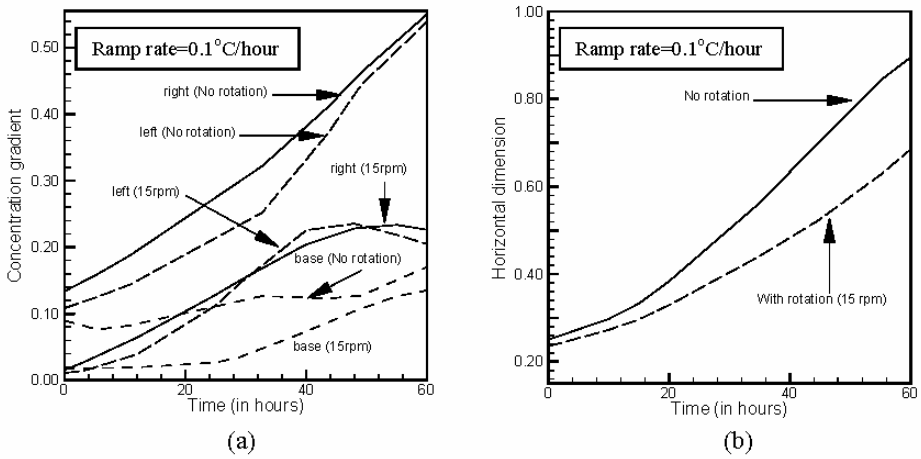

(c)

Figure 24. (a) Variation of normalized concentration gradients near the three faces of the growing crystal, (b) horizontal growth of the crystal relative to its maximum size as a function of time, and (c) photographs of grown crystals with and without crystal rotation. (Ramp rate=0.1°C/hour).

9.2.3. Effect of Crystal Size

In the above sections, it is seen that the crystal growth rate is positively correlated with the local concentration gradients. The gradients in turn depend on the size of the crystal, ramp rate and the rate of rotation. It is of interest to know if the gradients are explicit functions of time. An absence of time-dependence would show the process to be quasi-steady, and the results obtained in the present work would be applicable with greater generality.

To test the experimental data for the presence of growth history and inertia effects, the following experiments were performed: Previously grown crystals of small, medium and large sizes were suddenly inserted into the supersaturated solution. The solution was subjected to cooling at the prescribed ramp rate (of 0.1°C/hour). The short time convection currents around a passive crystal have been compared with those that evolve gradually around a growing one when the growth process takes place from a seed, for a longer duration of time

(~ 60-70 hours). A favorable comparison in terms of convection patterns is an indicator that the concentration gradients respond directly to the process parameters, and are not explicit functions of time.

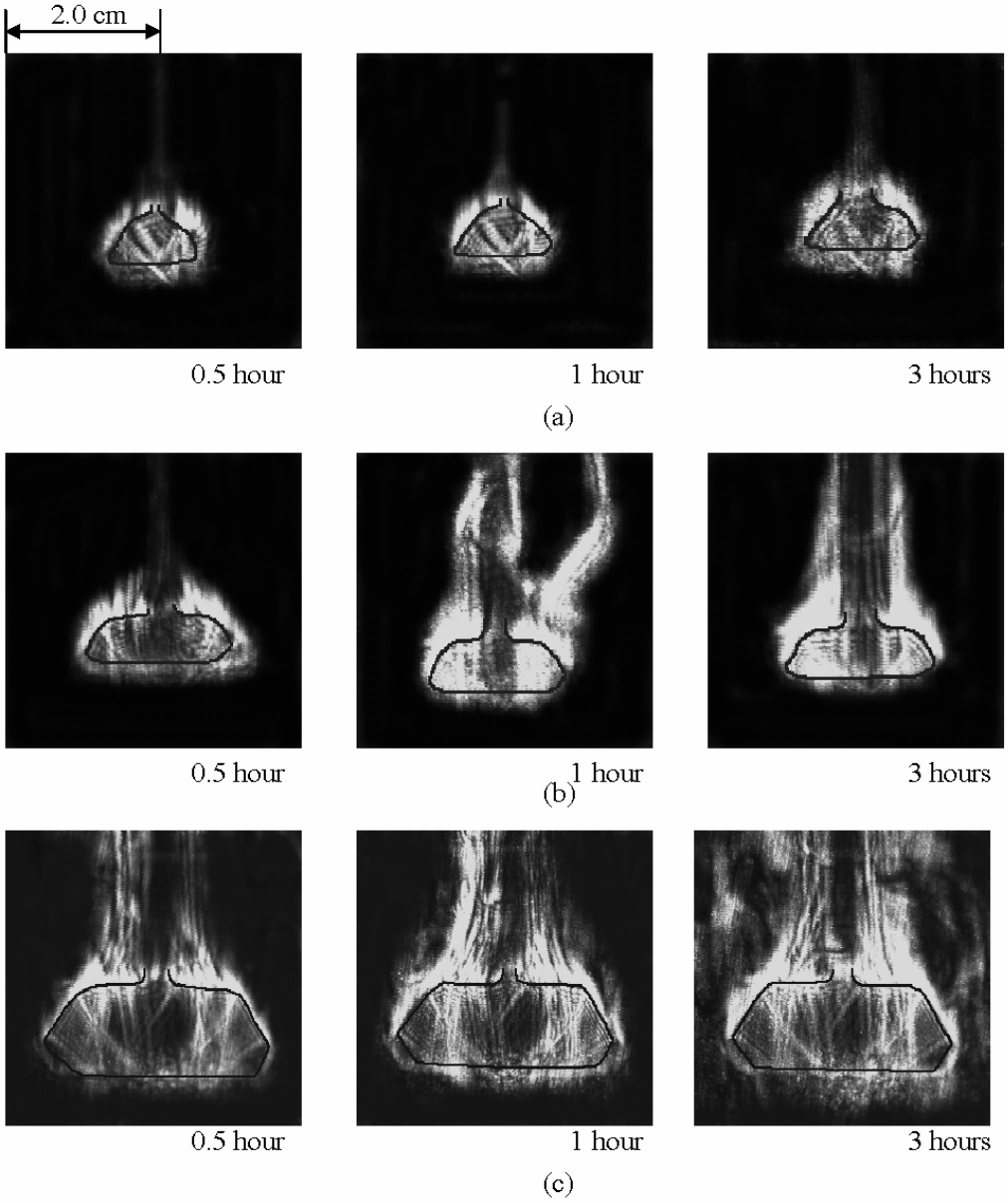

Figure 25. Schlieren images showing the instantaneous evolution of buoyancy-driven convection currents in the growth chamber when a crystal of (a) small, (b) medium and (c) large size is inserted into its supersaturated solution.

Figure 25 shows instantaneous schlieren images of buoyancy-driven convection around the crystal of varying sizes (small, medium and large) over duration of 3 hours. Compared to the time durations generally required, this is a small time scale. Figure 25 shows that short

time transients are indeed present in the solution, but they decay within a time frame of three hours for the three sizes considered. Over this time frame, the change in the crystal size was found to be negligible. Figure 25 shows that the strength of convection is weaker during the transient phase, and is the most vigorous when steady state appropriate for the size of the crystal is reached. The convection plumes during the transient phase can be unsteady and unsymmetrical. The loss of symmetry is related to the imperfections in the initial crystal geometry. The unsymmetrical plume is responsible for inducing flow unsteadiness above the crystal. With the passage of time, minor imperfections of the crystal are accommodated and the plume becomes symmetric as well as steady. The schlieren images in Figure 25 recorded at the end of 3 hours of experimentation correlate well with those shown in Figure 23. The similarity of buoyant plumes in the two configurations reveals that the long-time crystal growth process is indeed quasi-steady. Figure 25 also shows that departure from quasi-steady growth conditions can result in loss of symmetry and unsteady plume movement, both of which are undesirable from the view-point of crystal quality.

9.2.4. Competing Mechansims In Convection

The relative importance of buoyant convection over rotation is discussed in the present section in fundamental terms. Essentially, the increase in crystal size takes place owing to the deposition of excess salt in the solution on the crystal faces. The speed at which the deposition occurs is proportional to the gradients in solutal concentration prevailing in this region. The gradients in turn depend on the pattern of fluid motion in the crystal growth chamber. The influence of fluid motion on concentration gradients can be explained in terms of solutal boundary-layers (*diffusion boundary-layers*) adjacent to the crystal faces. The boundary-layer thickness decreases as the fluid velocity increases. Clearly vigorous convective motion will increase concentration gradients, ultimately leading to a rapid increase in crystal size.

The conditions under which flow is intensified can be understood in terms of the forces acting on the fluid particles. For the solution contained in the beaker, the external force arises from buoyancy (in a gravitational field), while inertia forces related to linear and rotational acceleration are also present. The motion, in all situations is retarded by fluid viscosity. The forces are conveniently explained in terms of the dimensionless parameters Ra, the Rayleigh number Ra and Re, the Reynolds number. As discussed in Section 4.1, Rayleigh number denotes the ratio of energy available in a buoyancy field and energy required to overcome viscous forces. Reynolds number is a ratio of rotational and viscous forces. These parameters are respectively defined as [2, 71]

$$\mathrm{Ra}=g\beta\Delta C L^3/\nu\alpha; \quad \mathrm{Re}=\omega L^2/\nu$$

Here, g is acceleration due to gravity and β is the volumetric expansion coefficient of the solution with respect to salt concentration (=0.1 per mol). Further ΔC is the concentration difference between the saturated (density 1.1717 gm/cm^3) and super-saturated solution, L the crystal thickness in the vertical direction, ν the kinematic viscosity (=1.073×10^{-6} m^2/s) and α the mass diffusivity (1.0×10^{-9} m^2/s). The symbol ω is the crystal rotational speed. In the present set of experiments, the linear dimension L increases with time, till the excess solute in the vicinity of the crystal is fully utilized.

The relative importance of the Rayleigh and Reynolds numbers is defined by the ratio $A=Ra/Re^2$, often called the Archimedes number [2]. When the parameter is far away from unity, Ra (for A>>1) or Re (for A<<1) alone will control the flow. For the ratio A close to unity, one can expect an interaction between the buoyant and rotational force fields. It is reasonable to expect that the critical value of the Archimedes number that defines transition from buoyancy to rotation-controlled flow regimes is geometry dependent. Two and three-dimensional geometries are expected to yield different critical values. In the absence of definite information, A=1 is used in the following discussion as a critical value.

For the experiments conducted in the present work, the Rayleigh number based on the smallest crystal diameter is $10^{4,}$ while based on the largest crystal diameter it is in excess of $10^{6.}$ The corresponding Reynolds numbers range from 0 (no rotation) to 8 (smallest crystal) to 110 (largest crystal). These changes occur primarily because of an increase in the crystal size, but also due to an increase in the concentration difference available in a higher ramp rate experiment. For a small rotating crystal, one can calculate the ratio A=156, while for a large rotating crystal, A=82. Clearly, A>>1 in all the experiments discussed above, and fluid motion is controlled by buoyancy, thus ensuring large-scale circulation in the crystal growth chamber. Rotation plays an important role locally in equalizing solutal concentrations and maintaining stable growth conditions.

The directional nature of gravity imparts certain peculiar properties to the buoyancy field. Specifically, the strength of convection patterns over the horizontal faces of the crystal depends on whether the face is aligned or opposed to the gravity vector. The downward facing surface is stabilized by gravity, experiences weak convection and has the smallest concentration gradients (as seen in Figure 22(a)). At a later point of time, convection in the bulk of the solution drives fluid flow over the lower surface as well, thus increasing the concentration gradients. A second consequence of weak convection is that the influence of rotation is felt strongly even at small time leading to a rapid increase in concentration gradients. This result is once again to be observed in Figure 22(a).

9.3. Tomographic Reconstrcution of Schlieren Data

The question of a correlation between the solutal distribution in the solution and the topography of the crystal can be partially addressed by reconstructing the solute concentration contours on select planes above the crystal. Reconstruction from schlieren images using principles of tomography is discussed in the present section. Unlike the hanging crystal configuration in Sections 9.1 and 9.2, the crystal in the set of experiments was mounted over a platform. With this arrangement, the interference of the rising convection plume with the crystal holder is eliminated. Recording projections requires the apparatus to be turned; in this respect, what is collected is time-lapsed data. For meaningful analysis, it is thus necessary that the convection pattern be steady in time. Only those experiments where this requirement was fulfilled have been included in the discussion.

One parameter that defines the quality of the growing crystal is the symmetry of its faces. Since growth from an aqueous solution is governed by the strength and movement of buoyancy-driven convection currents, the convective field plays an important role in transporting solute from the bulk of the solution to the crystal faces. Hence, to ensure symmetric growth of the crystal, it is necessary to ensure that the convective field in the

growth chamber retains a symmetry pattern. In the present work, a viewpoint that an axisymmetric convective field is favorable for crystal growth has been adopted. Thus, conditions under which the solutal distribution is axisymmetric have been delineated from the tomographic reconstructions.

Results are presented for experiments on crystal growth in the diffusion as well as steady convection regimes. In Section 9.4, results have been presented in the form of a time sequence of schlieren images recorded at four view angles, corresponding to four pairs of optical windows of the growth chamber. The crystal is not disturbed during the growth process. In this respect, the measurement process is truly non-invasive, though with a drawback of allowing only a limited number of projections. The emphasis is towards understanding the diffusion-dominated and the stable growth regimes of the crystal. In both regimes, the concentration field is practically steady, particularly during the recording of the individual projections. The reconstruction of the concentration field over selected planes above the crystal and their relationship to the crystal geometry are discussed. The influence of crystal rotation on the convective field is not covered in the present discussion.

9.4. Convection around a Growing KDP Crystal

Imaging of three dimensional convection patterns around the growing KDP crystal is discussed here. Four view angles are considered for tomographic reconstruction of the concentration field. In the experiments conducted, the crystal is not disturbed during the recording of the projection data. In addition, longer durations of crystal growth have been considered. Since finite time is required to turn the beaker and record projections, experiments have been conducted when the concentration field around the crystal is nominally steady. Occasionally, the plume above the crystal is marginally unsteady, and a time-averaged sequence of schlieren images has been used for analysis. The increment in the view angles is 45^o, covering the range of 0 to 180^o.

The crystal growth process has been initiated by inserting a spontaneously crystallized KDP seed into its supersaturated solution at an average temperature of 35^oC. This step is followed by slow cooling of the aqueous solution. The cooling rate employed is 0.05^oC/hour. The seed thermally equilibrates with the solution in about 20 minutes. With the passage of time, the density differences within the solution are solely due to concentration differences. Adjacent to the crystal, the solute deposits on the crystal faces, and the solution goes from the supersaturated to the saturated state. When the crystal size is small, salt deposition from the solution on to the crystal occurs by gradient diffusion. Diffusive transport has been sustained for a longer duration of time (and larger crystal sizes as well) by maintaining a small degree of supersaturation in the solution.

9.4.1. Growth Patterns in the Diffusion Regime

Figure 26 shows schlieren images of a growing crystal in the diffusion-dominated regime at three different time instants. All four view angles are included in the figure. Adjacent to the crystal the deposition of solute from the solution to the crystal surfaces results in a change of concentration. This introduces a variation in density, refractive index and hence results in intensity contrast. For small time (less than one hour), intensity changes are restricted to the vicinity of the crystal. Here, transport of the solute to the crystal is purely by diffusion. At

later times, a weak convection current is to be seen in the spread of light intensity above the crystal, though diffusion is still the dominant mechanism for solutal transport. For times greater than 70 hours, steady convection was seen to be clearly established in the form of a buoyant plume. In view of the small degree of supersaturation, the origin of convection here is related to an increase in the crystal size, rather than density differences.

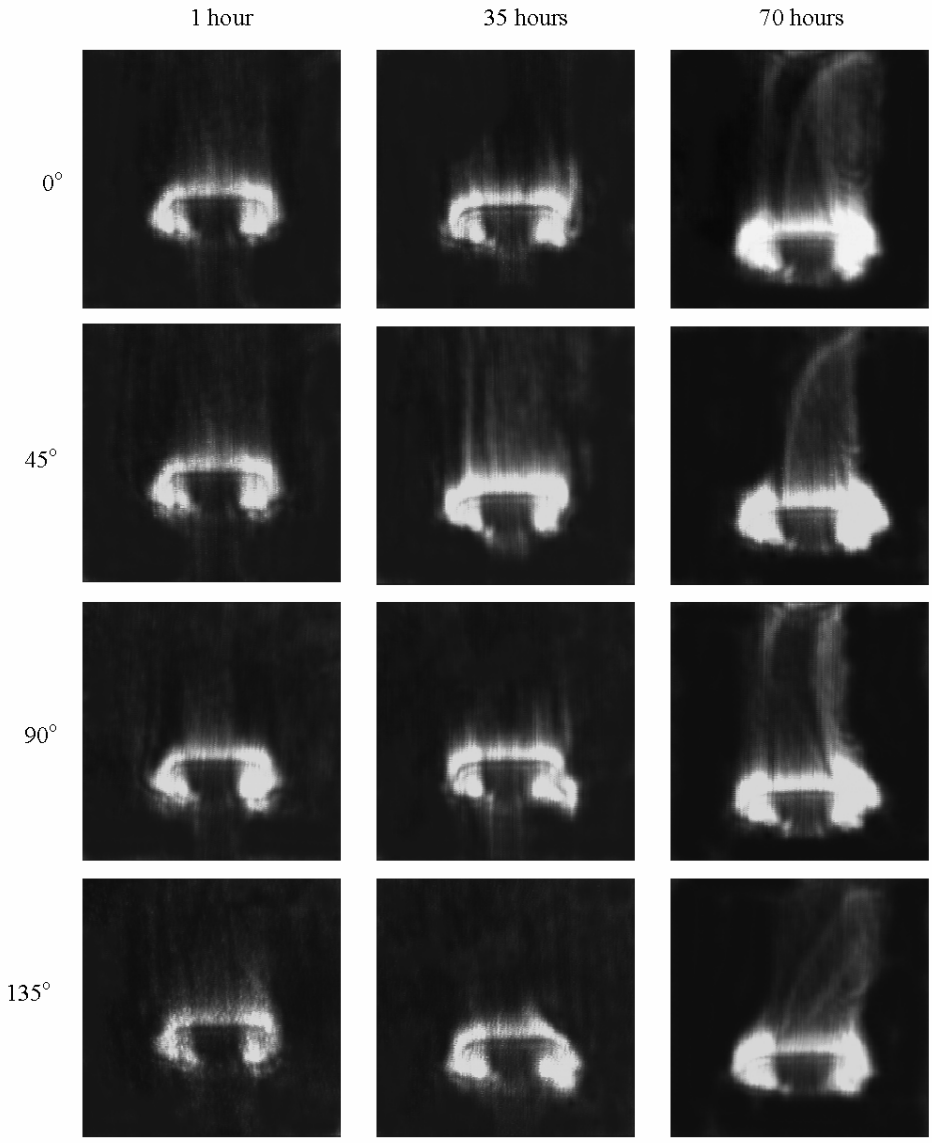

Figure 26. Schlieren images of the convective field around the crystal growing from its aqueous solution in a platform technique at three different time instants recorded from the four view angles are presented.

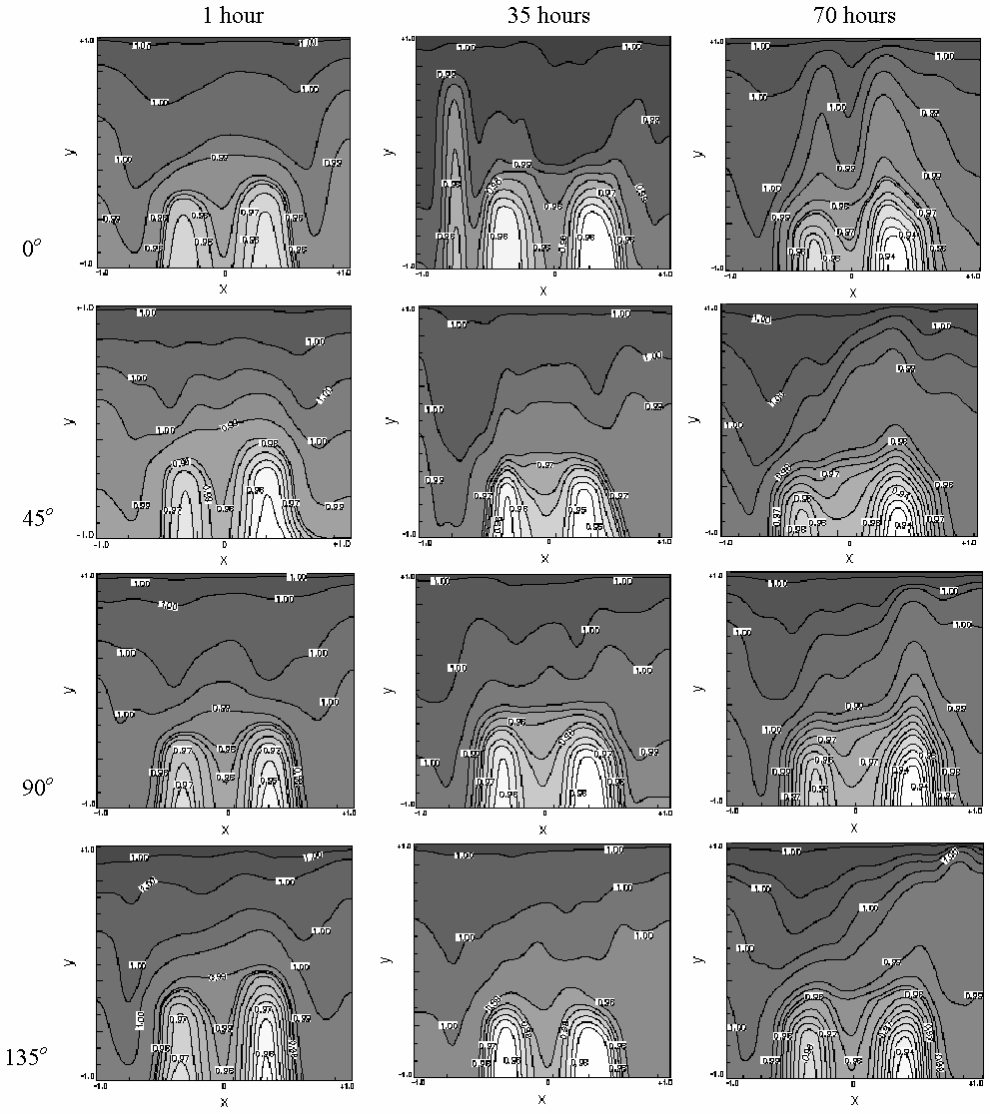

Figure 27. Concentration contours around a growing crystal at three different time instants in a diffusion dominated growth process for the four view angles.

Figure 27 shows normalized concentration maps above the growing crystal as derived from the schlieren images of Figure 26. The value of C=0 represents a saturated solution, while the limit C =1 refers to the supersaturated solution at its instantaneous temperature in the growth chamber. The maximum crystal size at the end of each experiment has been used to non-dimensionalize the x and y coordinates. For t=1 hour, the concentration contours of Figure 27 in the bulk of the solution reveal an almost symmetric solute distribution. Symmetry can also be gauged by the identical nature of contour distributions for each view angle. The contours are not densely spaced, indicating low concentration gradients. The contours are localized in the vicinity of the crystal, with the bulk of the solution being at the supersaturated state (C=1). Hence this phase of the experiments corresponds to the growth process with transport across a diffusion boundary layer attached to the crystal. With the

passage of time, the crystal size increases and the concentration gradients increase in strength. At this stage, the concentration field is accompanied by a partial loss of symmetry. Experiments of the present study revealed a marginal unsteadiness as well. This phase defines a transition process from diffusion-dominated transport of solute to the onset of convection. With the passage of time, a weak convection current is set up around the crystal. The images recorded at t=70 hours also show a greater loss of symmetry in the concentration contours and a denser spacing closer to the crystal are to be seen.

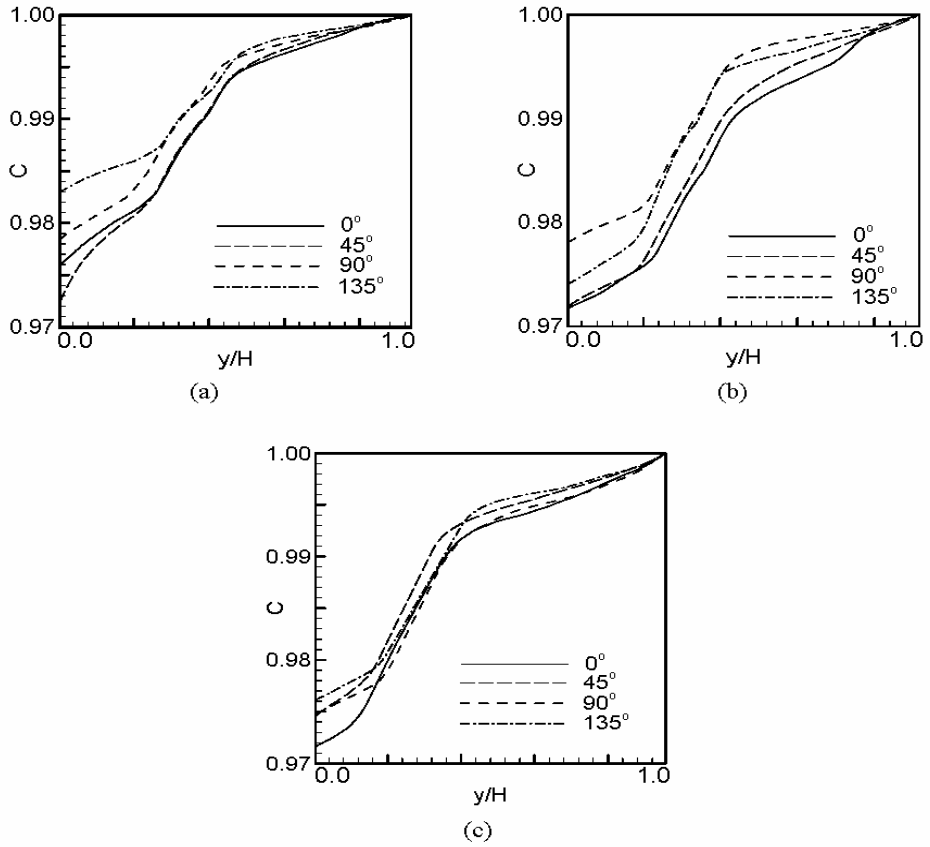

Figure 28. Width-averaged normalized concentration profile as a function of vertical coordinate for the diffusion-dominant crystal growth. Time elapsed (a) 1 hour, (b) 35 hours and (c) 70 hours.

Figure 28 shows the variation of concentration with respect to the (vertical) y-coordinate in the crystal growth chamber. The concentration referred here is an average obtained in the viewing direction of the laser beam and across the image as well. For averaging the concentration values in the x-direction, namely normal to the light beam, 11 columns along the width were selected. The concentration profiles for t=1 hour (Figure 28(a)) overlap in the bulk of the solution above the crystal for all the four view angles, thus revealing a uniform distribution of solute concentration in this region. At t=35 hours (Figure 28(b)), the differences in the profiles are quite noticeable. These differences can be attributed to the temporary unsteadiness that sets in when a transition from diffusion-dominated growth takes place towards convection. With the passage of time, the profiles become increasingly

symmetric and overlap with each other. The growth now takes place in the presence of an upward rising convective plume (Figure 28(c)). The symmetry in concentration distribution indicates an almost uniform and symmetric deposition of solute onto the crystal surfaces. It is to be noticed that for the three time instants, the profiles show differences in the vicinity of the crystal (y/H=0.0). The morphology of the KDP crystal is pyramidal, as shown in Figure 29 in a photograph of a grown KDP crystal in the diffusion-dominated regime, at the end of 70 hours. The differences in the average concentration near the crystal can be traced to the non-symmetric shape of the crystal as well as large gradients at the crystal edges.

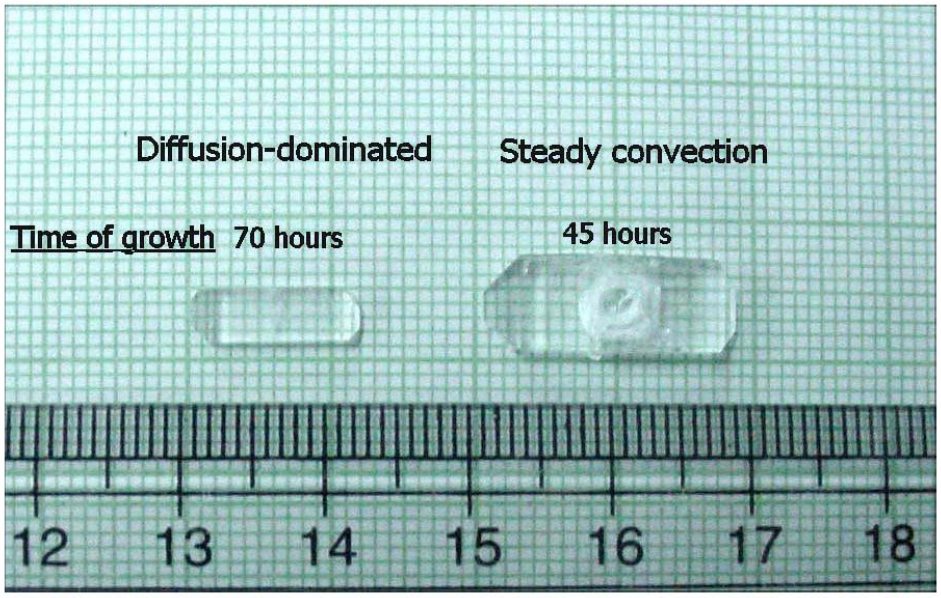

Figure 29. Photographs of as grown KDP crystals in diffusion-dominated (after 70 hours) and stable convection growth regimes (after 45 hours).

Figure 30 shows the concentration profiles reconstructed over five horizontal planes (y/H = 0.05, 0.15, 0.45, 0.60 and 0.90) above the growing crystal. The location y/H = 0.05 is just above the crystal while y/H = 0.90 represents a plane close to the top of the recorded schlieren image. The reconstructions correspond to the images presented in Figure 26. The outer circle represents the periphery of the beaker in which the crystal growth process is conducted. For a given time instant the images become progressively darker away from the crystal revealing the presence of supersaturated solution in the far field. At later times, as well as away from the crystal, the solution closer to the walls of the beaker is seen to be supersaturated, and the field is close to axisymmetric since the concentration contours here are circular. There is a significant departure from axisymmetry in the initial phase of crystal growth, as well as for longer times near the crystal itself. The second factor is explained by the fact that the crystal itself has a pyramidal structure and lacks circular symmetry. In the initial stages of growth, solutal transport is dictated by molecular diffusion from the solution to the crystal surface. Consequently, the lack of symmetry in the crystal morphology is felt on planes away from the crystal itself. At later times, a weak convection plume introduces the symmetry pattern of the

beaker in the solute distribution. Hence, a degree of regularity is seen in the concentration contours, particularly on planes away from the crystal.

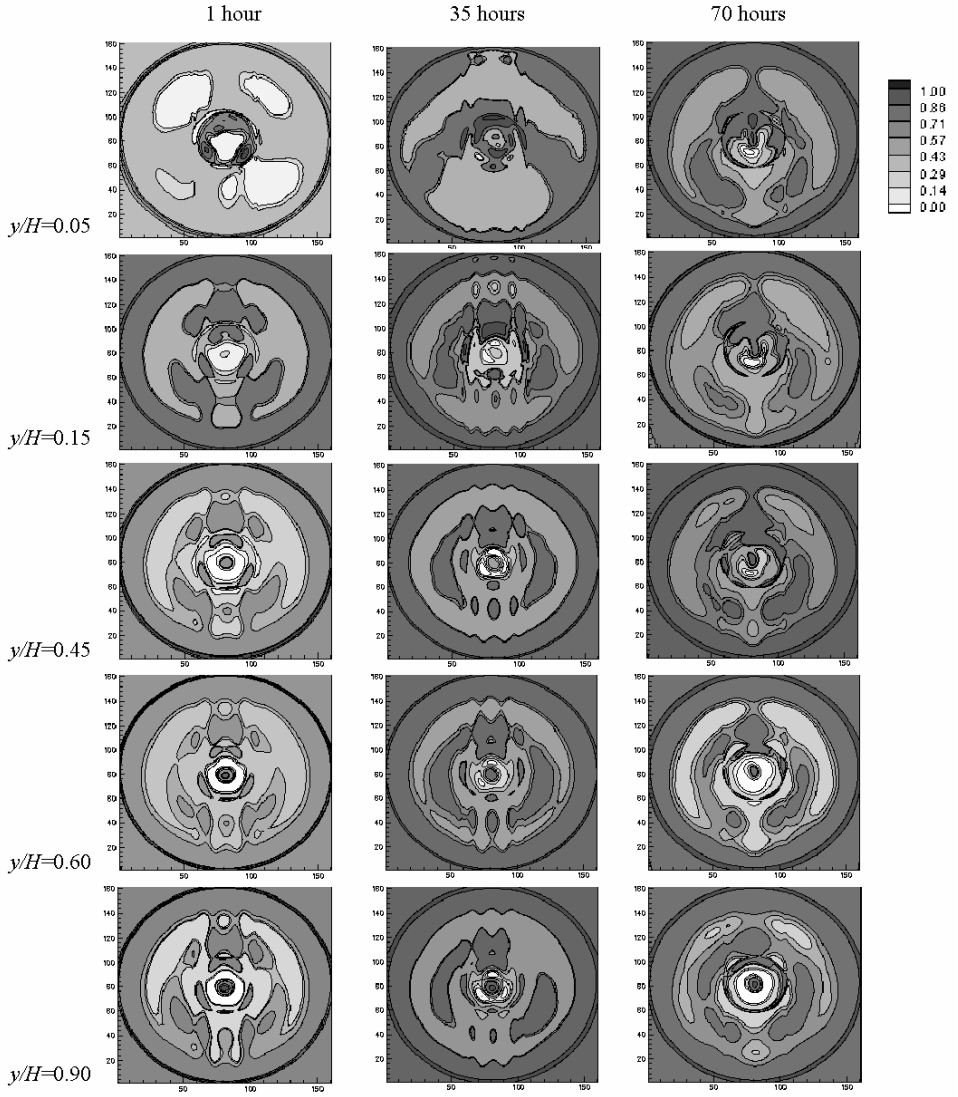

Figure 30. Reconstructed concentration profiles in the diffusion-dominated regime over five horizontal planes covering the range y/H=0.05-0.90, H being the vertical extent of the recorded schlieren image above the growing crystal.

There are several interesting features to be noticed in Figure 30.

1. At the central core of the reconstructed cross-section, the dark shade indicates the presence of a supersaturated solution. The surrounding region is bright, indicative of solution depleted of salt. Thus, the deposition of the salt on the crystal is seen to occur on the periphery of the crystal. This is a region of bright light intensity (Figure

26) and hence high concentration gradients. The relationship between high gradients and preferential growth rates of the crystal faces is brought out in Section 9.2.

2. The concentration contours near the crystal (y/H=0.05 and 0.15) show significant departure from symmetry during the initial stages of the growth process as well as during the transition phase (t=35 hours). The transition referred here is the appearance of a convection plume that is gradually set up around the crystal, resulting in the partial unsteadiness in fluid motion. The loss of symmetry in the reconstruction can be traced to the unsteadiness as well. Symmetry is partly restored on planes above y/H=0.45 at t=35 hours, indicating the influence of uniform solute concentration in the bulk of the solution. For t=70 hours, the convection plume is steady and the reconstructions are better structured closer to the crystal as well (for example, y/H=0.15).
3. The spacing of contours in the central region is smaller for the convection regime, when compared to diffusion. Thus, convection increases the concentration gradients near the crystal, increases the salt deposition rate and hence the overall increase in crystal size (Figure 30). This is possibly the most suitable transport regime for crystal growth.

9.4.2. Growth Patterns in the Convection Regime

Crystal growth from a solution in which the limit of supersaturation has been reached is now considered. The density differences (ramp rate of 0.05^{o}C per hour) as well as the crystal size (6 mm) are jointly large enough to sustain fluid motion in the beaker from the start. Experiments have been conducted under conditions of a steady plume rising from the crystal. Results for 30 hours of growth have been presented. For times greater than 30 hours, the plume became quite unsteady. Consequently, the projection data of individual view angles became uncorrelated.

Figure 31 shows the convective field in the form of schlieren images. A well-defined plume rising from the top surface of the crystal is seen at both times of t=2 and 30 hours for four view angles. At t=2 hours, the plume was temporally stable , though a swaying movement was seen from one projection angle to the other. The swaying motion was due to the disturbance of the flow field caused by the turning of the growth chamber for recording the projection data. The tilt in the plume at selected angles for small time is also related to the non-symmetric shape of the initial crystal itself. At a later time (t=30 hours), the gradients are large enough to give rise to a stable and symmetric convective field. This is accompanied by uniform deposition of the solute on the crystal surfaces. As discussed in Section 9.4.1, this regime yields the highest quality of the crystal in terms of symmetry of the faces and its transparency, along with the fastest growth rate.

Figure 32 shows concentration contours around the growing crystal derived from the schlieren images of Figure 31. The physical extent of the convective plume in the vertical direction can be estimated by the deformation of the concentration contours. Densely placed contours in the crystal vicinity are due to high concentration gradients. The contours at t=30 hours are seen to spread into the growth chamber, indicating that solute from the bulk of the solution itself is deposited over the crystal. The appearance of double peaks in the contour shape at the end of 30 hours confirms that the highest gradients and hence the deposition rates occur towards the edges of the crystal.

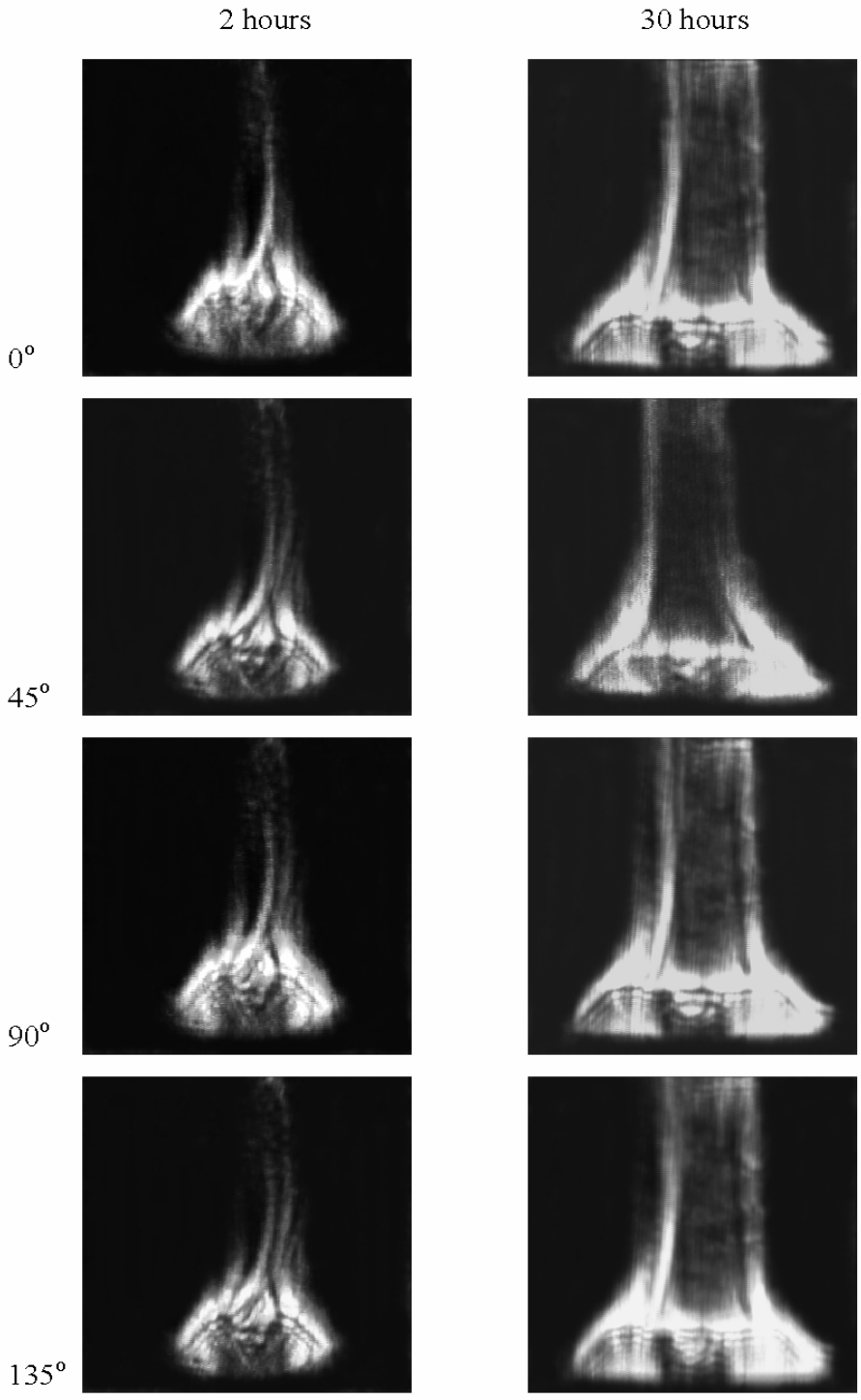

Figure 31. Schlieren images of the convective field around crystal growing from its aqueous solution as recorded from four different view angles at two different times instants (2 and 30 hours).

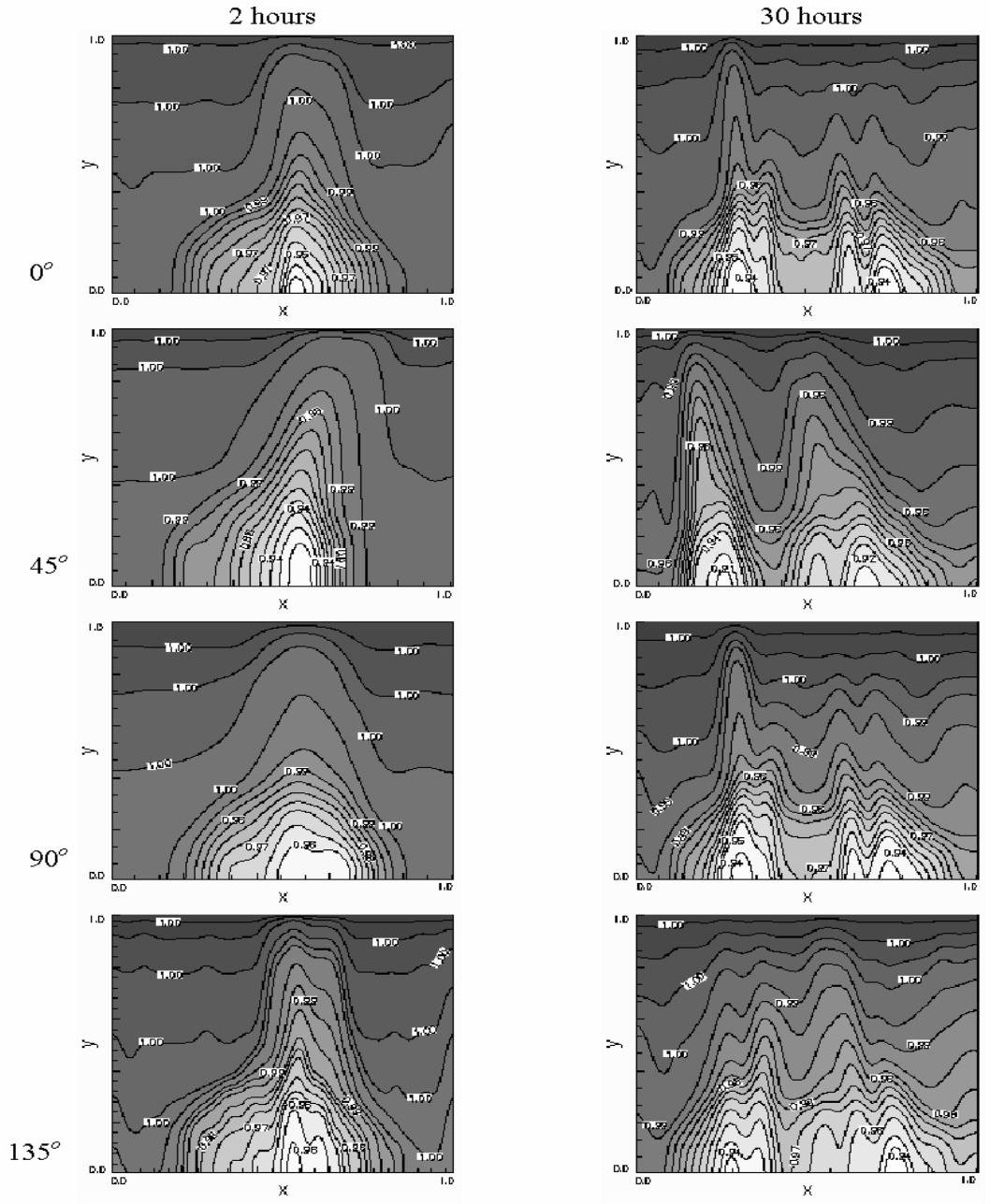

Figure 32. Concentration contours around a growing crystal in the presence of well-defined convective plume for the four view angles at two different time instants.

Figure 33 shows the distribution of width-averaged concentration with respect to the vertical coordinate at two time instants, namely 2 and 30 hours. The concentration data presented in the figure is integrated along the viewing direction by the light beam, and once again across the width of the image. The differences among the individual profiles for each of the view angles are a measure of loss of symmetry in the concentration distribution above the crystal. At t=2 hours, the differences are large in the bulk of the solution ($y/H \geq 0.55$). The

difference diminishes at locations closer to the crystal (y/H=0.0), Figure 33(a). With the passage of time, the convective plume stabilizes in terms of symmetry. The average concentration data corresponding to t=30 hours for the four view angles reveals a good degree of symmetry in the entire field of view above the crystal (Figure 33(b)).

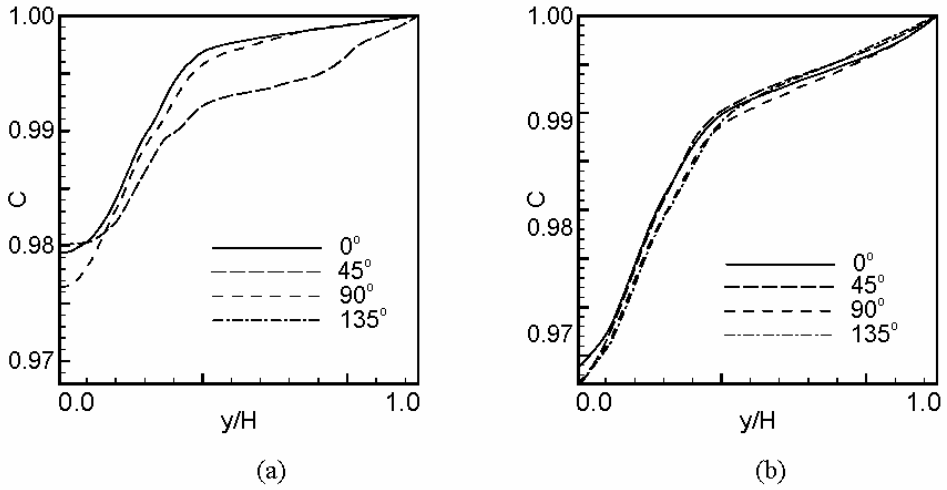

Figure 33. Width-averaged normalized concentration profile as a function of the vertical coordinate around a growing crystal in the stable convection regime after a period of (a) 2 hours, and (b) 30 hours.

Figure 34 shows reconstructed concentration profiles at selected horizontal planes above the growing crystal for the two time instants considered in Figure 31. The following observations can be recorded on the basis of the reconstruction.

1. At t=2 hours, the reconstructed concentration field reveals symmetry for the plane close to the crystal (y/H=0.05) both around the crystal and in the bulk of the solution. The presence of concentric rings indicates uniform distribution of concentration gradients on all the faces of the growing crystal. This feature is seen in Figure 31 as well, where the bright intensity region uniformly envelops the crystal faces. For planes away from the crystal ($y/H \geq 0.30$), the deformation of the concentric rings in the vicinity of the crystal is mainly due to the swaying motion of the convective plume introduced by turning the growth chamber. This movement is also to be seen in the schlieren images of Figure 31. On the other hand, the bulk of the solution closer to the beaker shows uniform and symmetric distribution of concentration. The appearance of only a few contours in the solution shows low concentration gradients here in the initial stages of growth.
2. For all planes (t=2 hours), the presence of a bright central core of the reconstructed cross-section is indicative of the solution depleted of salt. The spatial extent of the bright region at the center of the beaker is small, in agreement with the thin vertically rising buoyant plume above the growing crystal, Figure 31.

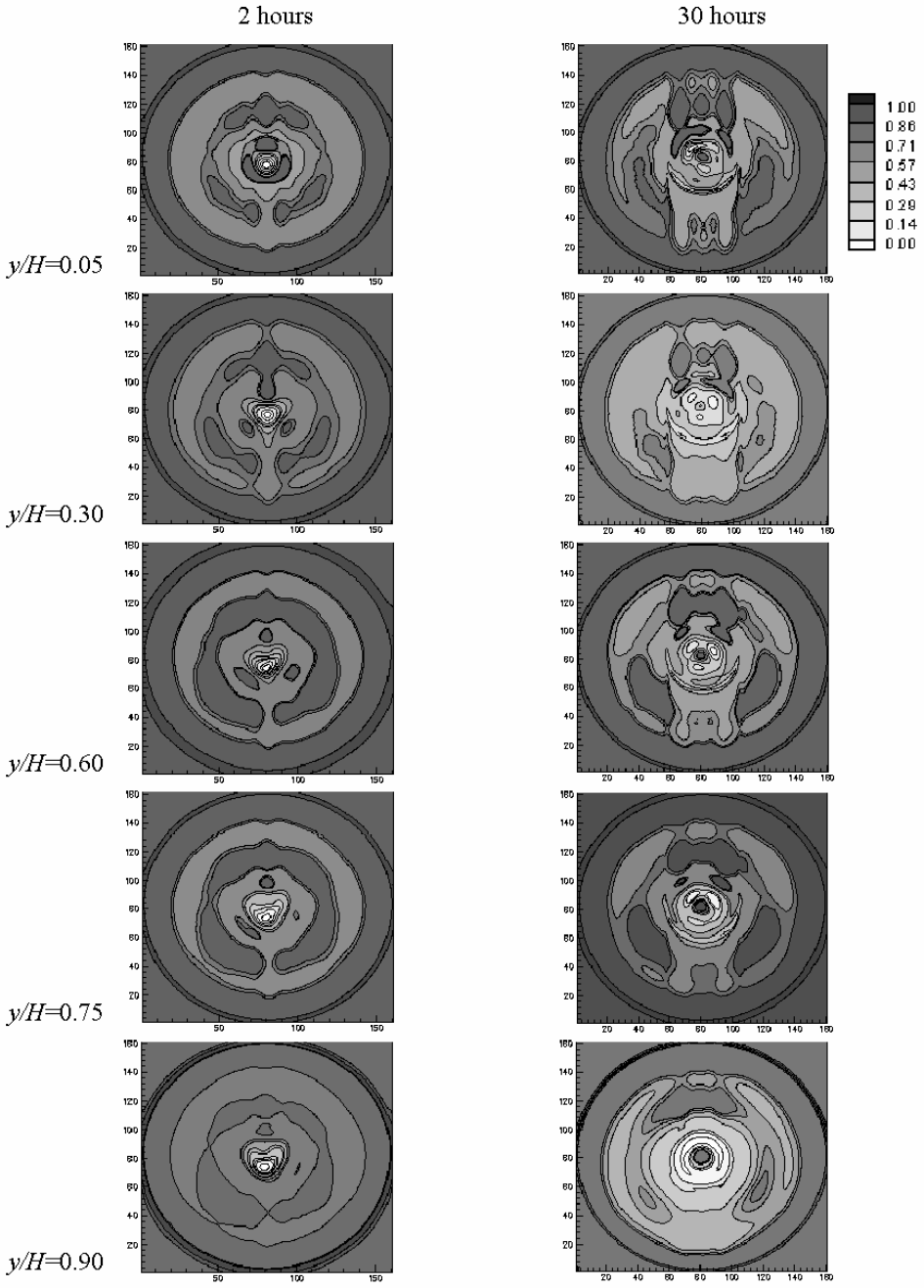

Figure 34. Reconstructed concentration profiles over five horizontal planes (y/H=0.05-0.90) above the crystal growing in the presence of a stable convection plume. Time instants of 2 and 30 hours of experimental run time are presented.

3. At later times (t=30 hours), the concentration field at planes near the crystal ($y/H \leq 0.30$) is not axisymmetric though the bulk of the solution near the boundaries of the growth chamber shows the presence of concentric rings. The loss of symmetry at the center of the reconstructed plane can be attributed to the role played by the

crystal geometry in deciding the overall orientation of convection pattern. The effect of crystal shape is negligible when the size is small (for example, at t=2 hours) but is significant when the crystal grows in size with a well-defined morphology (Figure 29). In addition, densely spaced contours in the core and the bulk reflect the presence of high concentration gradients in the growth chamber.

4. For planes located away from the crystal ($y/H \geq 0.60$), the effect of crystal geometry on the convective field is diminished. The presence of a dark central core (corresponding to a higher level of supersaturation) surrounded by a brighter region shows that high concentration gradients prevail on the crystal sides in comparison to its upper face.

10. CONCLUSIONS

The characterization of convection patterns around a crystal growing from its aqueous solution is the subject of the present investigation. The study has been conducted using three laser measurement techniques that rely on the variation of refractive index with density, and hence the solutal concentration. These techniques have been validated in a thermal buoyancy experiment in a rectangular cavity. Subsequently, they have been used to study convection patterns around the growing crystal for varying process parameters. While images contain line-of-sight averaged information in a vertical plane, the possibility of reconstructing concentration contours on horizontal planes has been studied *via* tomography. Experiments reported in the study show that convection does influence crystal growth rate as well as its quality. The laser measurement techniques succeed in capturing the solutal concentration field (or its derivatives) around the crystal. Hence they can be used for online process control. Specific conclusions arrived at are given in the following sections.

10.1. Comparison of Optical Techniques

Three refractive index-based optical techniques, namely interferometry, schlieren and shadowgraph have been applied to image the convective flow field in a differentially heated rectangular cavity. Air and water have been considered as working fluids. Experiments have been conducted over a wide range of temperature differences. The following conclusions have been arrived at in the present work.

1. In low temperature gradient experiments, all the three techniques correlate well with one another. Interferograms are limited by few fringes in air, and too many fringes in water. The shadowgraph image does not show sufficient contrast for analysis. In this respect, the schlieren technique is most amenable to data reduction.
2. In high gradient experiments, both schlieren and shadowgraph yield clear images. The interferograms are however corrupted by refraction errors. Schlieren and shadowgraph track the temporal response of the fluid medium in the form of the light intensity variation.

3. In high Rayleigh number experiments with water, the flow field is turbulent. Shadowgraph images are seen to be meaningful, as against interferograms and schlieren. They reveal a considerable amount of physical information, including boundary-layers, plumes and time scales.

10.2. Optical Techniques Applied to Crystal Growth

A direct comparison of interferometry, schlieren and shadowgraph in the context of growth of optical crystals from an aqueous solution has been conducted. The three techniques reveal similar trends in terms of the spatial distribution of concentration gradients in the vicinity of the growing crystal. The initial dissolution and unsteadiness, a stable and symmetric growth regime and the final stratification of the solution are brought out. The free convection crystal growth experiment is thus limited in the long run by the localization of high concentration gradients around the growing crystal. The stratification here is stable and suppresses fluid motion. This limits the size of the crystal that can be grown. Based on the ease of instrumentation, image clarity and simplicity of data analysis, the laser schlieren technique emerges as better suited for process control, as compared to interferometry and shadowgraph.

10.3. Influence of Process Parameters on Crystal Growth

The dependence of the convection patterns, concentration gradients and the crystal growth rate on ramp rate, rotation and crystal size is examined. Laser schlieren technique is employed as the measurement tool for determining the concentration distribution in the solution. Major conclusions to emerge from the study are:

1. The stable growth regime of the crystal at 0 rpm comprises of symmetric buoyancy-generated convection plumes. When rotation is imparted to the crystal, the stable growth regime reveals a helical flow path.
2. Buoyancy-driven convection intensifies with increasing size of the crystal as well as the ramp rate. It is ultimately limited by salt depletion and solute stratification in the growth chamber that bring the fluid particles to rest. Crystal rotation diminishes the concentration gradients, equalizes them over all faces, and improves the symmetry of the concentration distribution in the solution. This leads to a crystal of better quality. The rpm of the crystal required to improve crystal quality depends on the cooling rate of the solution.
3. Over the range of parameters studied, the large-scale convection pattern is buoyancy-driven, even when the crystal is rotated.
4. Growth rates of the crystal correlate with the magnitude of the concentration gradients over its individual faces. The gradients in turn respond to the convective field around the crystal.
5. Experiments with crystals of various sizes immersed in an aqueous solution show that the convection transients are short-lived. Thus, the growth process is quasi-steady and can be controlled by adjusting the ramp rate and crystal rotation.

10.4. Three Dimensional Reconstruction

Concentration distribution around a growing KDP on selected horizontal planes is reported. Partial images recorded at various view angles have been analyzed using the convolution back projection algorithm. A suitable extrapolation scheme has been employed to generate information about the entire measurement volume using the partial projection data. The performance of the extrapolation scheme has been assessed by reconstructing the numerically simulated three-dimensional temperature field in an axisymmetric differentially heated fluid layer. Steady crystal growth experiments have been conducted in two regimes that respectively are dominated by diffusion and buoyancy. The following conclusions emerge from the present study:

1. The extrapolation technique used in the present work was seen to perform adequately with simulated data. In particular, no new artifacts were seen even when the original data set was as small as 30%.
2. The concentration field in the vicinity of a crystal growing in a diffusion-dominated regime showed symmetry along the centerline of the beaker indicating a uniform deposition of solute on the crystal surfaces over a long period of time. The field in the bulk of the solution was entirely axisymmetric in the initial stages of the growth process.
3. The transition from diffusion-dominated growth to the onset of convection induced temporary unsteadiness in the flow field that was accompanied by a breakdown of the symmetry of the concentration field.
4. With an increase in the crystal size, the convection current was seen to increase in strength and thus determine the overall transport of solute from the bulk of the solution to the crystal surfaces. The geometry of the grown crystal fixed the orientation of the rising plume. Nearly symmetric distribution of concentration was realized in the stable growth regime in regions away from the crystal.

11. FUTURE WORK

In the context of measurements, we propose to analyze shadowgraph images of convection patterns, collect tomographic projections by synchronizing the crystal rotation with the frame rate of the camera, and implement grey-scale and color-filters for schlieren measurements. The suitability of iterative tomographic algorithms will be explored. The interaction of crystal rotation with buoyancy will be studied over a wider range of parameters. A closer connection between the facets of the crystal and convection patterns will be sought to be established.

ACKNOWLEDGEMENTS

The importance of fluid convection in many crystal growth processes was originally pointed out to the authors by Dr. Vishwanath Prasad, Dean of Engineering, Florida State

University, Florida. KM thanks Dr. V.K. Wadhawan, CAT Indore (India) for introducing him to crystal growth from an aqueous solution. AS is grateful to Department of Atomic Energy, Mumbai for awarding him the K.S. Krishnan Fellowship for the year 2004. The authors held several useful discussions on the aqueous solution technique with Mr. Sunil Verma, CAT Indore (India). Financial support of Department of Science and Technology, New Delhi during 2000-2003 is thankfully acknowledged.

NOMENCLATURE

A	Archimedes number, Ra/Re^2
C	Solute concentration, kmol of salt/kg of solution
ΔC_ε	Concentration difference between two successive fringes
ΔC	Concentration difference between the saturated and supersaturated solution
D	Distance of the screen from the optical window (also diameter of the growth chamber), m
E_1	Absolute maximum temperature difference
E_2	RMS error
f	Focal length of the de-collimating mirror, m
g	Acceleration due to gravity, m/s^2
H	Height of the fluid layer (rectangular cavity), m (also, image size as seen through the optical window)
I	Intensity distribution (digitized)
L	Distance traversed by the laser beam through the test cell (also, crystal thickness in the vertical direction), m
N	Molar concentration of the solution, moles per 100 gm of KDP solution (also, total number of grid points on the reconstructed plane for tomography reconstruction)
Nu	Local Nusselt number defined as wall heat flux×cavity height/fluid conductivity
n	Refractive index of the fluid
n_a	Refractive index of the ambient
Pr	Prandtl number of the fluid, ν/α
R	Spatial frequency in the CBP algorithm
Ra	Rayleigh number (thermal= $g\,\beta\,\Delta T\,H^3/\,\nu\alpha$)
Re	Rotational Reynolds number, $\omega L^2/\,\nu$
r	radial coordinate
s	Perpendicular distance of the data ray from the center of the object
t	Time, hr
T	Temperature, K
T_o	Reference temperature, K
ΔT_ε	Temperature difference between successive fringes, K
$W(R)$	Filter function
x,y,z	Cartesian coordinates, with z parallel to the direction of propagation of

light

Greek Symbols

α	Diffusivity (mass/thermal), m^2/s (also polarizability of the KDP solution)
β	Coefficient of volume expansion of the fluid, K^{-1}
λ	Wavelength of the laser, nm
δ	Angular deflection of laser beam
ϕ	Polar angle in the CBP algorithm
ν	Kinematic viscosity of the solution, m^2/s
ρ	Density of the solution, kg/m^3
ρ_o	Reference value of density, kg/m^3
θ	Position of the source-detector line with respect to a fixed axis
ω	Crystal rotation speed, rpm

Subscripts

a,o	Reference value
c	Cold
h	Hot
orig	Original (temperature)
recon	Reconstructed (temperature)

REFERENCES

[1] W.R. Wilcox, "Transport phenomena in crystal growth from solution", *Prog. Crystal Growth and Charact.* 26, 153-194 (1993).

[2] Gebhart B., Jaluria Y., Mahajan R.L., and Sammakia B., *Buoyancy-Induced Flows and Transport,* Hemisphere Publishing Corporation, New York (1988).

[3] R.W. Lewis, R.E. Teets, J.A. Sell, and T.A. Seder, "Temperature measurements in a laser-heated gas by quantitative shadowgraphy", *Applied Optics* 26(17), 3695-3704 (1987).

[4] S. Kosugi, K. Maeno, and H. Honma, "Measurement of gas temperature profile in discharge region of excimer laser with laser schlieren method", *Japanese Journal of Applied Physics*, 32(3), 4980-4986 (1993).

[5] K. Muralidhar, V.B. Patil, and R. Kashyap, "Interferometric study of transient convection in a square cavity", *Journal of Flow Visualization and Image Processing*, 2(4), 321-333 (1995).

[6] M.S. Chandrashekhara, D.D. Squires, M.C. Wilder, and L.W. Carr, "A phase-locked high-speed real-time interferometry system for large amplitude unsteady flows", *Experiments in Fluids* 20, 61-67 (1995).

[7] S. Zhong and L.C. Squires, "An interferometric study of organized structures in wakes of circular cylinders", *Experiments in Fluids* 20, 91-99 (1995).

[8] O. Dupont, J.L. Dewandel, and J.C. Legros, "Use of electronic speckle pattern interferometry for temperature distribution measurements through liquids", *Optics Letters* 20(17), (1995).

[9] W. Schopf, J.C. Patterson, and A.M.H. Brooker, "Evaluation of the shadowgraph method for the convective flow in a side-heated cavity", *Experiments in Fluids*, 21, 331-340 (1996).

[10] G. Tanda, and F. Devia, "Application of a schlieren technique to heat transfer measurements in free convection", *Experiments in Fluids*, 24, 285-290 (1998).

[11] L. Howle, R.P. Behringer, and J. Georgiadis, "Visualization of convective fluid flow in a porous medium", *Nature* 362, 230-232 (1993).

[12] A.K. Agrawal, N.K. Butak, S.R. Gollahalli, and D. Griffin, "Three-dimensional rainbow schlieren tomography of a temperature field in gas flows", *Applied Optics* 37(3), 485-497 (1998).

[13] W. Dezhong and Z. Tiange, "The measurement of 3-D asymmetric temperature field by using real time laser interferometric tomography", *Optics and Lasers in Engineering* 36, 289-297 (2001).

[14] R. Snyder and L. Hesselink, "Measurement of mixing fluid flows with optical tomography", *Optics Letters* 13(2), 87-89 (1988).

[15] D.W. Watt and C.M. Vest, "Turbulent flow visualization by interferometric integral imaging and computed tomography", *Experiments in Fluids* 8, 301-311 (1990).

[16] Y.C. Michael and K.T. Yang, "Three-dimensional Mach-Zehnder interferometric tomography of the Rayleigh-Benard problem", *ASME J. Heat Transfer* 114, 622-629 (1992).

[17] L. McMackin and R.J. Hugo, "High speed optical tomography system for imaging dynamic transparent media", *Optics Express* 1(11), 302-311 (1997).

[18] H.S. Ko and K.D. Kihm, "An extended algebraic reconstruction technique (ART) for density-gradient projections: laser speckle photographic tomography", *Experiments in Fluids* 27, 542-550 (1999).

[19] D. Mishra, K. Muralidhar, and P. Munshi, "Study of Rayleigh-Benard convection at intermediate Rayleigh numbers", *Fluid Dynamics Research*, 25(5), 231-255 (1999).

[20] D. Mishra, J.P. Longtin, R.P. Singh, and V. Prasad, "Performance evaluation of iterative tomography algorithms for incomplete projection data", *Applied Optics* 43(7), 1-11 (2004).

[21] P.S. Chen, P.J. Shlichta, W.R. Wicox, and R.A. Lefever, "Convection phenomena during the growth of sodium chlorate crystals from solution", *Journal of Crystal Growth* 47, 43-60 (1979).

[22] P.S. Chen, W.R. Wicox, and P.J. Shlichta, "Free convection about a rectangular prismatic crystal growing from a solution", *Int. J. Heat Mass Transfer* 22, 1669-1679 (1979).

[23] P.J. Shlichta, "Feasibility of mapping solution properties during the growth of protein crystals", *Journal of Crystal Growth* 76, 656-662 (1986).

[24] F. Bedarida, "Developments of holographic interferometryapplied to crystal growth from solution", *Journal of Crystal Growth* 79, 43-49 (1986).

[25] V.I. Bredikhin, V.P. Ershov, V.V. Korolikhin, V.N. Lizyakina, S.Yu. Potapenko, and N.V. Khlyunev, "Mass transfer processes in KDP crystal growth from solutions", *Journal of Crystal Growth* 84, 509-514 (1987).

[26] K. Onuma, K. Tsukamoto, and I. Sunagawa, "Role of buoyancy convection in aqueous solution growth; A case study of $Ba(NO_3)_2$ crystal", *Journal of Crystal Growth* 89, 177-188 (1988).

[27] K. Onuma, K. Tsukamoto, and I. Sunagawa, "Effect of buoyancy driven convection upon the surface microtopographs of $Ba(NO_3)_2$ and CdI_2 crystals", *Journal of Crystal Growth* 98, 384-390 (1989).

[28] K. Onuma, K. Tsukamoto, and I. Sunagawa, "Measurements of surface supersaturations around a growing K-Alum crystal in aqueous solution", *Journal of Crystal Growth* 98, 377-383 (1989).

[29] F. Bedarida, E. Piano, and C. Pontiggia, "Measurements of concentration profiles by diffraction techniques", *Journal of Crystal Growth* 106, 217-220 (1990).

[30] M. Mantani, M. Sugiyama, and T. Ogawa, "Electronic measurement of concentration gradient around a crystal growing from a solution by using Mach-Zehnder interferometer", *Journal of Crystal Growth* 114, 71-76 (1991).

[31] K. Onuma, K. Tsukamoto, and S. Nakadate, "Application of real time phase shift interferometer to the measurement of concentration field", *Journal of Crystal Growth* 129, 706-718 (1993).

[32] I.Sunagawa, K. Tsukamoto, K. Maiwa, and K. Onuma, "Growth and perfection of crystals from aqueous solution: Case studies on barium nitrate and K-Alum", *Prog. Crystal Growth and Charact*., 30, 153-190 (1995).

[33] X. Yu, Y. Liu, X. Yu, and Y. Sun, "Some new optical measurement techniques for the study of crystal growth and electrode processes", *Optics and Lasers in Engineering* 25, 191-204 (1996).

[34] S. Kleine, W.J.P. van Enckevort, and J. Derix, "A dark field-type schlieren microscope for quantitative, in situ mapping of solute concentration profiles around growing crystals", *Journal of Crystal Growth* 179, 240-248 (1997).

[35] M.J. Krasinski, "Evolution of diffusion fields around KDP crystals growing in gel", *Cryst. Res. Technol.* 34(5-6), 647-653 (1999).

[36] V.I. Bredikhin, G.L. Galushkina, and S.P. Kuznetsov, "Schlieren technique to in situ monitor-rapidly growing KDP crystal surface", *Journal of Crystal Growth* 219, 83-90 (2000).

[37] T. Inoue, K. Mori, Y. Kageyama, and H. Mori, "Various growth shapes of $Na_2S_2O_3.5H_2O$ crystals", *Cryst. Res. Technol.* 35(5), 587-593 (2000).

[38] E. Piano, G.A. Dall'Aglio, S. Crivello, R. Chittofrati, and F. Puppo, "New optical techniques for crystal growth from fluids", *Material Chemistry and Physics* 66, 266-269 (2000).

[39] E. Piano, G.A. Dall'Aglio, R. Chittofrati, S. Crivello, and F. Puppo, "A non-destructive interferometric technique for analysis of crystal growth and fluid dynamics", *Ann. Chim. Sci. Mat.* 26, 23-28 (2001).

[40] L. Duan, and J.Z. Shu, "The convection during $NaClO_3$ crystal growth observed by the phase shift interferometer", *Journal of Crystal Growth* 223, 181-188 (2001).

[41] N.A. Booth, A.A. Chernov, and P.G. Vekilov, "Characterestic lengthscales of step bunching in KDP crystal growth: in situ differential phase-shifting interferometry study", *Journal of Crystal Growth* 237-239, 1818-1824 (2002).

[42] S. Maruyama, K. Ohno, A. Komiya, and S. Sakai, "Description of the adhesive crystal growth under normal and micro-gravity conditions employing experimental and numerical approaches", *Journal of Crystal Growth* 245, 278-288 (2002).

[43] V.I. Bredikhin, G.L. Galushkina, A.A. Kulagin, S.P. Kuznetsov, and O.A. Malshakova, "Competing growth centers and step bunching in KDP crystal growth from solutions", *Journal of Crystal Growth* 259, 309-320 (2003).

[44] A. Srivastava, K. Muralidhar, and P.K. Panigrahi, "Comparison of interferometry, schlieren and shadowgraph for visualizing convection around a KDP crystal", *Journal of Crystal Growth* 267(1), 348-361 (2004).

[45] Atul Srivastava, K. Muralidhar, and P.K. Panigrahi, "A schlieren study of the effect of ramp rate and rotation on convection around a crystal growing from an aqueous solution", *Journal of Crystal Growth* 274(1-2), 191-208 (2005).

[46] S. Miyashita, H. Komatsu, Y. Suzuki, T. Nakada, "Observation of the concentration distribution around a growing lysozyme crystal", *Journal of Crystal Growth* 141, 419-424 (1994).

[47] P.G. Vekilov and F. Rosenberger, "Protein crystal growth under forced solution flow: experimental set up and general response of lysozyme", *Journal of Crystal Growth* 186, 251-261 (1998).

[48] W.B. Hou, A.B. Kudryavtsev, T.L. Bray, L.J. DeLucas, and W.W. Wilson, "Real time evolution of concentration distribution around tetragonal lysozyme crystal: case study in gel and free solution", *Journal of Crystal Growth* 232, 265-272 (2001).

[49] D. Yin, Y. Inatomi, and K. Kuribayashi, "Study of lysozyme crystal growth under a strong magnetic field using a Mach-Zehnder interferometer", *Journal of Crystal Growth* 226, 534-542 (2001).

[50] G. Sazaki, Y. Azuma, S. Miyashita, N. Usami, T. Ujihara, K. Fuziwara, Y. Murakami, K. Nakajima, "*In-situ* monitoring system of the position and temperature at the crystal-solution interface", *Journal of Crystal Growth* 236, 125-131 (2002).

[51] M. Kawaji, O. Gamache, D.H. Hwang, N. Ichikawa, J.P. Viola, and J. Sygusch, "Investigation of Marangoni and natural convection during protein crystal growth", *Journal of Crystal Growth* 258, 420-430 (2003).

[52] N. Ramachandran and F.W. Leslie, "Using magnetic field to control convection during protein crystallization-analysis and validation studies", *Journal of Crystal Growth* 274, 297-306 (2005).

[53] L. Gatti, F. Solitro, F. Bedarida, P. Boccacci, G.A. Dall'aglio, and L. Zefiro, "Three-dimensional measurements of concentration fields in crystal growth by multidirectional holographic interferometry," in *Laser Interferometry: Quantitative analysis of Interferograms*, Proc. SPIE 1162, 126-131 (1989).

[54] D.W. Sweeney and C.M. Vest, "Reconstruction of three-dimensional refractive index fields from multidirectional interferometric data," *Applied Optics* 12(11), 2649-2664 (1973).

[55] A.G. Notcovich, I. Braslavsky, and S.G. Lipson, "Imaging fields around growing crystals," *Journal of Crystal Growth* 198/199, 10-16 (1999).

[56] A Srivastava, K. Muralidhar, and P.K. Panigrahi, "Reconstruction of the concentration field around a growing KDP crystal using schlieren tomography", (manuscript in preparation).

[57] N.P. Zaitseva, L.N. Rashkovich, and S.V. Bogatyreva, "Stability of KH_2PO_4 and $K(H,D)_2PO_4$ solutions at fast crystal growth rates", *Journal of Crystal Growth* 148, 276-282 (1995).

[58] R.J. Goldstein, ed., *Fluid Mechanics Measurements,* second edition, (Taylor and Francis, New York, 1996).

[59] G.S. Settles, *Schlieren and shadowgraph techniques: Visualizing phenomena in transport media* (Springer-Verlag publications, New York, 2001).

[60] D. Mishra, K. Muralidhar, and P. Munshi, Performance Evaluation of Fringe Thinning Algorithms for Interferometric Tomography, *Optics and Lasers in Engineering*, Vol. 30, pp 229-249, (1998).

[61] G.T. Herman, *Image Reconstruction from Projections* (Academic, New York, 1980).

[62] F. Natterer, *The Mathematics of Computerized Tomography* (John Wiley, New York, 1986).

[63] F. Mayinger, ed., *Optical Measurements: Techniques and Applications* (Springer-Verlag, Berlin, Germany, 1994).

[64] K. Muralidhar, Temperature Field Measurement in Buoyancy-driven Flows using Interferometric Tomography, *Annual Review of Heat Transfer*, Vol. 12, pp. 265-376, 2001.

[65] P. Munshi, "Error analysis of tomographic filters. I: Theory," *NDT & E International* 25(4/5), 191-194 (1992); Part II: Results, *NDT & E International* 26(5), 235-240 (1993).

[66] M.G. Velarde and C. Normand, "Convection," *Scientific American* 243(1), 79-94 (1980).

[67] S.S. Leong, "Numerical study of Rayleigh-Benard convection in a cylinder," *Numerical Heat Transfer* (A) 41, 673-683 (2002).

[68] S. Punjabi, K. Muralidhar, and P.K. Panigrahi, Buoyancy-driven Convection in Superposed Fluid Layers in an Octagonal Cavity, *International Journal of Thermal Sciences*, Vol. 43(9), pp. 849-864 (2004).

[69] A.Srivastava, K. Muralidhar, and P.K. Panigrahi, Interferometric study of buoyancy-driven convection in a circular fluid layer, *Heat and Mass Transfer*, Vol. 41(4), pp. 353-359 (February 2005).

[70] Srivastava, A. Phukan, P.K. Panigrahi and K. Muralidhar, Imaging of a Convective Field in a Rectangular Cavity using Interferometry, Schlieren and Shadowgraph, *Optics and Lasers in Engineering*, Vol. 42(4), pp. 469-485 (2004).

[71] J.P. Vanyo, *Rotating Fluids in Engineering and Science,* Dover Publications, New York, (1993).